Delft University of Technology

Quantitative fermentation of sesquiterpene producing microorganisms

Rocha Essenfelder Abrahão, Meissa

Citation (APA)
Rocha Essenfelder Abrahão, M. (2024). *Quantitative fermentation of sesquiterpene producing microorganisms*. [Dissertation (TU Delft), Delft University of Technology]. https://doi.org/10.4233/uuid:460648f9-65ca-4ff7-ad95-f43f9f9b29d5

Important note
To cite this publication, please use the final published version (if applicable).
Please check the document version above.

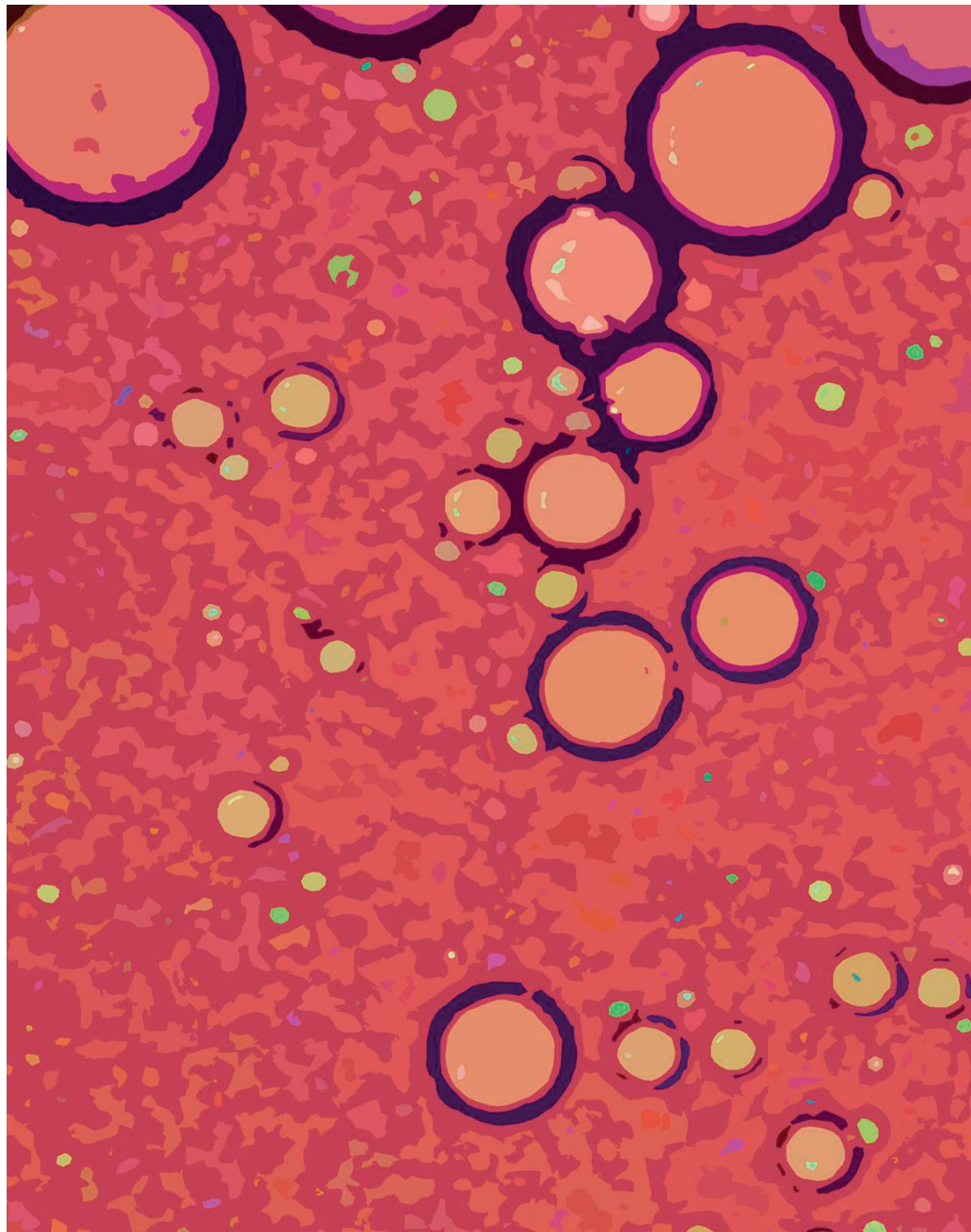# Quantitative fermentation of sesquiterpene producing microorganisms

Meissa Rocha Essenfelder Abrahão

Quantitative fermentation of sesquiterpene producing microorganisms

Dissertation

for the purpose of obtaining the degree of doctor
at Delft University of Technology
by the authority of the Rector Magnificus,
prof.dr.ir. T.H.J.J. van der Hagen
chair of the Board for Doctorates

to be defended publicly on
04 November, 2024 at 17:30 o' clock

by

Meissa ROCHA ESSENFELDER ABRAHÃO

Master of Food Science,
University of Campinas, Brazil
born in Governador Valadares, Brazil.

This dissertation has been approved by the promotors.

Composition of the doctoral committee

Rector Magnificus	Chairperson
Prof. dr. ir. L.A.M. van der Wielen,	Delft University of Technology, promotor
Dr. W. M. van Gulik,	Delft University of Technology, copromotor
Prof. dr. G. M. Pastore	University of Campinas (Brazil), promotor

Independent members

Prof. dr. ir. H. Noorman	Delft University of Technology
Prof. dr. J. T. Pronk	Delft University of Technology
Prof. dr. F. Hollmann	Delft University of Technology
Prof. dr. T. Teixeira Franco	University of Campinas (Brazil)

Reserve member

Prof. dr. ir. M. H. M. Eppink	Delft University of Technology

Dedicated to the memory of my dear father, Gilson Essenfelder, my most powerful example and inspiration.

Table of contents

Samenvatting

Door een toenemende vraag naar moleculen uit natuurlijke hulpbronnen, gecombineerd met heterogeniteit van productiegewassen, seizoensgebondenheid, lage opbrengsten met schaarste als gevolg, is de noodzaak van optimalisatie van biotechnologische processen voor de productie van dergelijke moleculen toegenomen. Belangrijke uitdagingen hierbij zijn de praktische en economische haalbaarheid van dergelijke productieprocessen, in veel gevallen gebaseerd op de grootschalige kweek van een hoog producerend micro-organismen (fermentatie).

Om de gevormde producten al tijdens het productieproces af te vangen kan "In situ product recovery" (ISPR) worden toegepast, bij voorbeeld middels het toevoegen van een organisch oplosmiddel tijdens de fermentatie. ISPR heeft als bijkomend voordeel dat ophoping van hydrofobe producten in het kweekmedium tot niveaus die de groei en productie van de producerende organismen remmen, wordt voorkomen. Niettemin brengt het gebruik van organische oplosmiddelen gecombineerd met oppervlakte-actieve stoffen (SACs) uitdagingen met zich mee voor de productterugwinning na stabilisatie van het kweekmedium.

Het onderzoek beschreven in dit proefschrift werd uitgevoerd binnen het Delft Integrated Recovery Column project (DIRC), dat zich richt zich op het ontwerp van een geïntegreerde reactor voor de productie en terugwinning van hydrofobe verbindingen zoals alkanen of isoprenoïden.

In dit proefschrift werd de productie van α-santaleen en α-humuleen bestudeerd, terpenen die van nature voorkomen in essentiële oliën van respectievelijk *Santalum album* en *Humulus lupulus*. De productie van deze verbindingen in twee verschillende *Escherichia coli* BL21(DE3) stammen werd bestudeerd tijdens fed-batch fermentaties met glycerol als

groeibeperkend substraat. Er werden duidelijke verschillen waargenomen tussen beide geteste stammen voor wat betreft de levensvatbaarheid van de cellen en de productiviteit.

Hoofdstuk 1 beschrijft waarom sesquiterpenen ($C_{15}H_{24}$) waardevolle apolaire moleculen zijn voor diverse industriële sectoren, op basis van hun bioactiviteit of gebruik als biobrandstoffen en geurstoffen. Verder wordt een overzicht gegeven van de biosyntheseroutes voor de productie van terpenen, met name de biosyntheseroute voor het gebruik van glycerol als koolstofbron. Als laatste wordt een overzicht gegeven van de literatuur waarin de resultaten van onderzoek naar de voordelen en beperkingen van *Escherichia coli* voor de expressie van heterologe producten wordt beschreven.

Hoofdstuk 2 presenteert de eerste resultaten van de biotechnologische productie van α-santaleen, daarbij gebruikmakend van ISPR (met toevoeging van dodecaan) in 2 L bioreactoren. Hierbij werden een aantal procesvariaties (zoals verschillende voedingssnelheden en inductiestrategieën) getest in fed-batch kweekexperimenten met een genetisch gemodificeerde *Escherichia coli BL21* (DE3) stam die bekend staat om zijn hoge variabiliteit in sesquiterpeen productiviteit. Bovendien werden de waarden van de black-box parameters (a, m_s) uit de Herbert-Pirt correlatie voor de specifieke consumptiesnelheid (q_s) van substraat geschat aan de hand van de verkregen experimentele gegevens.

Hoofdstuk 3 richt zich op dezelfde α-santaleen producerende stam die in hoofdstuk 2 is bestudeerd, rapporteert onderzoek naar de plasmidedynamiek tijdens een experiment zonder de extractant dodecaan, dat het process positief beïnvloedt maar de qPCR-analyse verstoord.

De biotechnologische productie van α-humuleen, ook uitgevoerd in 2L bioreactoren, wordt behandeld in Hoofdstuk 4. Daarbij werd gebruik

gemaakt van een beter producerende *E. coli* stam waartoe onze groep toegang had in de laatste fase van dit project. De productiviteit overtrof de verwachtingen in vergelijking met de bevindingen beschreven in de voorgaande hoofdstukken. De invloed van de toevoersnelheid van het substraat glycerol werd onderzocht, in combinatie met ISPR, evenals de invloed van de afwezigheid van dodecaan op de specifieke productiviteit. Herbert-Pirt parameters werden geschat voor een fed-batch experiment uitgevoerd met een constante glycerol voedingssnelheid. Daarnaast werden correlaties tussen de specifieke humuleen productiviteit (q_p) en de specifieke groeisnelheid (μ) gepresenteerd.

Om de modellering op realistische gegevens te baseren, zijn in Hoofdstuk 5 experimentele zuurstofoverdrachtssnelheden onder feitelijke extractieve ('overlay') en niet-extractieve omstandigheden voor sesquiterpeenfermentatie bepaald en vergeleken met de huidige inzichten in coalescerende en niet-coalescerende systemen. Terwijl de kLa-waarden bij extractieve fermentatie (ISPR) niet-coalescerend gedrag aangeven, volgt de kLa van oplosmiddelvrije fed-batch een algemene correlatie voor coalescerende systemen. Gecombineerd met de specifieke productiviteitsresultaten die zijn gerapporteerd voor de humuleenproducerende stam, zoals gerapporteerd in Hoofdstuk 4, beschrijft Hoofdstuk 5 het ontwerp van opgeschaalde productieprocessen, uit te voeren in 1 m^3 en 10 m^3 bioreactoren. Met gebruikmaking van een opgesteld black-box model werden de effecten van twee verschillende toevoerstrategieën van het substraat glycerol vergeleken, te weten een exponentiële toenemende voedingssnelheid (exponential feed (EF)) en een gecontroleerde voedingssnelheid gericht op een constante maximale zuurstofverbruikssnelheid (Constant Oxygen Consumption Rate (COCR)).

Hoofdstuk 6 vat de belangrijkste bevindingen samen en geeft aanbevelingen voor verder onderzoek en ontwikkeling.

Summary

Due to the increasing demand for molecules derived from natural resources, coupled with the heterogeneity of production crops, seasonality, and low yields leading to scarcity, the need for optimizing biotechnological processes for producing such molecules has grown. Key challenges in this area include the practical and economic feasibility of these production processes, often based on large-scale cultivation of high-yielding microorganisms (fermentation).

To capture the formed products during the production process, "In Situ Product Recovery" (ISPR) can be applied, for example, by adding an organic solvent during fermentation. ISPR also has the added benefit of preventing the accumulation of hydrophobic products in the culture medium to levels that inhibit the growth and production of the microorganisms. However, the use of organic solvents combined with surface-active compounds (SACs) poses challenges for product recovery after the stabilization of the culture medium.

The research described in this thesis was conducted within the Delft Integrated Recovery Column project (DIRC), which focuses on designing an integrated reactor for the production and recovery of hydrophobic compounds such as alkanes or isoprenoids.

This thesis explores the production of α-santalene and α-humulene, terpenes naturally found in the essential oils of *Santalum album* and *Humulus lupulus*, respectively. The production of these compounds in two different *Escherichia coli* BL21(DE3) strains was studied during fed-batch fermentations using glycerol as a growth-

limiting substrate. Significant differences were observed between the two tested strains regarding cell viability and productivity.

Chapter 1 describes why sesquiterpenes ($C_{15}H_{24}$) are valuable non-polar molecules for various industrial sectors, based on their bioactivity or use as biofuels and fragrances. It also provides an overview of the biosynthetic pathways for terpene production, particularly the biosynthetic route for using glycerol as a carbon source. Finally, it reviews the literature on the advantages and limitations of *Escherichia coli* for the expression of heterologous products.

Chapter 2 presents the initial results of the biotechnological production of α-santalene, using ISPR (with the addition of dodecane) in 2 L bioreactors. Various process variations (such as different feed rates and induction strategies) were tested in fed-batch culture experiments with a genetically modified *Escherichia coli* BL21 (DE3) strain known for its high variability in sesquiterpene productivity. Moreover, the values of the black-box parameters (a, m_s) from the Herbert-Pirt correlation for the specific substrate consumption rate (q_s) were estimated based on the experimental data obtained.

Chapter 3 focuses on the same α-santalene-producing strain studied in Chapter 2, but instead investigates plasmid dynamics during an experiment without dodecane: while this organic solvent improves bioprocess performance, it interferes with qPCR assays.

The biotechnological production of α-humulene, also carried out in 2L bioreactors, is discussed in **Chapter 4**. This was done using a better-producing *E. coli* strain that our group gained access to in the final phase of this project. The productivity exceeded expectations compared to the findings described in the previous chapters. The influence of the substrate glycerol feed rate was examined, in

combination with ISPR, as well as the impact of the absence of dodecane on specific productivity. Herbert-Pirt parameters were estimated for a fed-batch experiment conducted with a constant glycerol feed rate. Additionally, correlations between specific humulene productivity (q_p) and specific growth rate (μ) were presented.

To base the modeling on realistic data, **Chapter 5** determined and compared experimental oxygen transfer rates under actual extractive ("overlay") and non-extractive conditions for sesquiterpene fermentation with current insights into coalescing and non-coalescing systems. While the kLa values in extractive fermentation (ISPR) indicate non-coalescing behavior, the kLa of solvent-free fed-batch follows a general correlation for coalescing systems. Combined with the specific productivity results reported for the humulene-producing strain in Chapter 4, Chapter 5 outlines the design of scaled-up production processes, to be carried out in 1 m³ and 10 m³ bioreactors. Using a developed black-box model, the effects of two different glycerol feed strategies were compared: an exponentially increasing feed rate (Exponential Feed, EF) and a controlled feed rate aimed at a constant maximum oxygen consumption rate (Constant Oxygen Consumption Rate, COCR).

Chapter 6 summarizes the key findings and provides recommendations for further research and development.

Resumo

Devido à crescente demanda por moléculas provenientes de recursos naturais, juntamente com a heterogeneidade das culturas de produção, sazonalidade e baixos rendimentos que levam à escassez, houve o aumento da necessidade de otimizar os processos biotecnológicos para produzir tais moléculas. Os principais desafios nesta área incluem a viabilidade prática e econômica desses processos de produção, frequentemente baseados no cultivo em larga escala de microrganismos de alto rendimento (fermentação).

Para capturar os produtos formados durante o processo de produção, a "Recuperação de Produto *In Situ*" (ISPR) pode ser aplicada, por exemplo, adicionando um solvente orgânico durante a fermentação. A ISPR tem o benefício adicional de prevenir o acúmulo de produtos hidrofóbicos no meio de cultura a níveis que inibem o crescimento e a produção dos microrganismos. No entanto, o uso de solventes orgânicos combinados com compostos tensoativos (SACs) impõe desafios para a recuperação do produto após a estabilização do meio de cultura.

A pesquisa descrita nesta tese foi desenvolvida como parte do projeto "Delft Integrated Recovery Column" (DIRC), cujo objetivo é em projetar um reator integrado para a produção e recuperação de compostos hidrofóbicos, como alcanos ou isoprenóides.

Esta tese explora a produção de α-santaleno e α-humuleno, terpenos encontrados naturalmente nos óleos essenciais de *Santalum album* e *Humulus lupulus*, respectivamente. A produção desses compostos em duas diferentes cepas de *Escherichia coli* BL21(DE3) foi estudada durante fermentações em batelada alimentada usando glicerol como substrato limitante de crescimento. Diferenças significativas foram

observadas entre as duas cepas testadas em relação à viabilidade e produtividade celular.

O Capítulo 1 descreve motivos pelos quais os sesquiterpenos ($C_{15}H_{24}$) são moléculas não polares valiosas para vários setores industriais, com base em sua bioatividade ou uso como biocombustíveis e fragrâncias. Ele também fornece uma visão geral das vias biossintéticas para a produção de terpenos, com ênfase na rota bioquímica para a utilização de glicerol como fonte de carbono. Finalmente, tal capitulo oferece uma revisão bibliográfica sobre as vantagens e limitações de *Escherichia coli* para a expressão de produtos heterólogos.

O Capítulo 2 apresenta os resultados iniciais da produção biotecnológica de α-santalene, usando ISPR (por adição de dodecano) em biorreatores de 2 L. Variações de processo (como diferentes taxas de alimentação e estratégias de indução) foram testadas em experimentos de cultura em batelada alimentada com uma cepa *Escherichia coli BL21* (DE3) geneticamente modificada, conhecida por sua alta variabilidade na produtividade de sesquiterpeno. Além disso, os valores dos parâmetros de caixa preta (a, m_s) da correlação de Herbert-Pirt para a taxa de consumo de substrato específico (q_s) foram estimados com base em resultados experimentais.

O Capítulo 3 destaca-se por estudos com a mesma cepa produtora de α-santaleno estudada no Capítulo 2, mas desta vez investiga a dinâmica de plasmídeos durante um experimento sem dodecano: enquanto este solvente orgânico tende a impactar positivamente o bioprocesso, ele também pode interferir em técnicas de qPCR.

A produção biotecnológica de α-humuleno, também pesquisada em biorreatores de 2L, é discutida no Capítulo 4. Isso foi feito através do cultivo de uma cepa de *E. coli* de melhor performance de produção, à qual nosso grupo obteve acesso na fase final deste projeto. A

produtividade superou as expectativas em comparação com as descobertas descritas nos capítulos anteriores. O efeito da taxa de alimentação de glicerol do substrato foi examinada, em combinação com ISPR, bem como o impacto da ausência de dodecano na produtividade específica. Os parâmetros de Herbert-Pirt foram estimados para um experimento de batelada alimentada conduzido com uma taxa de alimentação de glicerol constante. Além disso, foram apresentadas correlações entre a produtividade específica de humuleno (q_p) e a taxa de crescimento específica (μ).

Para basear a modelagem em dados realistas, o Capítulo 5 determinou e comparou as taxas de transferência de oxigênio sob condições experimentais extrativas ("sobreposição") e não extrativas em fermentação de sesquiterpeno com referências atuais em sistemas coalescentes e não coalescentes. Enquanto os valores de kLa na fermentação extrativa (ISPR) indicam comportamento não coalescente, o kLa de batelada alimentada sem solvente segue uma correlação geral para sistemas coalescentes. Combinado com os resultados de produtividade específicos relatados para a cepa produtora de humuleno no Capítulo 4, o Capítulo 5 descreve o design de processos de produção em escala, a serem realizados em biorreatores de 1 m³ e 10 m³. Usando um modelo de caixa-preta, os efeitos de duas estratégias diferentes de alimentação de glicerol como substrato foram comparados: uma taxa de alimentação exponencialmente crescente ("Alimentação Exponencial","AE") e uma taxa de alimentação controlada com o objetivo de obter uma taxa máxima e constante de consumo de oxigênio ("Taxa de Consumo de Oxigênio Constante","TCOC").

O Capítulo 6 resume as principais descobertas e fornece recomendações para futuras pesquisas e desenvolvimento.

Chapter 1

Introduction and Thesis Outline

1.1. Terpenes: categories, applications in biotechnology and pathways

Remarkable for their chemical diversity in nature, bioactivity and organoleptic properties, terpene-like molecules or terpenes are represented by more than 70000 different molecules [1] acting on signalling, cell protection, photosynthesis, membrane structure, respiration [2], and exerting further biological activities (antioxidant, anti-inflammatory or anticancer) [3]. Several terpenes or their oxygenated compounds (terpenoids) are considered fine chemicals due to unique properties. Their relevance as aroma compounds, biofuels and pharmaceutical compounds have been widely described [2, 4].

Terpenes and their derivatives, called terpenoids, are found mostly in plants. The chemical structures of terpenes are based on isoprene units (5C). The prefixes "hemi", "mono"," sesqui", "di", "sester" and "tetra" indicate terpenes with 5, 10, 15, 20, 25, 40 carbon atoms, respectively. Isopentenyl diphosphate (IPP) and dimethylallyl diphosphate (DMAPP) are key intermediates towards the synthesis of isoprenoids with high molecular weight [2].
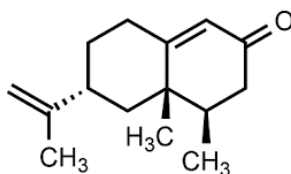

Figure 1.(+)-Nootkatone.

Specific compounds such as nootkatone, β-carotene, and astaxanthin are molecules of massive industrial interest [2]. The companies Evolva and Isobionics have dedicated efforts to the production of valencene, nootkatone and sandalwood oil (for the later, the characteristic odor is mainly due to the presence of β-santalol) [5]. Nootkatone (figure 1) is a key compound with grapefruit-like notes and biological activities that suggest potential as insecticide. As a result, a strong interest has arisen from several industry segments, including pharmaceutical, cosmetics, food and fragrances [6]. Metabolic engineering of *Pichia pastoris* towards alcohol dehydrogenase overexpression resulted in 208 mg · L^{-1} of (+)-nootkatone in cell culture [7].

Remarkable for its potent antimalarial property, the sesquiterpene endoperoxide artemisinin (figure 3) has been recommended by the Word Health Organization (WHO) in combined therapies for uncomplicated malaria caused by *Plasmodium falciparum*. Despite the availability of artemisinin in natural sources such as *Artemisia annua*, the supply of this plant is restricted, due to price changes and shortages [8].
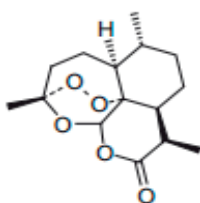

Figure 2. Artemisinin.

Amongst the leaders for the development of processes for the production of valuable sesquiterpenes and related intermediates, the company Amyris announced the successful production of artemisinic acid (25 g · L^{-1}) using an engineered *Saccharomyces cerevisiae* strain. In addition, an efficient chemical process was developed to convert the produced artemisinic acid to artemisinin [8].

The heterologous expression of farnesene synthases from several different sources has been reported, aiming at farnesene formation from farnesyl diphosphate (FPP). Isomers including (E)-β-farnesense, (E, E)- α-farnesene and (Z, E)-α farnesene are referred to as farnesene and have also been described as chemically signaling molecules in nature [2]. The reduced form farnesane (figure 3) exerts potential as an isoprenoid-derived biosynthetic fuel [9].
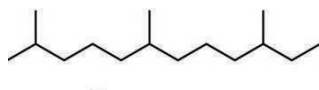
Figure 3. Farnesane.

The yeast *S. cerevisiae* was engineered for the high level production of farnesene, to act as a precursor for renewable chemicals and fuels. This resulted in a process capable of producing 130 g·(kg broth)$^{-1}$ of farnesene after two weeks of fermentation [10]. A license for this process was sold to DSM [11].

Tricyclic sesquiterpenes have been considered as alternative jet fuel precursors: the combination of promotor engineering and mevalonate (MVA) pathway expression in *E. coli* led to 727.9 mg · L^{-1} epi-isozizaene, 77.5 mg · L^{-1} α-isocomene and 780.3 mg · L^{-1} of

pentalenene. The same pathway expressed, instead, in *S. cerevisiae* aiming at the latter molecule resulted in 344 mg·L^{-1} [12].

1.2. Metabolism and sesquiterpene synthase expression in *E. coli*

Sugar compounds have been traditionally the main source of carbon for the biotechnological production of fuels and chemicals [1, 13]. However, the increasing population is expected to raise sugar demands around the world, encouraging a continuous search for attractive and non-competing carbon sources by scientists [14]. Crude glycerol is a by-product from biodiesel production (10 % w·w^{-1}) [15]. High availability and decreased costs have renewed the interest in glycerol as carbon and energy source to obtain valuable chemicals. Elucidation of glycerol metabolizing pathways has led to the development of production processes with high potential for industry, such as for dihydroxyacetone and organic acids [16]. This work is focused on the aerobic production of sesquiterpenes ($C_{15}H_{24}$) using glycerol ($C_3H_8O_3$) as carbon source.

Glycerol as carbon source has been tested as substrate for sesquiterpene production in *Escherichia coli.* The final titer of α-farnesene, a potential biodiesel precursor, has been reported to reach 380 mg·L^{-1} after codon optimization of heterologous α-farnesene synthase (from *Malus domestica*) and protein fusion between this enzyme and FPP (farnesyl-diphosphate) synthase [17]. *Escherichia coli* can convert glycerol into ethanol and organic acids (such as succinic, acetic, and formic) [18]. It was reported that, from unrefined

glycerol, the yield of ethanol and by-products (such as hydrogen and formate) was higher than 95 % of the theoretical maximum by engineered *E.coli* strains SY03 and SY04 using fermentative pathways [19].

Although the metabolic pathways can differ, after glycerol uptake (in the presence of GlpF, a facilitator in *E. coli*), usually the next step consists of phosphorylation by ATP-dependent kinases. Next, glycerol-3-phosphate (G3P) is oxidized by G3P dehydrogenases to dihydroxyacetone-phosphate (DHAP), further isomerized to glyceraldehyde-3-phosphate (Ga3P) towards the lower part of the glycolytic pathway. The last enzyme here could be NAD-dependent or linked to the electron transport chain via ubiquinone [16].

From the many known chemical structures of isoprenoids, only genes associated with the synthesis of a few hundred of those have been cloned until 2007 [20]. However, exponential interest in sequencing terpene synthases has been shown, given the increase of genome-sequencing projects and industrial relevance of the fine molecules [21]. Sterols and quinones are isoprenoids, naturally produced as central metabolites in some microorganisms, but in general host strains used for heterologous expression are not naturally capable of producing a range of different terpenoids [20]. Improvements of isoprenoid production pathways have been limited, due to factors such as storage capacity and tolerance of hosts, since terpenes have been known for their antimicrobial activity and thus toxic effects on microorganisms, including E. *coli* [22].

The building blocks of terpenes (DMAPP (dimethylallyl diphosphate) and IPP (isopentenyl diphosphate)) result either from the

MEP (C-methyl-D-erythritol-4-phosphate pathway) or the MVA (mevalonate) pathways [23, 24], which differ mainly for the first steps. The MEP (or DXP, meaning 1-deoxy-d-xylulose 5-phosphate) stem pathway is characterized by glycerol-3-phophate (G3P) condensation to pyruvate, resulting in 1-deoxy-D-xylose-5-phosphate (DXP), subsequently reduced to MEP. For the mevalonate (MVA) pathway, instead, the condensation of three acetyl-CoA molecules leads to HMG-CoA (3-hydroxy-3-methylglutaryl-CoA) formation, further reduced to mevalonate [22].

There are two different pathways for isoprenoid biosynthesis, the mevalonate pathway and the methylerythritol phosphate pathway (MEP). The mevalonate pathway is present in eukaryotic cells, archaea and some bacteria, while most bacteria as well as chloroplasts of plants and algae employ the MEP pathway [23]. Several metabolic engineering projects have focused on improving the flux through these pathways [4]. The utilization of heterologous hosts such as *E. coli* and *S. cerevisiae* for terpene biosynthesis has the advantage that they have been widely studied and are genetically well accessible. In addition their native isoprenoid metabolism is very limited, thus minimizing challenges with competing metabolic fluxes [20].

The mevalonate pathway (MVA) is naturally present in *S. cerevisiae*, while *E. coli* is known for the MEP pathway system, which encouraged scientific efforts to test complementary options in combination with endogenous pathways to obtain microbial platforms [21]. The MVA pathway for isoprenoids production in *Escherichia coli* is extended in two further main phases beyond the central metabolism.

In the so called "stem pathway", the main units for synthesis of isoprenoids, DMAPP and IPP, are produced. From the glycolysis towards the MVA pathway, three molecules of acetyl-coA are condensed by thiolase (THL) and HMGS (HMG-Coa synthase) to form HMG-CoA (3-hydroxy-3-methylglutaryl-coa) [22].

The next step, performed by HMG-CoA reductase, leads to mevalonate, which is further phosphorylated and decarboxylated to IPP. Named "branched pathway", the final phase is characterized by the head-to-tail condensations of the previously mentioned "building blocks" to form linear isoprenyl diphosphates. Terpene synthases and their diverse characterization steps such as acylation, oxidation or cleavage results in a diversity of different isoprenoids [22]. Alternatively, other authors suggest that while terpene synthases are responsible for the cyclization steps towards chains of polyisoprenoid diphosphates, other tailoring enzymes enhance structural diversity of final molecules by addition of functional groups. These tailoring enzymes include oxygenases, acetyltransferases, glycosyltransferases and methyltransferases [25].

Advances for the production of Taxadiene, an intermediate of the Taxol (effective against cancer) biosynthesis pathway, in *E. coli* reached more than $1 \text{ g} \cdot \text{L}^{-1}$ after significant improvements towards the native upstream and heterologous downstream parts of the pathway [26]. Likewise, mevalonate and amorphadiene concentrations were raised after the improvement of the pyruvate dehydrogenase bypass, enhancing the availability of acetyl-CoA [27]. As result, 1.9-fold increase in productivity had been reported, as compared to the control strain. The highest titer of sesquiterpene achieved was $120 \text{ mg} \cdot \text{L}^{-1}$

using a genetically modified strain (PDB108), engineered for overexpression of ALD6 (encoding cytosolic acetaldehyde dehydrogenase) and a gene from *Salmonella* (hosting a gene for acetyl-CoA synthetase). This host had been optimized earlier for steps related to the mevalonate pathway, such as activities for FPP synthase and hydroxymethylglutaryl-CoA reductase (HMGR) [27].

1.3. Advantages and challenges: *E. coli* as a work horse for protein expression

Factors such as structure, size and stability of the gene product are essential for the selection of the host system, so are post-translational modification demands, in order to achieve the proper biological activity of the protein of interest. *Escherichia coli* has become an example of a microbial cell factory [28] for cost-efficient expression of proteins on a large scale, especially those with limited size and relatively simple structural complexity [29]. Features for this bacterium such as low cost, known genetic data, simplicity and fast high-density cultivation have led to this popularity [30]. Also, the high maximum specific growth rate of *E. coli* is an advantage. For the strain *E. coli* K-12, for instance, a doubling time of 20 min in Luria-Bertani broth was reported [31].

Limitations in performing disulfide bond formation, specific posttranslational modifications typical of eukaryotic proteins, and the absence of an efficient mechanism of protein secretion are some of the drawbacks of the utilization of *Escherichia coli* as host for heterologous protein expression [32]. To accomplish the production of

recombinant proteins, some essential steps (identification of the gene of interest, selection of a proper host organism, cloning and transformation of expression vectors, induction of protein expression) are very clear in theory, but in practice, problems occur, such as unsatisfactory production or inactivity of proteins, insufficient growth and the formation of inclusion bodies (IBs) [28].

Despite the advances in the genetic engineering of *E. coli*, the expression of some genes is susceptible to the degradation and/or the toxicity of the protein of interest, peculiarities of gene sequences, stability of mRNA and differences between host and original source for codon usage [32] .To address the later, and related translational problems [33], works on codon optimization have been published [34], [35], [36].

Certain special features are key for strains to be successful in recombinant protein expression, such as the presence of elements required in the expression system, deficiency in some harmful natural proteases and capability to maintain the plasmid [30]. In *Escherichia coli* BL21, for instance, the mutation *hsd*SB (inherited from the parental strain (B834)), hinders DNA methylation and degradation, minimizing plasmid loss [28]. BL21 and B834 strains are also deficient in *ompT* proteases, which has applications not only against cleavage of proteins during purification, but also for recombinant protein expression, because this type of proteases could also cleave T7 RNA polymerases [37, 38].

Generally, a system-compatible genetic background which harbors the induced plasmid is required for protein expression [30]. A compatibility with diverse hosts such as prokaryotes and eukaryotes

has been reported for the T7 system. Traditionally, the integration of the gene encoding T7 polymerase into the host genome and transcription by RNA polymerase of the host is performed in order to minimize the lethal effects associated with over transcription [39].

The commercial strain *Escherichia coli* BL21(DE3) (bearing the T7 gene I, regulated in its chromosome by the lacUV5 promoter) has been widely applied for non-toxic protein expression [28, 40, 41]. Orientation and strength of promoters on the plasmids are known for their impact on protein expression [42]. While BL21(DE3) strains are focused on proteins from cloned genes controlled by a promoter for T7 RNA polymerase in suitable vectors, BL21 are less specific, used for expressing genes controlled by other promoters [43, 44].

In case that the T7 promoter is driving the expression of the gene of interest, the supply of T7 RNA is required [28]. Ideally, cells should be able to induce enough T7 RNA polymerase to trigger high level expression of the target protein [45]. Bacteriophage T7 RNA polymerase is a product of the T7 gene I and differs physically and biochemically from RNA polymerase in the *E. coli* host cells. A high r-strand specificity (> 95%) for that enzyme is known, indicating that the formation of RNA chains is originated at specific sites on the T7 template [46]. For T7 RNA polymerase, a fast mechanism for RNA synthesis occurs, as well as high affinity for their own promoters [47]. In the strain BL21(DE3), prophage ʎDE3 is present in the chromosome, leading to a single copy of the gene for T7 RNA polymerase under control of an inducible promoter (*lac* UV5) [28, 45].

Some environmental stimuli trigger the action of specific proteins with high affinity for DNA sequences towards activation or repression

of some genes in prokaryotic and eukaryotic cells [48]. Special molecules modify the affinity of repressors towards operators. Under the presence of anti-inducers, the referred affinity can be increased with a factor five, while it could be decreased with a factor of 1000 under standard conditions, in the presence of inducers such as IPTG (Isopropyl β-D-1-thiogalactopyranoside), an allolactose analog [48, 49].

For plasmids properly maintained in the cells, the *lac* UV5 promoter responds to the chemical inducer, IPTG, producing T7 RNA polymerase [45]. The promoters *lac* UV5 and T7/lac hybrid are repressed by gene *Lac*I, present in the *E. coli* genome and vectors under control of the T7 lac hybrid promoter. The presence of IPTG leads to the release of *Lac*I from the lac operator and subsequent transcription of the target gene [30].

In the absence of a chemical inducer, though, some T7 RNA polymerase is also produced, characterizing a leaky feature of *lac* UV5, and resulting in basal transcripts of cloned genes. As a consequence, the maintenance of plasmids containing certain genes becomes a concern: plasmids cannot be established in BL21(DE3) if the gene is considerably toxic, risking the accumulation of non-functional mutants as outcome [45].

Robust vectors designed for high production of proteins and built up to carry strong promotors (T7, *lac, tac, trc*) are commercially available [40]. Suitable prokaryotic expression vectors are characterized by selection markers, origin of replication, SD (Shine-Dalgarno) site, an efficient transcription terminator, gene-specific translational and transcriptional "enhancers" acting on the stringent

regulation of promoter activity [32]. Additionally, a tightly regulated promoter is required, especially for the production of toxic proteins [50].

The overconsumption of metabolites involved in general pathways can result in a decreased production of crucial cell components, and overall, a balance between optimizing production and maintaining the viability of the host cells is required. The utilization of low-copy plasmids has been recommended for long-term expression of pathways involving multiple steps. They are compatible with strong promoters, enhancing the chances to maximize gene expression, while minimizing the metabolic burden compared to high-copy number vectors [51]. Depending on the origin of replication, between 25-50 copies per cell are present of low-copy vectors, in contrast to high-copy number vectors such as pUC derivatives, responsible for about 200 copies per cell [29, 52]. For the later, the translation of foreign mRNA into proteins could potentially represent a metabolic burden and negatively impact the production yields [28].

Plasmid maintenance in cells during division and related stability are influenced by the copy-number characteristics [29]. Despite their versatility as expression tools, the use of plasmids can represent challenges related to segregational instability in biotechnological applications [53, 54].

1.4. Selection pressure in bioprocesses

To ensure a satisfactory accumulation of proteins of interest, most cells must be able to express the target genes after induction. The growth of plasmid-bearing cells tend to be surpassed by the plasmid-lacking fraction in a short time range, as the loss of selective pressure happens [45].

Antibiotic-based selection has been discouraged in production systems as a consequence of regulatory requirements [55] or their utilization has even been forbidden in processes aiming at human nutrition related products [56]. Not only side effects such as allergic responses have been described for certain types of antibiotics (β-lactam category) [55], but the removal of antibiotics in general during downstream processing is a costly drawback, raising demands towards strategies for gene expression free of these specific selection markers [56].

As an alternative to the utilization of antibiotics, the selection of bacterial transformants has been achieved after the complementation of auxotrophic mutations in the chromosome strategically placed in the vector containing the functional gene [57].

Chromosomal integration has also been suggested an alternative to overcome limitations associated to the maintenance of plasmids [53]. Based on this strategy, genes in the chromosome can either be replaced or inserted in intercistronic regions, resulting in stable strains, with genes maintained independently of selection markers [58]. The integration of recombinant genes into the chromosome of *Escherichia coli* JM109 as individual expression

cassettes resulted in the plasmid-free production of 2′-fucosyllactose in fed-batch experiments. The bioprocess scaled up to a 30 L stirrer tank reached a titer of 20.28 ± 0.83 g $\cdot$ L^{-1} of 2'-fucosyllactose (2-'FL) and a productivity of 0.57 g $\cdot$ (L $\cdot$ h)$^{-1}$ [56].

1.5. Driving forces towards biotechnological production of apolar molecules

Traditional methods of extraction for volatile compounds from essential oils are susceptible to seasonal and geographical limitations, climate disasters and plant diseases, not to mention the price and quality fluctuations. In essential oils, for instance, many molecules of interest occur in very low concentrations in natural sources, representing a small fraction of the chemically comparable substances, challenging purification. The ongoing search for techniques to replace the traditional methods for the production of fine chemicals led to a great interest towards biotechnological strategies, whereby the feasibility depends on the target molecule [59].

Biocatalytic routes can be carried out using mild conditions, for instance, as for the allylic oxidation of valencene into nootkatone [6]. Moreover, regio and stereoselectivities in enzymatic reactions reinforce the trending preference for a biotechnology strategy over chemical synthesis and extraction from natural sources [24].

Chemical synthesis and the linked concept for artificial products can lead to rejection by the consumers, while specific customer

preferences for natural ingredients appear as market opportunities, strengthening the driving force towards alternative processes [59].

The engineering of efficient strains led to a diverse collection of molecules in either bench or industrial scales [60]. The first decade of the 21st century has advanced towards new molecules, achieved through biotechnological routes. More than 100 flavors originated from bioprocesses were commercially available five years ago [59].

Fundamentally, there are two options for the biotechnological production of aroma compounds: *de novo* synthesis or biotransformation. During *de novo* ("from the new"), synthesis in most cases an extensive pathway is required synthesize the compound of interest from simple building blocks. On the other hand, biotransformation requires often only one or a few steps to modify a certain compound to another (with comparable chemical structure) either by isolated enzymes or whole cells [61, 62].

Biotransformation of terpenes, focused on highly available molecules, such as industrial by - products, into fine chemicals, has been extensively researched using relatively simple pathways [63]. Limonene is highly available in *Citrus aurantium* (90.0 %) and *Citrus limon* (59.7%) oils, mainly obtained from the peels of these fruits [64]. Further conversion of this monoterpene into carvone and α-terpineol was reported, as was the biotransformation of geraniol into linalool and linalool oxide [65].

Optimization of the biotransformation of R-(+)-limonene into R-(+)-α-terpineol with the fungus *Fusarium oxysporum* 152b*,* using response surface methodology (RSM), thereby including parameters as temperature, incubator speed, substrate concentration and the

utilization of co-substrate resulted in a final titer of 2.4 g · L^{-1}. Optimal R-(+)-α-terpineol concentrations were accomplished after 72 h at 26 °C/240 rpm, from 0.5 % R-(+)-limonene in pure distilled water [66]. High limonene concentrations (180 g · L^{-1}) converted by *Sphingobium sp*, resulted in 130 g · L^{-1} α-terpineol using sunflower oil as organic phase [67].

Pinenes (consisting of 60 - 70 % of the *α*- isomer and 20 - 25 % and of the *β*-isomer) are the major terpene forms available in sulphate turpentine, a by-product from softwood used in paper manufacturing industries [68]. From *α*-pinene, biotransformation into verbenone, a key compound of rosemary oil, was reported [63]. Likewise, the synthesis of the speciality chemical responsible for the grapefruit-like aroma, (+)-nootkatone, is possible from (+)-valencene [6].

Feasibility and sustainability are key goals for the bioprocesses. However, the challenge to make the processes feasible for commercial scale still remains dependent on the target molecules. Once further optimizations of the production of isoprenoids by biocatalysts have been carried out, a great potential for biotechnological processes to reach new markets currently dominated by chemical manufacturers based on fossil sources or plant biosynthesis, is predicted, expanding the opportunities for renewable processes [2].

1.6. *In situ* product recovery (ISPR) and challenges due to emulsification

The biotechnological production of aroma derivatives is susceptible to factors as low solubility of product and substrate in water, chemical instability and the impact of substrate and products on the viability of the biocatalysts. One of the most popular approaches to overcome or minimize some of these challenges is *in situ* product recovery [69]. A suitable ISPR strategy should be chosen according to specific physicochemical properties of the compounds of interest, such as charge, volatility, molecular weight and hydrophobicity [70].

Solvent extraction is widely used as a form of ISPR. Through the affinity towards hydrophobic compounds, the addition of a solvent with low water solubility to the aqueous phase leads to the compartmentalization between biocatalyst and the product. Therefore, the tolerance of biocatalysts against cytotoxicity and inhibition effects of certain molecules is encouraged. However, bottlenecks in productivity and yield using this method could be expected due to interfacial mass transfer fluxes of these compounds, assuming the choice for this recovery method [4]. Stirred tanks have been the most popular reactors described for two-liquid phase bioprocesses using ISPR. The correlation between agitator speed and droplet diameter on interfacial area in organic phase is considered a key aspect in recovery [71].

An emulsion is a system characterized by instability of one immiscible liquid dispersed in another, thus, likely to separate into the original liquids in the absence of stabilizing components [72]. An

undesirable stable emulsion effect, though, results from the interaction between the solvent chosen for extraction [73] and surface-active compounds (SACs), also produced by microorganisms, hampering phase separation. SACs are excreted for protection or to increase the substrate access [4]. Phospholipids, glycolipids, polymeric surfactants and lipopeptides or lipoproteins were described for their defined hydrophobic and hydrophilic groups and related properties as SACs [74].

In the presence of SACs, the droplet interface remains stabilized, demanding extra steps to force droplet coalescence from concentrated emulsion (referred to as "cream") in order to obtain a continuous oil phase [72]. Given these drawbacks from the perspective of product recovery, actions towards their control in the broth include: minimizing the stress of microorganisms in processes or adapting pretreatment strategies, for instance [75]. Diverse factors influencing the product recovery become crucial from an economic perspective, when considered for the scale - up of processes, especially for products demanded in high amounts, such as biofuels.

An efficient organic phase must be chosen taking into consideration factors such as biocompatibility and phase volume ratio between organic and aqueous volumes, usually not exceeding 0.4 for the last [4]. Suitable solvents for biocatalysis are selected according to general guidelines for specific log P (logarithm of the partition coefficient standard octanol–water system). This indicator is related to polarity and toxicity, as follows: inactivation or denaturation of biocatalysts is expected for solvents with log P below 2, while those with log P higher than 4 are not supposed to impact the viability and

activity necessary for reactions. Between 2 < log P < 4, the effects are hard to predict, since solvents are usually weak water coat-biocatalyst distorters and may affect, to some extent, the biological activity [76]. The terpene limonene (log P 4.46), for instance, is able to accumulate in the membrane and damage the cell [77].

Overall, a correlation between different organic phases with suitable partition coefficients and the resulting biocatalyst activity determines biocompatibility, which is specific to the type of the microorganism and the contact with the tested solvent. Many factors influence such extent of contact: concentrations of SACs, biomass and solvent, power input by mixing, interfacial area for mass transfer and others [4].

Remarkable strain improvements have been published, encouraging the concept of microbial cell factories with high metabolic flux and the diversification of products [24]. Despite all these achievements focused on biocatalysts, challenges in the optimization of the complete bioprocess and related process technology remain to allow a competitive production of apolar molecules. Many strategies developed at laboratory scale (under controlled conditions and from pure chemicals) show poor performance after scale-up. [73].

Based on the potential of isoprenoids and alkane molecules [75] for the microbial production as advanced biofuels, the DIRC (Delft Integrated Recovery Column) project was initiated in 2008, aiming at the construction of a reactor able to integrate the fermentation and alternative separation method and minimize costs. A patent for this reactor was registered in 2010, describing the initial concepts [78].

Within the DIRC project in 2016, the thesis from Heeres [79] discussed the advanced biofuels production and proposing suitable methods of integration, resulting in three publications. The causes of stabilization for emulsions from a microscale perspective were reviewed, remarking different mechanisms: electrostatic, steric and mechanical. Factors for a successful coalescence process and specific steps were described: droplet collision, film drainage and film rupture. The interference of surface-active compounds blocking the droplet interface and the coalescence process, essential for continuous oil layer formation and product recovery, was explained [72].

The following experimental work revealed a minimal droplet size required for oil layer formation and process conditions influencing coalescence. Testing either microfluidic chips or stirred vessels with 1 $g \cdot L^{-1}$ of mannoprotein and 100 μm of initial droplet size led to stable droplet size after 1.5 h. An even longer duration could be required for smaller initial droplet sizes [75].

A method based on the flow of gas bubbles through glass columns to stimulate the formation of a continuous oil layer was presented, so were further possibilities for integration in reactors and reutilization of cells. The authors reported the influence of superficial gas velocity and nozzle diameter on separation. Despite the action of air bubbles as coalescence facilitators, their influence on axial dispersion occurred [80].

Replacing expensive available methods such as centrifugation and eliminating the addition of de-emulsifiers turned out to be a challenging goal due to the complex profile of polyphasic systems and

the presence of surface-active compounds, but the research towards more environmentally friendly methods of recovery continues to progress [79].

1.7. Scope and outline of the thesis

In addition to the interest in the DIRC project in integrated recovery strategies, this thesis is focused on research towards the biotechnological production of industrially valuable sesquiterpenes ($C_{15}H_{24}$). For this, bench-scale fed-batch experiments were performed using engineered *Escherichia coli* strains, which were not designed in our facilities, but kindly provided by our industrial partner. Research questions established for this specific project are:

- What are the values of the Herbert-Pirt parameters, related to biomass yield on glycerol and maintenance energy requirements of the engineered strains and how can we obtain them from fed-batch experiments;
- What are the effects of a second liquid-phase on aerobic microbial sesquiterpene production by these strains;
- Which factors affect strain stability and thus sesquiterpene production;
- How can Black-Box modeling be applied to support model simulations of larger scale processes.

In the subsequent chapters of this thesis these research questions are addressed as follows:

In Chapter 2, an engineered santalene-producing *E. coli* strain was cultivated in fed-batch mode in bench-scale bioreactors (2 L) using dodecane for ISPR. The values of the Herbert-Pirt parameters for biomass formation (a) and maintenance (m_s) were estimated from the obtained data. The strategies applied include variations for induction step and feed rate variations. The performance of the same santalene-producing *E. coli* strain was the main topic of Chapter 3, presenting Real time PCR to check on plasmid copy numbers for different timepoints in the absence of *in situ* product recovery (ISPR).

For Chapter 4, a different engineered *E. coli* strain was tested for the biotechnological production of the α-humulene, a sesquiterpene naturally available in *Humulus lupulus*. The α-humulene productivities were compared for different feeding strategies and for the absence or presence of ISPR using dodecane. Also, for this strain the Herbert-Pirt parameters were estimated from the obtained fed-batch data.

In chapter 5 a scale-up study is performed using Black-box modeling, based on the estimated parameters and metabolic model of the α-humulene producing strain that followed from Chapter 4. Feed strategies (Exponential feed versus Constant Oxygen Consumption Rate) were compared for productivities and general processes demands.

1.8. Acknowledgements

1.9. References

1.   Krieg, T., et al., *CO2 to Terpenes: Autotrophic and Electroautotrophic α-Humulene Production with Cupriavidus necator.* Angewandte Chemie International Edition, 2017. **57**(7): p. 1879-1882.

2.   Chandran, S.S., J.T. Kealey, and C.D. Reeves, *Microbial production of isoprenoids.* Process Biochemistry, 2011. **46**(9): p. 1703-1710.

3.   Felipe, L.d.O., A.M.d. Oliveira, and J.L. Bicas, *Bioaromas – Perspectives for sustainable development.* Trends in Food Science & Technology, 2017. **62**: p. 141-153.

4.   Schewe, H., M.A. Mirata, and J. Schrader, *Bioprocess Engineering for Microbial Synthesis and Conversion of Isoprenoids*, in *Biotechnology of Isoprenoids*, J. Schrader and J. Bohlmann, Editors. 2015, Springer International Publishing: Cham. p. 251-286.

5.   Leavell, M.D., D.J. McPhee, and C.J. Paddon, *Developing fermentative terpenoid production for commercial usage.* Current Opinion in Biotechnology, 2016. **37**: p. 114-119.

6.   Fraatz, M.A., R.G. Berger, and H. Zorn, *Nootkatone—a biotechnological challenge.* Applied Microbiology and Biotechnology, 2009. **83**(1): p. 35-41.

7.   Wriessnegger, T., et al., *Production of the sesquiterpenoid (+)-nootkatone by metabolic engineering of Pichia pastoris.* Metabolic Engineering, 2014. **24**: p. 18-29.

8.   Paddon, C.J., et al., *High-level semi-synthetic production of the*

potent antimalarial artemisinin. Nature, 2013. **496**: p. 528-532.

9.   Peralta-Yahya, P.P., et al., *Microbial engineering for the production of advanced biofuels.* Nature, 2012. **488**(7411): p. 320-328.

10.   Meadows, A.L., et al., *Rewriting yeast central carbon metabolism for industrial isoprenoid production.* Nature, 2016. **537**: p. 694-697.

11.   Amyris. *DSM Expands Strategic Alliance with Amyris*. 2019 27-March-2019]; Available from: https://amyris.com/dsm-expands-strategic-alliance-with-amyris/.

12.   Liu, C.-L., et al., *Renewable production of high density jet fuel precursor sesquiterpenes from Escherichia coli.* Biotechnology for Biofuels, 2018. **11**(285): p. 1-15.

13.   Carroll, A.L., S.H. Desai, and S. Atsumi, *Microbial production of scent and flavor compounds.* Current Opinion in Biotechnology, 2016. **37**: p. 8-15.

14.   Sonntag, F., et al., *Engineering Methylobacterium extorquens for de novo synthesis of the sesquiterpenoid α-humulene from methanol.* Metabolic Engineering, 2015. **32**: p. 82-94.

15.   McCoy, M., *Glycerin surplus.* Chemical & Engineering News Archive, 2006. **84**(6): p. 7.

16.   Sprenger, G.A., *Glycerol as Carbon Source for Production of Added-Value compounds*, in *Engineering of Microorganisms for the Production of Chemicals and Biofuels from Renewable Resources*, G. Gosset, Editor. 2017, Springer International Publishing. p. 39-123.

17.   Wang, C., et al., *Metabolic engineering of Escherichia coli for*

α-farnesene production. Metabolic Engineering, 2011. **13**(6): p. 648-655.

18. Murarka, A., et al., *Fermentative utilization of glycerol by Escherichia coli and its implications for the production of fuels and chemicals.* Applied and environmental microbiology, 2008. **74**(4): p. 1124-1135.

19. Shams Yazdani, S. and R. Gonzalez, *Engineering Escherichia coli for the efficient conversion of glycerol to ethanol and co-products.* Metabolic Engineering, 2008. **10**(6): p. 340-351.

20. Withers, S.T. and J.D. Keasling, *Biosynthesis and engineering of isoprenoid small molecules.* Applied Microbiology and Biotechnology, 2007. **73**(5): p. 980-990.

21. Daviet, L. and M. Schalk, *Biotechnology in plant essential oil production: progress and perspective in metabolic engineering of the terpene pathway.* Flavour and Fragrance Journal, 2010. **25**(3): p. 123-127.

22. Wang, C., et al., *Metabolic engineering and synthetic biology approaches driving isoprenoid production in Escherichia coli.* Bioresource Technology, 2017. **241**: p. 430-438.

23. Boronat, A. and M. Rodriguez-Concepcion, *Terpenoid Biosynthesis in Prokaryotes*, in *Biotechnology of Isoprenoids*, J. Schrader and J. Bohlmann, Editors. 2015, Springer International Publishing: Switzerland. p. 475.

24. Schempp, F.M., et al., *Microbial Cell Factories for the Production of Terpenoid Flavor and Fragrance Compounds.* Journal of Agricultural and Food Chemistry, 2018. **66**(10): p. 2247-2258.

25.   Bian, G., et al., *Releasing the potential power of terpene synthases by a robust precursor supply platform.* Metabolic Engineering, 2017. **42**: p. 1-8.

26.   Ajikumar, P.K., et al., *Isoprenoid pathway optimization for Taxol precursor overproduction in Escherichia coli.* Science, 2010. **330**(6000): p. 70-74.

27.   Shiba, Y., et al., *Engineering of the pyruvate dehydrogenase bypass in Saccharomyces cerevisiae for high-level production of isoprenoids.* Metabolic Engineering, 2007. **9**(2): p. 160-168.

28.   Rosano, G.L. and E.A. Ceccarelli, *Recombinant protein expression in Escherichia coli: advances and challenges.* Frontiers in microbiology, 2014. **5**: p. 172-172.

29.   Jonasson, P., et al., *Genetic design for facilitated production and recovery of recombinant proteins in Escherichia coli.* Biotechnology and Applied Biochemistry, 2002. **35**(2): p. 91-105.

30.   Sørensen, H.P. and K.K. Mortensen, *Advanced genetic strategies for recombinant protein expression in Escherichia coli.* Journal of Biotechnology, 2005. **115**(2): p. 113-128.

31.   Sezonov, G., D. Joseleau-Petit, and R. D'Ari, *Escherichia coli physiology in Luria-Bertani broth.* Journal of bacteriology, 2007. **189**(23): p. 8746-8749.

32.   Makrides, S.C., *Strategies for achieving high-level expression of genes in Escherichia coli.* Microbiological reviews, 1996. **60**(3): p. 512-538.

33.   Kane, J.F., *Effects of rare codon clusters on high-level expression of heterologous proteins in Escherichia coli.*

Current Opinion in Biotechnology, 1995. **6**(5): p. 494-500.

34.   Jenkins, M.C., et al., *Effects of codon optimization on expression in Escherichia coli of protein-coding DNA sequences from the protozoan Eimeria.* Journal of Microbiological Methods, 2023. **211**: p. 106750.

35.   Fu, H., et al., *Codon optimization with deep learning to enhance protein expression.* Scientific Reports, 2020. **10**(1): p. 17617.

36.   Fei, D., et al., *Codon optimization, expression in Escherichia coli, and immunogenicity analysis of deformed wing virus (DWV) structural protein.* PeerJ, 2020. **8**: p. e8750.

37.   Gottesman, S., *Proteases and their targets in Escherchia coli* Annual Review of Genetics, 1996. **30**(1): p. 465-506.

38.   Grodberg, J. and J.J. Dunn, *ompT encodes the Escherichia coli outer membrane protease that cleaves T7 RNA polymerase during purification.* Journal of bacteriology, 1988. **170**(3): p. 1245-1253.

39.   Wang, W., et al., *Bacteriophage T7 transcription system: an enabling tool in synthetic biology.* Biotechnology Advances, 2018. **36**(8): p. 2129-2137.

40.   Chao, Y.-P., C.-J. Chiang, and W.-B. Hung, *Stringent Regulation and High-Level Expression of Heterologous Genes in Escherichiacoli Using T7 System Controllable by the araBAD Promoter.* Biotechnology Progress, 2002. **18**(2): p. 394-400.

41.   Yau, S.Y., E. Keshavarz-Moore, and J. Ward, *Host strain influences on supercoiled plasmid DNA production in*

Escherichia coli: Implications for efficient design of large-scale processes. Biotechnology and Bioengineering, 2008. **101**(3): p. 529-544.

42.   Weickert, M.J., et al., *Optimization of heterologous protein production in Escherichia coli.* Current Opinion in Biotechnology, 1996. **7**(5): p. 494-499.

43.   William Studier, F., et al., *[6] Use of T7 RNA polymerase to direct expression of cloned genes*, in *Methods in Enzymology*. 1990, Academic Press. p. 60-89.

44.   Daegelen, P., et al., *Tracing Ancestors and Relatives of Escherichia coli B, and the Derivation of B Strains REL606 and BL21(DE3).* Journal of Molecular Biology, 2009. **394**(4): p. 634-643.

45.   Studier, F.W. and B.A. Moffatt, *Use of bacteriophage T7 RNA polymerase to direct selective high-level expression of cloned genes.* Journal of Molecular Biology, 1986. **189**(1): p. 113-130.

46.   Chamberlin, M., J. McGrath, and L. Waskell, *New RNA Polymerase from Escherichia coli infected with Bacteriophage T7.* Nature, 1970. **228**(5268): p. 227-231.

47.   Tabor, S. and C.C. Richardson, *A bacteriophage T7 RNA polymerase/promoter system for controlled exclusive expression of specific genes.* Proceedings of the National Academy of Sciences of the United States of America, 1985. **82**(4): p. 1074-1078.

48.   Figge, J., et al., *Stringent regulation of stably integrated chloramphenicol acetyl transferase genes by E. coli lac repressor in monkey cells.* Cell, 1988. **52**(5): p. 713-722.

49.   Barkley, M.D., et al., *Interaction of effecting ligands with lac repressor and repressor-operator complex.* Biochemistry, 1975. **14**(8): p. 1700-1712.

50.   Hannig, G. and S.C. Makrides, *Strategies for optimizing heterologous protein expression in Escherichia coli.* Trends in Biotechnology, 1998. **16**(2): p. 54-60.

51.   Jones, K.L., S.-W. Kim, and J.D. Keasling, *Low-Copy Plasmids can Perform as Well as or Better Than High-Copy Plasmids for Metabolic Engineering of Bacteria.* Metabolic Engineering, 2000. **2**(4): p. 328-338.

52.   Balbas, P. and F. Bolivar, *[3] Design and construction of expression plasmid vectors in escherichia coli*, in *Methods in Enzymology*. 1990, Academic Press. p. 14-37.

53.   Martinez-Morales, F., et al., *Chromosomal integration of heterologous DNA in Escherichia coli with precise removal of markers and replicons used during construction.* Journal of bacteriology, 1999. **181**(22): p. 7143-7148.

54.   Peredelchuk, M.Y. and G.N. Bennett, *A method for construction of E. coli strains with multiple DNA insertions in the chromosome.* Gene, 1997. **187**(2): p. 231-238.

55.   Peubez, I., et al., *Antibiotic-free selection in E. coli: new considerations for optimal design and improved production.* Microb Cell Fact, 2010. **9**: p. 65.

56.   Baumgärtner, F., et al., *Construction of Escherichia coli strains with chromosomally integrated expression cassettes for the synthesis of 2'-fucosyllactose.* Microbial Cell Factories, 2013. **12**(1): p. 1-13.

57. Olempska-Beer, Z.S., et al., *Food-processing enzymes from recombinant microorganisms--a review.* Regul Toxicol Pharmacol, 2006. **45**(2): p. 144-158.

58. Albermann, C., N. Trachtmann, and G.A. Sprenger, *A simple and reliable method to conduct and monitor expression cassette integration into the Escherichia coli chromosome.* Biotechnology Journal, 2010. **5**(1): p. 32-38.

59. Berger, R.G., *Biotechnology as a source of natural volatile flavours.* Current Opinion in Food Science, 2015. **1**: p. 38-43.

60. Ekas, H., M. Deaner, and H.S. Alper, *Recent advancements in fungal-derived fuel and chemical production and commercialization.* Current Opinion in Biotechnology, 2019. **57**: p. 1-9.

61. Bicas, J.L., et al., *Production of Aroma Compounds by White Biotechnology*, in *White Biotechnology for Sustainable Chemistry*. 2016, The Royal Society of Chemistry. p. 310-332.

62. Sales, A., et al., *Biogeneration of aroma compounds.* Current Opinion in Food Science, 2018. **19**: p. 77-84.

63. Schrader, J., *Microbial Flavour Production*, in *Flavours and Fragrances: Chemistry, Bioprocessing and Sustainability*, R.G. Berger, Editor. 2007, Springer Berlin Heidelberg. p. 507-574.

64. Soković, M., et al., *Antibacterial Effects of the Essential Oils of Commonly Consumed Medicinal Herbs Using an In Vitro Model.* Molecules, 2010. **15**(11): p. 7532-7546.

65. Molina, G., et al., *Monoterpene bioconversion for the production of aroma compounds by fungi isolated from Brazilian fruits.* Food Science and Biotechnology, 2013. **22**(4):

p. 999-1006.

66.   Bicas, J.L., et al., *Optimization of R-(+)-α-terpineol production by the biotransformation of R-(+)-limonene.* Journal of Industrial Microbiology & Biotechnology, 2008. **35**(9): p. 1061-1070.

67.   Bicas, J.L., et al., *A bioprocess for the production of high concentrations of R-(+)-α-terpineol from R-(+)-limonene.* Process Biochemistry, 2010. **45**(4): p. 481-486.

68.   van der Schaft, P.H., *Chemical Conversions of Natural Precursors*, in *Flavours and Fragrances: Chemistry, Bioprocessing and Sustainability*, R.G. Berger, Editor. 2007, Springer International Publishing. p. 285-301.

69.   Berger, R.G., *Biotechnology of flavours—the next generation.* Biotechnology Letters, 2009. **31**(11): p. 1651-1659.

70.   Freeman, A., J.M. Woodley, and M.D. Lilly, *In situ product removal as a tool for bioprocessing.* Bio/Technology, 1993. **11**(9): p. 1007-1012.

71.   Wang, D.I.C. and A. Ochoa, *Measurements on the interfacial areas of hydrocarbon in yeast fermentations and relationships to specific growth rates.* Biotechnology and Bioengineering, 1972. **14**(3): p. 345-360.

72.   Heeres, A.S., et al., *Microbial advanced biofuels production: overcoming emulsification challenges for large-scale operation.* Trends in Biotechnology, 2014. **32**(4): p. 221-229.

73.   Cuellar, M.C. and L.A.M. van der Wielen, *Recent advances in the microbial production and recovery of apolar molecules.* Current Opinion in Biotechnology, 2015. **33**: p. 39-45.

74. Healy, M.G., C.M. Devine, and R. Murphy, *Microbial production of biosurfactants.* Resources, Conservation and Recycling, 1996. **18**(1): p. 41-57.

75. Heeres, A.S., et al., *Fermentation broth components influence droplet coalescence and hinder advanced biofuel recovery during fermentation.* Biotechnology Journal, 2015. **10**(8): p. 1206-1215.

76. Laane, C., et al., *Rules for optimization of biocatalysis in organic solvents.* Biotechnology and Bioengineering, 1987. **30**(1): p. 81-87.

77. Sikkema, J., J.A. de Bont, and B. Poolman, *Interactions of cyclic hydrocarbons with biological membranes.* Journal of Biological Chemistry, 1994. **269**(11): p. 8022-8028.

78. van der Wielen, L.A.M. and J.J. Heijnen, *Process for the continuous biological production of lipids, hydrocarbons or mixtures thereof. European Patent EP 2 196539 A1, publication date16/06/2010.* p. 13.

79. Heeres, A.S., *Integration of Product Recovery in Microbial Advanced Biofuel Production: Overcoming Emulsification Challenges, PhD thesis,.* Delft University of Technology: Delft Repository (2016), https://doi.org/10.4233/uuid:7dd55824-96ae-4dfc-9b36-95f21490612e.

80. Heeres, A.S., et al., *Gas bubble induced oil recovery from emulsions stabilised by yeast components.* Chemical Engineering Science, 2016. **145**: p. 31-44.

Chapter 2

Kinetic parameters and strategies for biotechnological α-santalene production

Kinetic parameters and strategies for biotechnological α-santalene production

Abstract

Volatile compounds typically found in the essential oil from *Santalum album* exert organoleptic and biological activities of outstanding industrial interest. Multiple companies have focused on the research and development of processes for the production of sesquiterpenes such as α-santalene and chemically related molecules.

In the development of such processes several challenges might be encountered, for instance, the sensitivity of the strain to shear stress, time of induction and inducer concentrations, the concentration of solvents such as dodecane for product recovery and its impact on emulsion formation, due to the presence of surface-active compounds (SACs).

In this chapter biotechnological α-santalene-production was performed using *E. coli* BL21 (DE3) through three experiments using glycerol as substrate and dodecane for *in situ* product recovery (ISPR) in 2L bench-scale bioreactors. Hereby, factors impacting on productivity were researched, such as induction strategies, varying fed-batch ages and different IPTG concentrations. For one experiment, the absence of antibiotics in feed was tested to evaluate the effect of the decrease of selection pressure over product formation.

The fed-batch strategy consisting of early induction and intermediate IPTG concentrations resulted in α-santalene specific productivities starting from $2.28 \cdot 10^{-4}$ to $2.87 \cdot 10^{-4}$ Cmol P $\cdot$ (Cmol X)$^{-1}$ and led to the highest product concentration after 69.5 h of feed phase: 0.39 g/kg ± 0.01. The strategy using continuous induction and

antibiotics in feed resulted in the second higher specific productivity, reaching $1.8 \cdot 10^{-4}$ Cmol P $\cdot$ (Cmol X)$^{-1}$).

Averaged Herbert-Pirt parameters for biomass formation and maintenance of cells for the experiments with lower santalene specific productivity were $a = -\frac{1}{Y_{X/S}^{max}}$ = - 0.42 [mol glycerol $\cdot$ (Cmol X)$^{-1}$] ± 0.07 and m_s = - 0.021 [mol glycerol consumed $\cdot$ (h $\cdot$ Cmol X present)$^{-1}$] ± 0.0004. For the experiment with the highest ranges on specific santalene productivity, different parameters (a = - 0.70 [mol glycerol $\cdot$ (Cmol X)$^{-1}$] ± 0.11 and m_s = - 0.008 [mol glycerol consumed $\cdot$ (h $\cdot$ Cmol X present)$^{-1}$] ± 0.0027) were estimated.

Keywords: *Escherichia coli,* glycerol, α-santalene, fed-batch, ISPR, dodecane

2.1. Introduction

2.1.1. α- Santalene as target compound and the relevance of santalol isomers

Terpenoids present remarkable applications as flavors and fragrances. They can either be chemically synthesized or obtained from essential oil and natural extracts [1]. Sandalwood oil is obtained by steam distillation of the heartwood of East Indian species of *Santalum album* L. (Santalaceae family), and is mainly composed of santalols, complex structured sesquiterpenoids [2-4]. The sandalwood oil is known for its sweet fragrance, balanced with delicate woody notes [5] and regarded as a stable and a valuable fixative in perfumery [4]. Santalene (figure 1) and santalols are responsible for the unique odor of sandalwood [6]. Nearly 90 % of this essential oil is composed by four specific molecules: epi-β-santalol, α-exo-bergamotol and both santalol isomers: α and β [7]. Usually the sandalwood oil yield is 4 to 6.5 %, based on trees aged for at least 30 years [8].

The precursor of santalols, santalene ($C_{15}H_{24}$), represents between 21 % and 24 % of hydrocarbons for sandalwood oils, higher in Australian than in Indian varieties [9]. The terpene can be hydroxylated at position C12 by cytochrome P450 monooxygenases to form santalol, assisted by a NADPH dependent reductase. At least nine different cytochrome P450 enzymes (family CYP76F) with varying specificities for substrates are known [10].

Patents have been registered for the production of both isomers: β-santalene [11] and α-santalene [12], focusing on obtaining them from the precursor of sesquiterpenes, farnesyl diphosphate (FPP). The last patent [12] specifically cites the overexpression of α-santalene synthase *in vivo* using *Escherichia coli* BL 21(DE3). Even though the expression of foreign enzymes had been performed during the strain transformation, according to the author, they were not essential for the target terpene formation, but focused on increase of intermediates.
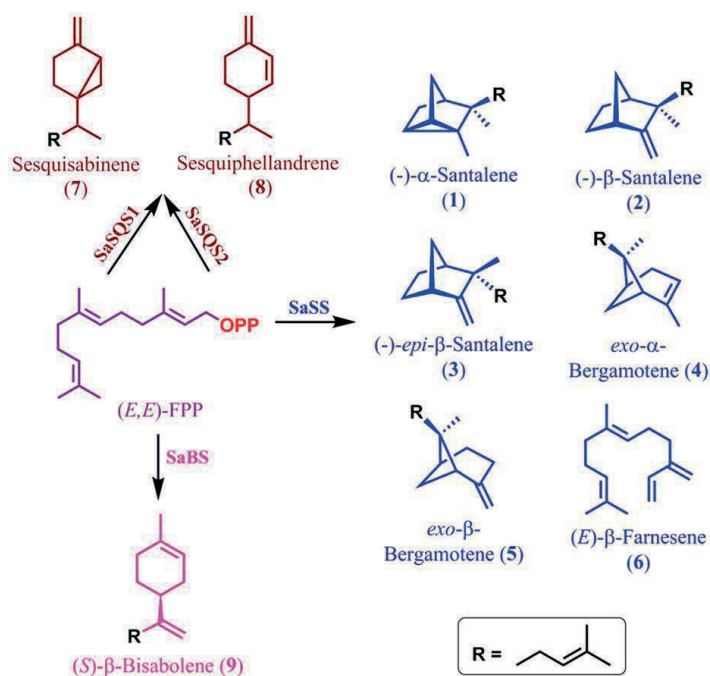
Figure 1. Different sesquiterpene synthases and products from (E,E)-FPP: farnesyl-diphosphate. Santalene synthase (Sass), bisabolene synthase (SaBS), sesquisabinene synthase (SaSQS1 and SaSQS2) [16]. Published under a CC BY 4.0 license.

Both santalol isomers (α and β) are key molecules for several industries from the flavors and fragrances market, for example, Evolva [13] and Isobionics [5]. The *Santalum album* oil characterization in terms of santalol isomers composition is a good indication of quality: authors proposed a minimal composition of 43 % for the α-isomer and no less than 18 % for the β-isomer using GC-MS and considering geographical and taxonomical variations [14]. These isomers should represent 90 % of the yellow oil from the East Indian Sandalwood tree [15], distinguished from the variant known as *Amyris balsamifera* (or west Indian sandalwood, a less costly option), which has been used for *S. album* oil depreciation [14].

Given that the composition of the sandalwood oil depends on several factors, such as geography, taxonomy and age, a flexibilization for international standards in terms of composition for both alcohols had been requested. Due to the influence of age, higher concentrations in β-santalol were present in *S. album* oils from the oldest woods, compared to younger sources [17].

In vivo tests with mice revealed anti-hyperglycemic and antioxidant activities for α-santalol and sandalwood oil, confirming potential applications for the pharmaceutical industry [18]. Furthermore, properties against skin cancer have been suggested for the same alcohol through *in vitro* and *in vivo* tests. Once human prostate cancer cells were exposed to α-santalol, apoptosis was observed, suggesting an inhibition effect [19].

Even though more biochemical background similarities with plant cells have been reported for *S. cerevisiae* (MVA pathway, primarily found in eukaryotes) as compared to *E. coli* (MEP pathway),

an overview performed by authors indicated the prevalence of research articles using *Escherichia coli* as heterologous host for the expression of several isoprenoids [20]. Contrastingly, most publications specifically related to the expression of santalene synthases found in this chapter described the utilization of *S. cerevisiae* for the biotechnological production of α-santalene.

Engineering of *Saccharomyces cerevisiae* for the production of α-santalene was firstly reported by Scalcinatti *et al* [21], through the expression of SanSyn (santalene synthase, original from *Clausena lansium*). Through strain modifications and performing fed-batch experiments with exponential feed and glucose de-repressed growth conditions, bottlenecks in the mevalonate pathway, were elucidated. One of most controlling steps appeared to be the conversion from 3-hydroxyl-3-methyl-glutaryl-CoA into mevalonate, catalyzed by HMGR (3-hydroxyl-3-methyl-glutaryl-CoA reductase). In order to increase the availability of the universal precursor of sesquiterpenes, as a first strategy, farnesyl diphosphate (FPP), a truncated form of this enzyme was overexpressed. FPP can be directed to different molecules, such as farnesol and ergosterol, the last compound being a constituent of cell membranes, required for cell maintenance and growth.

The second strategy was focused on the squalene synthase (SQS) activity, involved in the balance between the formation of non-sterol sesquiterpenes and sterol. The gene *ERG9*, which encodes the key-enzyme for ergosterol formation was down-regulated by the replacement of its promoter by the HXT1 promoter, increasing the α-

santalene productivity by 260 %, thereby accomplishing a specific productivity of 0.18 mg $\cdot$ (g biomass $\cdot$ h)$^{-1}$.

As the formation of ergosterol was decreased, an increase of farnesol production occurred, indicating a saturation of santalene synthase, the enzyme required for santalene formation. The best concentration of α-santalene (92 mg $\cdot$ L^{-1}) and specific productivity 0.21 mg $\cdot$ (g biomass $\cdot$ h)$^{-1}$ occurred after this improvement was combined with a deletion of the DPP1 gene, encoding for pyrophosphate phosphatase that converts FPP into farnesol. This resulted in a 24 % decrease of farnesol accumulation, and a 54 % increase of the santalene titer [21].

Another paper published by Scalcinati *et al.* [22] reported the continuous production of α-santalene (dilution rate of 0.05 $\cdot$ h^{-1}) under glucose limited conditions and using dodecane for *in situ* product recovery. Combined modifications of different pathways resulted in a 1.8-fold increase of the overall α-santalene yield (5.2$\cdot$10^{-3} Cmmol $\cdot$ (Cmmol glucose)$^{-1}$), as compared to the previous publication from the same group [21]. Under specific process conditions, a productivity of 490.2 mg $\cdot$ (g DCM$\cdot$h)$^{-1}$ was achieved. To ensure more genetic stability, most of the modifications described were integrated into the genome. During this work, a codon-optimized version of the sesquiterpene synthase (SanSyn$_{opt}$) was used to engineer *S. cerevisiae.* Likewise, an increase of NADPH availability, the reductive cofactor (given its demand for the mevalonate pathway), was accomplished. However, wash-out was observed for the best performing strains when the operational dilution rate was increased from 0.05 $\cdot$ h^{-1} to 0.1 $\cdot$ h^{-1}**.**

Dodecane has been described for its hydrophobicity, low volatility and biocompatibility. Authors report absent or negligible toxic effects towards the biocatalysts from this solvent or for santalene accumulation, for which log P values have been published as 6.6 and 6.2, respectively [21], [23]. The partitioning effect due to the solvent addition facilitates the capture of compounds with low solubility in water and minimizes the loss of volatile compounds through the gas stream.

Cloning and functional characterization of key sesquiterpene synthases linked to biosynthesis of FPP, sesquisabinene, β-bisabolene and santalenes was carried out, enabling developments for heterologous microbial production of sesquiterpene-like molecules from *Santalum album* L. (Indian sandalwood) [16]. A metabolic engineering approach led to a four-fold increase of α-santalene production by *S. cerevisiae* after increasing the flux towards acetyl-CoA, which is also required for the production of lipids, polyketides, and 1-butanol. Strategies included blocking the competing pathways for acetyl-CoA and ethanol conversion into the intermediate via acetaldehyde [24].

Later on, another group [25] reported santalene production with ISPR in Fed-batch cultivations. After 30 h of feeding, the santalene concentration reached 163 $mg \cdot L^{-1}$ in 2.5 L bioreactors, expressing santalene synthase (Sass) from *C. lansium* in *S. cerevisiae.* A feed strategy based on an exponential feed profile, controlled by the respiratory quotient, was used in a feedback loop. Starting from the same precursor (FPP), a 50 % lower product yield on biomass (Y_{Xsant} =0.006 $g \cdot (g \ DCW)^{-1}$) was observed, as compared to the farnesene

yield on biomass (Y_{Xfar}) described for a farnesene producing strain with similar biochemical background. The authors suggested a more efficient catalytic activity for farnesene synthase, as compared to santalene synthase: this could be due to the complexity associated to the cyclization step, key for the synthesis of santalene (see figure 1 for details on chemical structure).

As will be detailed in chapter 3 of this thesis, the instability of genetically modified strains is a concern, as it directly influences the productivities of bioprocesses. Once the plasmids were built up with special genes required for sesquiterpene production, it is important that the cells keep the original plasmids active. For the santalene-producing strain, each plasmid was constructed with a resistance gene to antibiotics (chloramphenicol and carbenicillin, as shown in table 1). Microbiological assays performing the incubation in plates had been initially used here to track the percentage of viable cell count with plasmids, as compared to the total population.

2.1.2. Black-box modelling

Consumption of the carbon and energy source, further on called the substrate, during heterotrophic growth of microorganisms can be described by a simple linear equation, thereby dividing the consumed substrate over growth, product formation and maintenance, the so called Herbert-Pirt equation [26]:

$$q_s = a \cdot \mu + b \cdot q_p + m_s \text{ [mol glycerol} \cdot (h \cdot Cmol\ X)^{-1}],$$

$$\text{for a} = -\frac{1}{Y_{X/S}^{max}} \text{ and b} = -\frac{1}{Y_{P/S}^{max}}$$

The first term on the right side represents the substrate consumption for biomass formation (a·μ), with the parameter a being the amount of substrate (here glycerol) required to produce one Cmol of biomass [mol glycerol · (Cmol X)$^{-1}$] and μ the biomass specific growth rate [Cmol X produced · (Cmol X present · h)$^{-1}$]. The second term represents the substrate consumption for product formation with the parameter b being the amount of substrate required to produce one mol of product [mol glycerol · (mol P)$^{-1}$] (in the absence of growth or maintenance) and q_p [mol P · (Cmol X · h)$^{-1}$] the biomass specific rate of product formation. Finally, the third term represents the specific rate of substrate consumption for maintenance m_s [mol glycerol · (h · Cmol X)$^{-1}$].

The approach used in this chapter for the HP (Herbert - Pirt) correlation has been simplified, considering only the biomass and maintenance terms, as the rate of santalene production is very low and therefore the product term of the Herbert - Pirt equation is negligible compared to the total specific rate of substrate consumption q_s. Published values of the Herbert - Pirt parameters for growth of *Escherichia coli* MG1655 on glycerol can be found in [27].

An important aim of this chapter is the identification of kinetic and stoichiometric parameters through quantitative data processing. For this, Black-Box modeling was applied based on experimental data from fed-batch experiments for the estimation of the Herbert-Pirt parameters related to biomass formation (a) and maintenance (m_s), using glycerol as the carbon source. Furthermore, the impact of

chemical inducer concentrations on product formation was tested, as well as different strategies for the induction of santalene production. Additionally, the performance of santalene production was tested for a strain submitted to increased levels of inducer and antibiotics.

2.2. Materials and Methods

2.2.1. Strains and pre-culture preparation

2.2.1.1. Standard α-santalene-producing strain (SS)

Escherichia coli BL21(DE3) (Novagen) was the basic biocatalyst used. The santalene-producing strain (SS) used during this project was built up with two plasmids and was kindly provided by an industrial partner. The plasmid pACYCDuet™-1 (built up with a gene for resistance against chloramphenicol) contained genes for the expression of typical enzymes of the mevalonate pathway [28], towards the production of farnesyl diphosphate (FPP or FDP, the precursor for all the sesquiterpenes). The other plasmid (pETDuet™-1), contained the gene for the final step, α-santalene synthase, converting FDP into the final product and a gene coding for resistance to the beta-lactam antibiotic ampicillin.

Table 1. Plasmid features for the santalene-producing strain:

Identification	Selection marker
pACYCDuet-1	Chloramphenicol
pETDuet-1	Carbenicillin

2.2.1.2. Strain (named SS*) obtained after screening different levels of inducer and antibiotics

Due to the instability regarding α-santalene productivities for the standard SS strain (described by colleagues from Delft Advanced Biorenewables (DAB) [29]) and considering the mix of bacterial populations often reported for some bioprocesses using GMOs depending on selection pressure (see chapter 1), an attempt to select a more resistant version to increasing antibiotics and IPTG concentrations was caried out in plates according to table 2. The rationale used here consisted on early exposure of strains to selective stress in plates to evaluate the performance of the biomass resulting from the resistant colonies for α-santalene production cultivated in bioreactors.

Different concentrations of chloramphenicol, carbenicillin and IPTG (Isopropyl β-D-1-thiogalactopyranoside) were added to LB-agar medium in Petri plates. Level one was similar to the batch medium initial concentrations and the next levels (2, 3) consisted of the doubled concentrations from level 1 and 2, respectively (table 2). Colonies able to growth in plates for a specific level were transferred to plates with the next level, then incubated at 30 °C during 48 h (Heraeus instruments). The plating step was carried out at least three times per level before the transfer to higher concentrations.

Table 2. Composition of LB-agar medium per level in Petri plates:

Level	Chloramphenicol	Carbenicillin	IPTG
	$g \cdot L^{-1}$	$g \cdot L^{-1}$	$g \cdot L^{-1}$
1	0.025	0.1	0.24
2	0.050	0.2	0.48
3	0.100	0.4	0.96

2.2.1.3. Pre-culture

The pre-culture preparation was adapted from to the reference article [30] [supporting info, section "Sclareol production in *E. coli*"]. From frozen glycerol (25 % m $\cdot$ v^{-1}) stocks kept at - 80 °C, 400 µL was transferred to 50 mL of LB (Luria-Bertani medium, composition 10 g. kg^{-1} bacto-tryptone, 5 g $\cdot$ kg^{-1} yeast extract and 5 g $\cdot$ kg^{-1} sodium chloride) supplemented with carbenicillin (50 mg $\cdot$ L^{-1}), chloramphenicol (34 mg $\cdot$ L^{-1}) and thiamine (4.5 mg $\cdot$ L^{-1}) in baffled *Erlenmeyer* flasks (250 mL). The first incubation (35 °C and 250 rpm) lasted approximately 5 h, whereafter the required culture volume to reach an initial OD_{600nm} of around 0.2 in pre-culture 2 was transferred to 100 mL of the same fresh medium and incubated under the same conditions for another 4 h in baffled *Erlenmeyer* flasks (500 mL). These flasks were incubated in an orbital shaker (Sartorius Stedim Biotech S.A., France), for approximately 4 h. As soon as the second preculture reached and OD_{600nm} between 2 and 4, it was used for bioreactor inoculation, aiming at an initial OD_{600nm} of around 0.2.

2.2.2. Experimental set up

Aerobic fed-batch experiments were performed in jacketed 2 L reactors (Applikon, Delft, The Netherlands) equipped with a single 6-blade Rushton impeller (diameter 45 mm), controlled by a BIOSTAT® Bplus (Sartorius). Mass flow controllers (Brooks, U.S.A.) were used for aeration rates between 1.2 and 2 $nL \cdot min^{-1}$ (normal liters per minute, ideal gas assumption) Phosphoric acid (3 M) and Ammonium hydroxide/ Sodium hydroxide (6 M/0.4 M) solutions were used for pH control. An aqueous solution 10 % $w \cdot w^{-1}$ of Pluronic® L-81(Sigma-Aldrich) was used as antifoam. Pumps integrated in the controller were used for antifoam, acid and base solutions. A Masterflex peristaltic pump (Cole Parmer, U.S.A) was used for addition of the glycerol solution.

2.2.3. Batch phase

For the batch phase, the vessel with mineral "AM" medium, adapted from the reference article by Schalk [30], was autoclaved at 121°C for 20 minutes after pH probe calibration. Exceptions were the experiments 1 and 2, which batch medium was sterilized by filtration (0.22 μm pore).

Glycerol (30 $g \cdot kg^{-1}$) was used as the carbon source, in combination with other components as 4.2 $g \cdot kg^{-1}$ KH_2PO_4, 11.98 $g \cdot kg^{-1}$ K_2HPO_4, 2 $g \cdot kg^{-1}$ $(NH_4)_2SO_4$, 1.7 $g \cdot kg^{-1}$ citric acid, 8.4 $mg \cdot kg^{-1}$ EDTA. Next, filter-sterilized (0.22 μm) solutions to reach 0.1 $g \cdot kg^{-1}$

carbenicillin, 17 mg $\cdot$ kg^{-1} chloramphenicol, and 4.5 mg $\cdot$ kg^{-1} thiamine$\cdot$HCl were added. 10 mL trace metal solution (composition: 10 g $\cdot$ kg^{-1} Fe$_{(III)}$citrate, 0.25 g $\cdot$ kg^{-1} CoCl$_2$$\cdot$6H$_2$O, 1.5 g $\cdot$ kg^{-1} MnCl$_2$$\cdot$4H$_2$O, 0.118 g $\cdot$ kg^{-1} CuCl$_2$$\cdot$2H$_2$O, 0.3 g $\cdot$ kg^{-1} H$_3$BO$_3$, 0.25 g $\cdot$ kg^{-1} Na$_2$MoO$_4$$\cdot$2H$_2$O, and 1.3 g $\cdot$ kg^{-1} Zn(CHCOO)$_2$$\cdot$2H$_2$O), 1.23 g $\cdot$ kg^{-1} MgSO$_4$$\cdot$7H$_2$O) were added in sterile conditions. A sterile solution of yeast extract (5 g $\cdot$ kg^{-1}) was the last addition, after which sterile water was used to complete 1 kg of medium. Under sterile conditions the vessel was connected to the controller and bottle connections. After dissolved oxygen probe calibration, the temperature and pH were controlled (30 °C and 7.0, adjusted with NaOH 4 M prior to inoculation). The stirrer speed was kept between 1200 - 1250 rpm during the batch phase.

2.2.4. Fed-batch phase

Feed solution (1 kg) was prepared according to the supporting information file in the previously cited article [30], but with lower concentrations of glycerol as compared to this article (between 20 % w$\cdot$w^{-1}and 35 % w$\cdot$w^{-1} depending on the experiment, as shown in table 6). MgSO$_4$$\cdot$7H$_2$O and EDTA concentrations in the feed solution were 24.6 g $\cdot$ kg^{-1} and 26 mg $\cdot$ kg^{-1}, respectively.

Filter sterilized (0.22 µm) antibiotic solutions were added to the feed medium (66.5 mg $\cdot$ L^{-1} carbenicillin and 11.2 mg $\cdot$ L^{-1} chloramphenicol) for experiment 3, in comparable concentrations to those used for Exp 1: 50 mg $\cdot$ L^{-1} carbenicillin and 8.5 mg $\cdot$ L^{-1}

chloramphenicol. Exp 2 on the other hand, was performed in absence of antibiotics in feed medium: the selection pressure decreased more with time, as compared to Exp$_s$ 1 and 3.
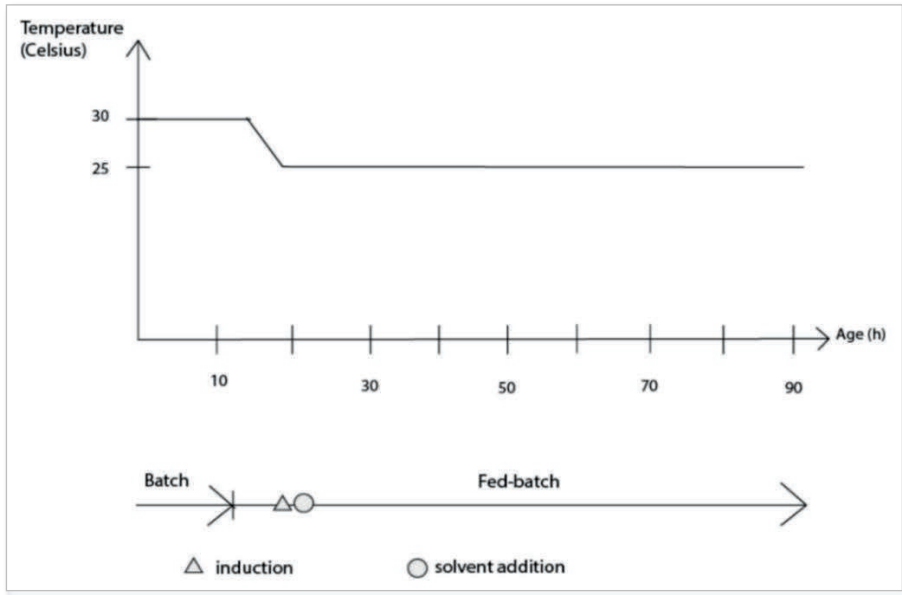

Figure 2. Fed-batch process: general temperature profile versus time performed for the production of santalene.

Prior to the induction step, the temperature was adjusted from 30 °C to 25 °C, method adapted from the reference article [30] and according to the protocol provided by our industrial partner. The temperature decrease step presented in figure 2 was performed from the start of this PhD project, and is justified from the correlation between lower cultivation temperatures and improved recombinant protein quality [31]. After the temperature decrease step, filter

sterilized dodecane (containing the dye Oil red O as 50 μg · g^{-1} organic phase) was used as the organic phase, for *in situ* product recovery.

When OD_{600nm} reached at least 40, filtered IPTG (Isopropyl β-D-1-thiogalactopyranoside) was injected under sterile conditions into the reactor (except for experiment 1, for which IPTG was supplied in feed medium). Volumetric inducer concentrations differed between experiments (figure 10). See table 8 for induction ages.

2.2.5. On-line analyses

The gas stream left the system through a condenser and subsequently passed through an off-gas analyzer (Rosemount NGA-2000, Fisher Rosemount, Germany). O_2 and CO_2 contents (mol·mol^{-1}) were logged through the software MFCS/Win 2.1 software (Sartorius Stedim Biotech S.A., France), which was also used to record the masses of base and feed bottles, using load cells (Mettler Toledo, The Netherlands). Temperature, pH and DOT were monitored with probes (Applikon or Mettler Toledo, The Netherlands).

2.2.6. Off-line analyses

2.2.6.1. Dry mass and optical density for aqueous phase samples:

For dry biomass determinations, 1.5 mL microcentrifuge tubes (in duplicates, previously dried at 24 h at 70 °C), containing 1 mL broth were placed in a centrifuge (Heraeus, Biofuge Pico) at 13000 rpm for 5 minutes and dried for 72 h at 70 °C in an oven (Heraeus instruments) after the supernatant had been disposed. The amount of biomass in the sample was obtained from the mass difference with the pre-weighed empty tube.

To determine the optical density (OD_{600nm}), the absorbance measurements of diluted broth were carried out in a spectrophotometer (Biochrom) at $\lambda = 600$ nm. The quantifications were corrected for the dilution factor between the original and the diluted samples.

2.2.6.1.1. Samples from the two-phase system (in the presence of dodecane): dried mass (DM_{CS}) and optical density ($OD_{600nm\ CS}$):

After the dodecane addition, the tubes for biomass measurement were carefully cleaned after centrifugation to minimize interference of remaining solvent with the dry mass and OD_{600nm} analyses. The centrifugation of 1 mL of broth in 1.5 mL microcentrifuge tubes was performed in the same centrifuge (Heraeus Biofuge Pico)

at 13000 rpm for 5 minutes, followed by the disposal of supernatant and the organic phase removal from the tube surface using cotton swabs. Next, the biomass pellet was re-suspended in distilled water (figure 4) and centrifuged again.

These washing steps were performed until the organic phase was absent, whereafter the microtubes with cell pellets were dried for 72 h at 70 °C in oven (Heraeus instruments). For the tubes that were used for OD_{600nm} measurements the last centrifugation step was omitted, after which the absorbance was read using the spectrophotometer (Biochrom, λ = 600 nm). After cleaning the sample and re-suspending the biomass, the new mass of tube was determined (m_{CS}), to obtain the correction factor (f), for the cleaning step (table 10, appendix B).

2.2.6.2. Viable cell count

Samples (50 μL) from original broth were diluted in 4.95 mL of sterile 0.9 % w·v^{-1} NaCl solution sequentially (four times 10^{-2} diluted, resulting in final dilution of 10^{-8}). The plated volume was 150 μL in duplicates on Petri plates only containing LB medium (5 g · kg^{-1} bacto-tryptone, 10 g · kg^{-1} yeast extract, 10 g · kg^{-1} sodium chloride) with 1.5 % agar, according to the spread-plate method, placed at 30 °C for 48 h in an incubator (Heraeus instruments). The colony-forming units (CFUs) were counted to determine the number of colony-forming units per mL (or CFU · mL^{-1}) for the original sample. Two replicate dilutions of the same factor (usually 10^{-8}) were prepared per sample. Based on

density, and biomass concentration based on dry cell mass, the viable cell count was reported in CFU per g of DCW (dry cell weight).

To estimate the impact of the dilution step on the number of colony-forming units, for some experiments two different dilutions were used. When necessary, 500 µL from tubes (with 10^{-6} or 10^{-8} dilutions) were further diluted in 4.5 mL of sterile saline solution (0.9 % w·v^{-1} NaCl), resulting in dilutions 10^{-7} or 10^{-9}, respectively.

2.2.6.3. Sesquiterpene extraction

Sterile glass tubes were attached to the bioreactor for direct sampling (5 mL approximately) to avoid early phase separation by density differences (multiphasic broth). Tubes with samples were frozen at - 20 °C until the product extraction procedure.

A similar volume of dodecane was added to the broth volume for every sample. Next, the samples in the tubes were mixed with a vortex for 10 seconds and centrifuged at 4000 rpm for 10 minutes, after which the solvent was removed using a glass pipette. Finally, dodecane was again added to the sample tubes, repeating the clarification step, followed by a last solvent removal.

The total mass of the dodecane added to the samples was registered for data processing, so were all the intermediate tube weights relevant for the extraction process. The concentration of product in the solvent was estimated, based on the respective peak areas obtained by gas chromatography (GC) and on previous calibrations of the terpene of interest dissolved in dodecane. The amount of organic phase (g) already present in the sample for ISPR

prior the extraction was also estimated using as reference the concentration (g solvent $\cdot$ kg broth^{-1}) calculated by the mass balance (since the fed-batch operation mode was used, the solvent was diluted in broth with time).

The original amount of terpene in the original sample (mg) was obtained by multiplying the concentration of sesquiterpene measured (mg $\cdot$ g^{-1}) in GC for the total dodecane added (during extraction plus the solvent amount already present in the sample before extraction). This amount of terpene was finally divided by the original mass of sample in the tube, resulting in the product concentration in the frozen sample (g $\cdot$ kg^{-1}).

2.2.6.4. Gas Chromatography for sesquiterpene quantification

A gas chromatography (GC/FID) system with a HP-1 column (Agilent Technologies, Santa Clara, CA, U.S.) length 25 m, film 0.33 µm, and a 0.2 mm internal diameter was used for the quantification of the α-santalene extracted from samples according to section 2.2.6.3 using an Agilent Technologies 6890N Network GC System with a 7683 Series injector. The injection volume of dodecane was 1 µL. The temperatures of the injector, detector and oven (initial) were respectively 230, 250 and 100 °C. Three minutes after injection the temperature of the oven was increased with 20 °C $\cdot$ min^{-1} and after reaching a temperature of 220 °C it was kept constant for 4 minutes. The column flow was 1.7 mL $\cdot$ min^{-1}, with a constant pressure of 234

kPa and a split ratio of 20 (total flow 10 mL · min^{-1}). A retention time of 7.8 min is expected for α-santalene using this method.

2.2.6.5. High Performance Liquid Chromatography (*HPLC*)

For the detection of metabolites in the supernatant, a Refractive Index Detector (Waters 2414) at sensitivity 1024 at 30 °C and a U.V detector (Waters 2489 at 210 nm) were used. The column used was a BioRad HPX-87H 300 * 7.8 mm. at 59 °C, equipped with a guard column (BioRad Cation-H refill cartridge 30* 4.6 mm). Phosphoric acid 1.5 mmol · L^{-1} in Milli-Q water at 70 °C was the eluent; blanket: He. The flow rate of the mobile phase was 0.6 mL · min^{-1} (Waters 515 pump). The injection volume was 10 µL and was performed by a Waters 2707 auto sampler at 15 °C.

2.2.7. Chemicals

α-Santalene (75 % purity) was provided by our industrial partner. Dodecane (BOOM) was used for ISPR. Glycerol (99.5 % m · v^{-1}) from Merck was the substrate.

2.2.8. Growth rate and Herbert-Pirt parameter calculations:

The parameters $M_x(0)$, a and m_s were estimated from the experimental data of total biomass versus time during constant feed fed-batch cultivation, by weighed non-linear regression using the SciPy curve_fit function in python. The applied relation for biomass accumulation versus time for a carbon limited fed-batch cultivation with a constant feed was derived from the Herbert-Pirt equation, wherein substrate consumption for product formation was neglected ($q_s = \alpha \cdot \mu + m_s$) and the growth equation ($dMx/dt = \mu \cdot Mx$). The resulting equation is shown in Appendix B (table 10, equation 11).

2.2.9. Estimation of specific productivities

For the estimation of specific productivities' trends per experiment, the derivative of each fit resulting of product accumulation versus time was divided by the fit of biomass accumulation versus time for same time interval. This modeling was done by using the Matlab software R2019b for fits obtained from Excel.

2.3. Results

Details for all experiments are available in appendix A. Table 5 represents an overview. The total and feed phase ages for samples are listed in tables 6 and 7, while table 8 presents the key steps.

Due to limited time of the experimental phase in this project and limited availability of bench scale bioreactors, it was not possible to perform the fed-batch experiments described here in duplicates. The standard deviations presented (such those for Herbert-Pirt parameters) follow from measurements in multiple samples replicates.

2.3.1. The effect of the induction procedure (pulse wise vs continuous)

Two fed-batch experiments were performed using *E. coli* BL21 (DE3), as provided by our industrial partner (paragraph 2.2.1.1). Here, the standard strain (SS) was tested for continuous induction (experiment 1) in one reactor, while the induction for the other vessel was performed through injection (experiment 2). Similar constant glycerol feed rates were used for both reactors, approximately $3.2 \cdot 10^{-2}$ mol $\cdot$ h^{-1}. The temperature was kept at 25 °C during the entire process, including the initial batch phase, to avoid effects of temperature on the α-santalene formation and specific rates.

For experiment 1, a method of continuous induction was tested to investigate the effect on product accumulation, specific productivity of α-santalene compared to the traditional induction step, usually

performed by injection. The inducer was added under sterile conditions after 18.0 h of fed-batch cultivation to the bottle with the glycerol feed solution (20 % w·w^{-1}) resulting in an IPTG concentration of 5.3 mM in the bottle. Antibiotics were also present in the feed (50.0 mg · L^{-1} carbenicillin and 8.5·mg · L^{-1} chloramphenicol).

In contrast to experiment 1, for experiment 2 the IPTG solution was filter sterilized (0.22 µm pore size) and injected into the reactor after 19.5 h of fed-batch cultivation, starting with a IPTG concentration of 0.1 mM in the broth, (2.4 ·10^{-2} g inducer · kg^{-1} broth). In this experiment, a lower selection pressure for plasmid retention was expected with time, due to the absence of antibiotics in the feed solution (only for Exp 2).

The aim of using a lower batch temperature for Exp$_s$ 1 and 2 was to have an indication of the effect of a 5 °C decrease (which occurs in the regular fed-batch process (figure 2)) over the estimation of specific rates versus time, using as reference the known q$_{max}$ for 30 °C. For these experiments, neither of the conditions described by [32] as likely to interfere on the modeling parameters were changed, thus during the batches performed for experiments 1 and 2, no great variation would be expected for the maximum specific rates. On the other hand, specific rates during fed-batch could be influenced by several factors such as glycerol feed and conversion rate. It is expected that specific rates will decrease with time for a fed-batch designed with constant feed [33]. However, in the case of some experiments where the temperature is decreased during feed phase, such switch could also contribute to a certain extent to the decrease of specific rates versus time.

Figure 3 shows the santalene accumulation versus time for both experiments. The santalene accumulation for Exp 1, carried out with continuous IPTG and antibiotics addition in the feed, was clearly higher as compared to when the antibiotics and IPTG were added at once (Exp 2).
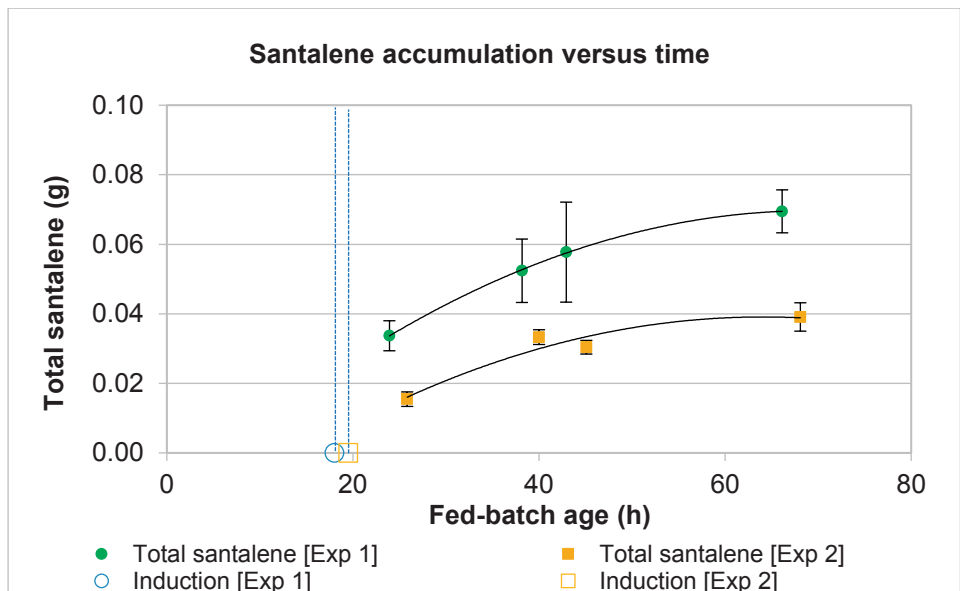

Figure 3. Santalene accumulation versus time for fed-batch cultivations 1 and 2. Vertical bars represent the standard deviations (n = 3). Dashed lines indicate induction steps, per experiment.
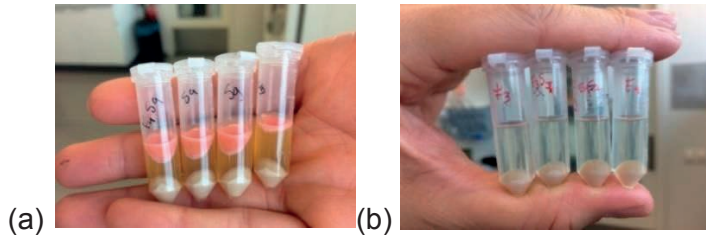
(a)　　　　　　　　　(b)

Figure 4.(a) Tubes after centrifugation; (b) after removal of dodecane.
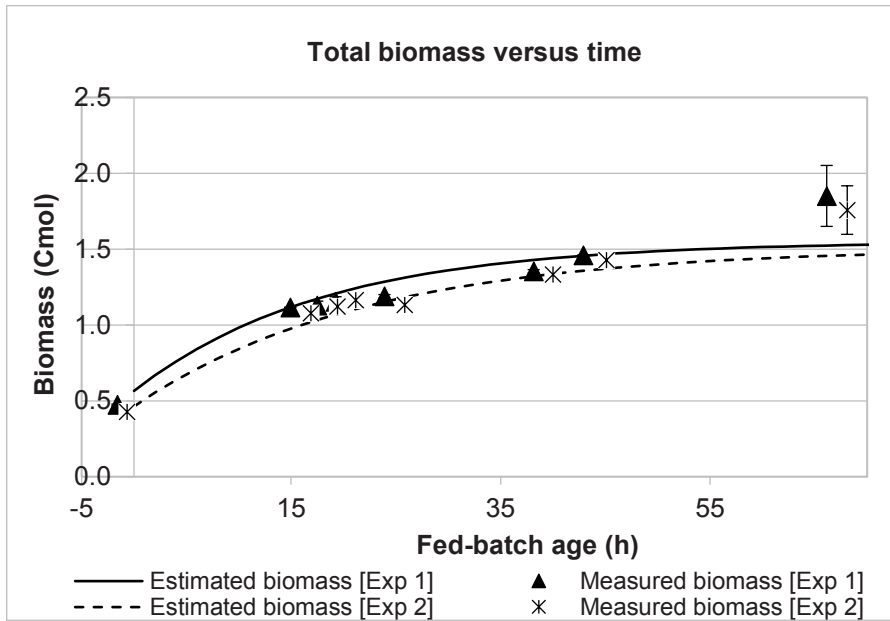
Figure 5. Total biomass versus time during constant feed fed-batch cultivations Exp. 1 and 2. Symbols represent measured values, lines represent model predictions (Appendix B, Eq. 11).

Figure 5 shows the total biomass amount versus time for both reactors. For biomass concentrations based on the dry cell weight (DCW) assay (figures 4a and 4b), most samples presented low standard deviation compared to average, except for the last sample.

As can be seen from figure 5, the biomass accumulation was comparable for both experiments. As seen in figure 9, also the specific productivity (biomass normalized) was similar for most of the samples between Exp 1 and Exp 2. As there is a difference in antibiotic levels between the experiments, no hard conclusions could be drawn on the effect of the induction method.

2.3.2. Experiment using *E. coli* BL21 obtained from screening in plates

Aiming at bioprocess evaluations for the santalene producing strain adapted to higher IPTG and antibiotic concentrations (strain SS*, see materials and methods, section 2.2.1.2), experiment 3 was carried out using this strain.

2.3.2.1. Average inducer concentrations and early induction [experiment 3]

The adapted strain (SS1*) was tested for viable cell count, biomass concentration, α-santalene production. From the cumulative obtained biomass, the values of the HP parameters (a and m_s) were

estimated. The reactor was fed using a concentrated glycerol solution (35 % $w \cdot w^{-1}$) and constant feed rate ($5.7 \cdot 10^{-2}$ mol glycerol $\cdot h^{-1}$) to accomplish a high biomass density.
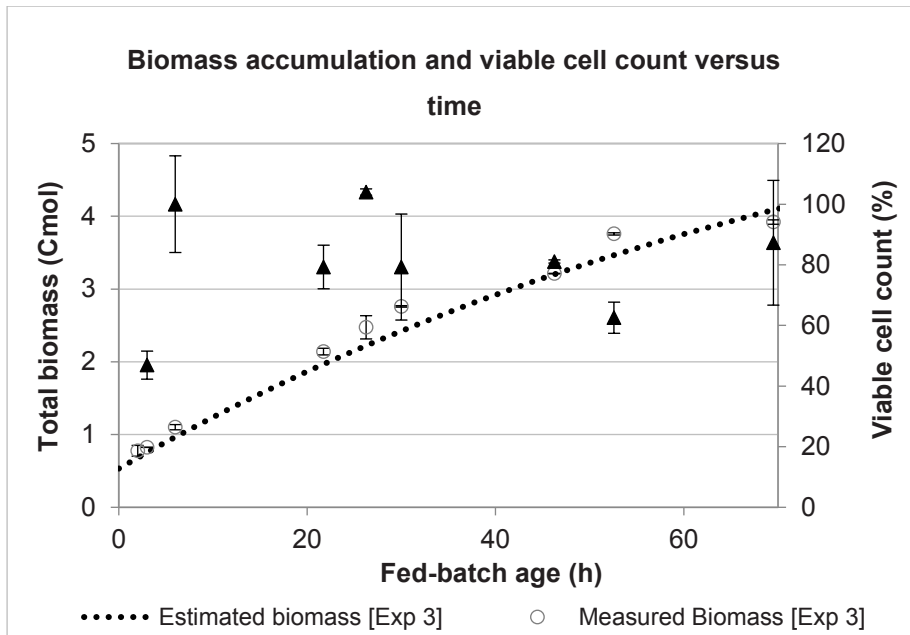

Figure 6. Measured total biomass (open circles) and viable cell count (closed triangles) versus time for constant feed fed-batch cultivation Exp. 3. Bars represent standard deviations for n = 2. The dotted line represents the model prediction for total biomass versus time (Appendix B, Eq. 11).

In this experiment early induction was carried out during the feed phase (table 8), using an intermediate volumetric inducer concentration (figure 10) and continuous selection pressure, as the

antibiotics were supplied in the feed medium (0.067 g·kg^{-1} carbenicillin and 0.011 g·kg^{-1} chloramphenicol). After 5 hours of fed-batch cultivation, the induction was carried out by injecting 10 mL of the freshly prepared IPTG solution (100 mM) under sterile conditions into the bioreactor to reach an initial inducer concentration of approximately 1 mM (see figure 10 for overview between experiments). As represented in figure 2, for this experiment the batch was performed at 30 °C, and the temperature was set to 25 °C during the feed phase, approximately 30 min prior to induction.

After 69.5 hours of fed-batch cultivation, a total biomass of 3.92 Cmol was produced at the end (figure 6), as was calculated from the measured dry cell weight (DCW) and the estimated broth mass versus time. The final biomass for Exp 3 reached approximately 2-fold the amount measured for Exp 1 and 2 (2 Cmol, figure 5).

As compared to the first two experiments, a significantly higher amount of santalene was produced at the end of Exp 3 (69.5 h of fed-batch cultivation), reaching 0.71 g (figure 7). Likewise, high specific productivities were reported for this experiment (figure 9), especially at lower growth rates (figure 8).

Even though a decrease in growth rate could have been expected from the temperature decrease step performed in this experiment, glycerol in excess was not detected in HPLC assays: most of the samples taken in the timepoints after induction had indications of negligible glycerol concentration.
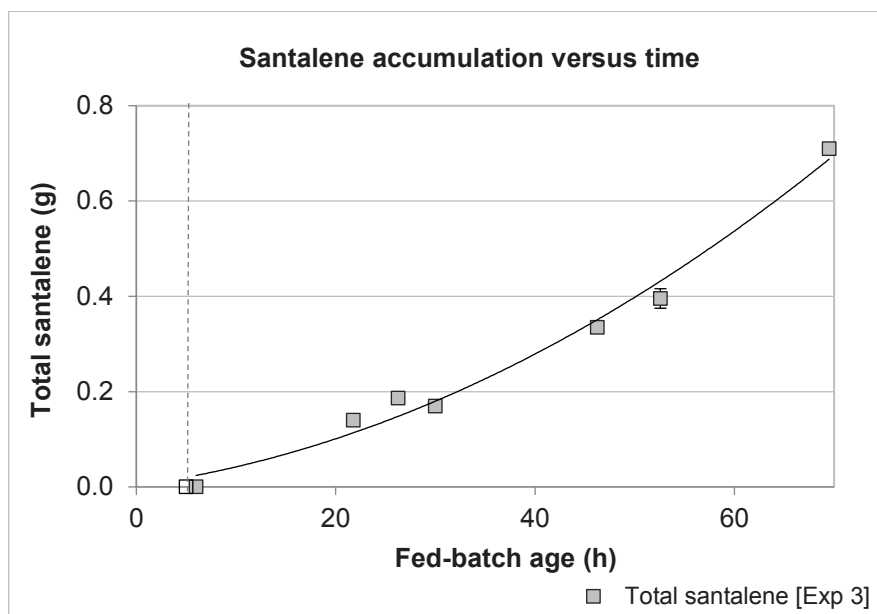
Figure 7. Product accumulation profile for the SS* strain (section 2.2.1.2) versus time, using early (5 h fed-batch age) induction and initial inducer volumetric concentration of approximately 0.9 mM IPTG. Fed-batch Exp 3 (bars represent standard deviations based on injections, n = 2). The vertical dashed line indicates the induction time.

The product extraction assay is described in section 2.2.6.3. Usually, several layers of separations are visible for centrifuged broth. Due to the lower density of dodecane as compared to water, a dark red solvent top is observed if coalescence occurs (not always visible), on a "pink cream layer" (see figure 4a as example), a brown aqueous intermediate layer and finally, the cells sediment at the bottom of the tube. Some other examples of phase separation on broth using this strain are available at [34].

For Exp 3, the precipitation of biomass as pellets after centrifugation and the top gel formation for extraction tubes were visible for all samples. Despite the lack of visual indications of biomass destruction in extraction tubes, it is possible that the tip speed as high as 3.5 m · s^{-1}, reported only for short intervals of this fed-batch, has increased cell lysis, resulting in the observed decreasing viable cell count over time (figure 6). For Exp 1 and Exp 2, unfortunately no viable cell count data are available.
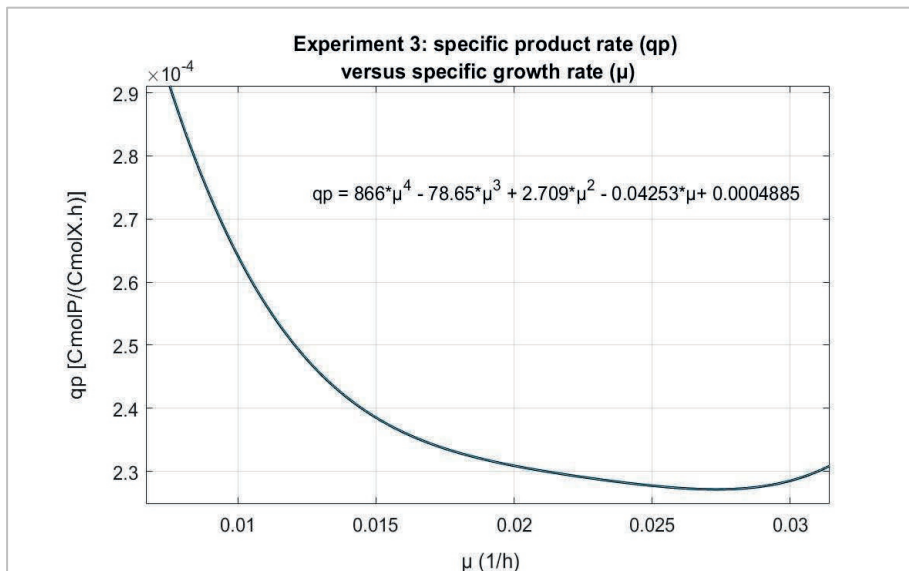
Figure 8. Polynomial fit of specific product formation rate (q_p) versus specific growth rate (μ). For fed-batch experiment 3, the experiment with the highest specific productivities reported in this chapter (induction at 5 h of fed-batch age, with approximately 0.9 mM IPTG).

2.3.2.2. Overview: specific productivities and inducer concentrations.

Inducer concentrations as high as 1 mM were used here for bioprocesses using *Escherichia coli*. For the next pictures, the same symbols/line formats refer to the same experiments. The figures 9 and 10 present, respectively, the specific productivities and estimated volumetric inducer concentrations versus time.

Intermediate specific productivities (figure 9) were reported for Exp_s 1 and 2 ($1.8 \cdot 10^{-4}$ to $1.0 \cdot 10^{-5}$ Cmol P $\cdot$ (Cmol X $\cdot$ h)$^{-1}$ and $1.3\ 10^{-4}$ to $3.0 \cdot 10^{-5}$ Cmol P $\cdot$ (Cmol X $\cdot$ h)$^{-1}$, respectively. The strategy of continuous induction combined with the presence of antibiotics in the feed medium (experiment 1) could have only impacted the specific santalene productivity to a certain extent. The productivities of Exp 1 discretely exceeded those from Exp 2 (which used standard induction and no antibiotics in the feed medium) during the first hours of the fed batch phase (25 h to approximately 40 h). Overall, both experiments (1 and 2) showed a decreasing profile for the specific α-santalene productivity during fed-batch cultivation.
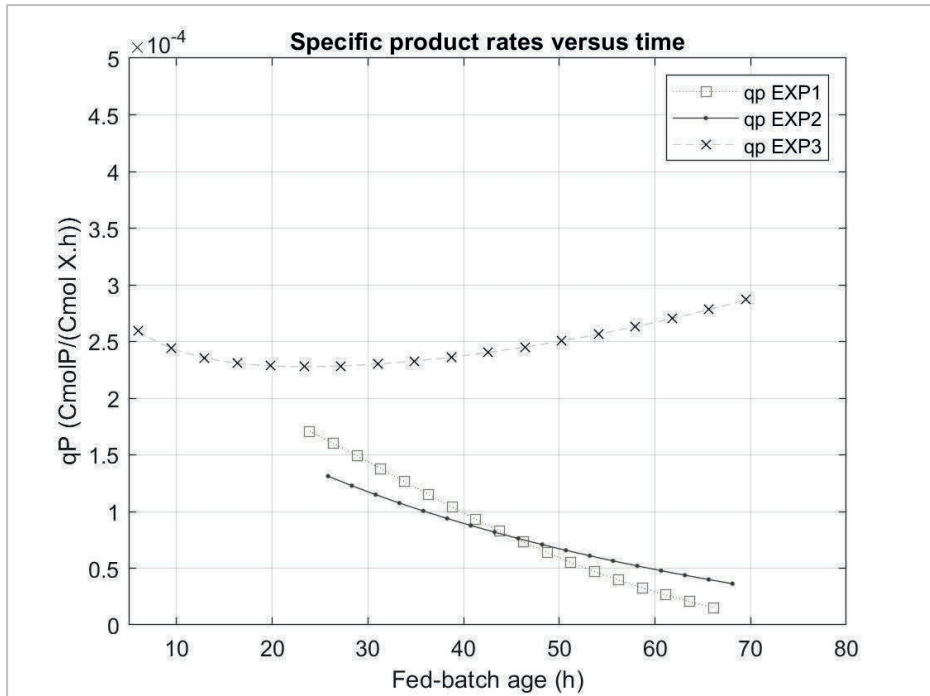
Figure 9. Calculated specific santalene rate formation (q_p) versus time for fed-batch experiments 1, 2, and 3.

It is noteworthy that for experiment 3 the highest specific santalene productivity occurred, increasing from $2.28 \cdot 10^{-4}$ to $2.87 \cdot 10^{-4}$ Cmol $P \cdot$ (Cmol $X \cdot h)^{-1}$. The early induction, combined with maintenance of the selection pressure, seems to represent an attractive strategy. The optical density prior to induction was 55.6 ± 0.1 for experiment 3], which did not differ much as compared to the other experiments in this chapter: OD_{600nm} next to 63. The timing of induction step on the other hand, differed between experiments: 5 h fed-batch (Exp 3) versus others (18.0 h to 19.5 h of fed-batch age). It could have

been that the timing influenced productivity, as reported by [35] for a 3 h difference interval between induction step.
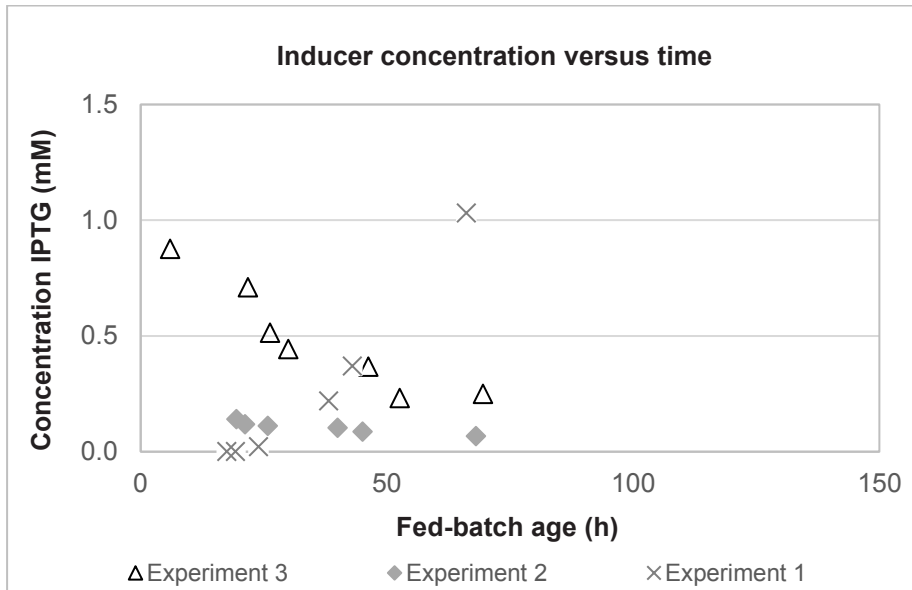

Figure 10. Calculated inducer (IPTG) concentrations versus time for fed-batch experiments 1, 2 and 3.

For experiment 3, characterized for early induction, an inverse relationship between specific productivity (figure 9) and the volumetric inducer concentration (figure 10) occurred. For Exp 3 the inducer concentrations were intermediate, as compared to others shown here. It is therefore, difficult to compare the results of experiments 1 and 2 with the results of experiment 3. Furthermore, experiment 3 differs with respect to the batch phase temperature setpoint (30 °C). The volumetric concentrations shown in figure 10 indicate that in

experiment 1 the IPTG concentration increased during cultivation to reach a value of approximately 1 mM at 66.1 h of fed-batch age. In experiment 3, outstanding for higher santalene productivities as compared to others, the initial IPTG concentration was below 1 mM and decreased during cultivation.

Experiment 2 had initial volumetric inducer concentration according to the recommendations of the product supplier [36] (approximately 0.2 mM) which did not result in high productivity. The decrease of selection pressure also has to be considered, though. The inducer concentrations trends for figure 10 rely on the initial IPTG addition and broth mass balance per experiment, whereby degradation was not taken into account.

2.3.2.3. Estimation of the a and m_s parameters (Herbert-Pirt correlation)

It is possible that the utilization of yeast extract in medium could have influenced the parameter estimations presented in table 3. This is due to variations described in yeast extract composition resulting from subtle differences between the production process used and raw materials [37]. Here, the addition of yeast extract was performed according to our industrial partner protocol [30] and batch number differences between experiments were not tracked, but to the best of our knowledge, the product supplier did not change. On the other hand, the fact that yeast extract was only added during the start of the batch phase indicates that the effects of its utilization over the determination of Herbert - Pirt parameters of feed-phase are most

likely negligible, due to very low remaining concentrations. Table 3 lists the estimated Herbert - Pirt parameters and fed-phase growth rates of experiments 1, 2, and 3:

Table 3. Estimated values of the Herbert-Pirt parameters and calculated initial specific growth rates during the constant-feed fed-batch experiments described in this chapter. The estimated parameter values are shown with their standard errors, which were obtained from the non-linear regression procedure for each individual experiment:

Exp	$M_{x(0)}$* $Cmol_x$	a $\dfrac{mol_{glycerol}}{Cmol_x}$	m_s $\dfrac{mol_{glycerol}}{Cmol_x \cdot h}$	$\mu_{initial}$** $\dfrac{1}{h}$
1	0.57 ± 0.03	-0.37 ± 0.01	-0.0205 ± 0.0002	$9.57 \cdot 10^{-2}$
2	0.46 ± 0.03	-0.47 ± 0.07	-0.0211 ± 0.0014	$1.02 \cdot 10^{-1}$
3	0.53 ± 0.04	-0.70 ± 0.11	-0.008 ± 0.0027	$1.40 \cdot 10^{-1}$

*= estimated initial biomass amount, **= calculated μ (specific growth rate) at the start of the fed-batch phase.

For fed batch processes designed with a constant feed of the growth limiting substrate, it can be derived that the specific growth rate decreases with time [33]. In case of experiment 3, there is also the temperature decrease (from 30 °C to 25 °C) near induction time. A comparison between the average μ_{max} of experiments 1 and 2 and a batch cultivation at 30 °C is listed in table 4 for estimating an effect of the temperature decrease. Maximum growth rates at 25 °C were 32.1

% lower based on dry cell mass and 30.5 % based on OD_{600nm}, as compared to the growth rates of experiment 3, which batch cultivation had been performed at 30 °C. In figure 11, the growth rates estimated versus time are shown.
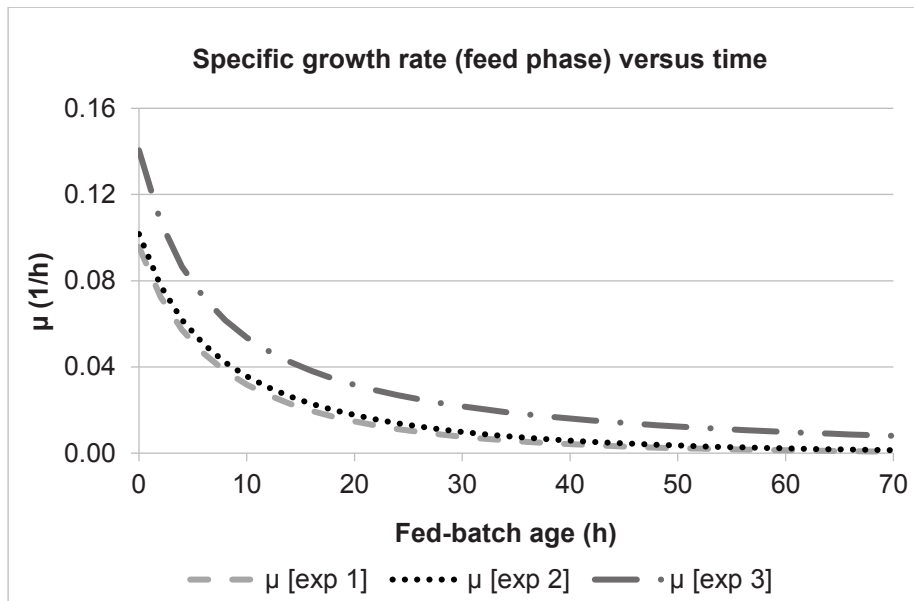

Figure 11. Calculated (Eq 12, Appendix B) specific growth rate (μ) profiles during constant feed fed-batch cultivations 1, 2 and 3.

Table 4. Batch specific rates using the standard α-santalene-producing strain (SS):

Batch	μ_{max}* $\dfrac{1}{h}$	μ_{max}** $\dfrac{1}{h}$	q_{O2}* $\dfrac{mol_{O_2}}{Cmol_x \cdot h}$	q_{CO2}* $\dfrac{mol_{CO_2}}{Cmol_x \cdot h}$	q_S* $\dfrac{mol_{glycerol}}{Cmol_x \cdot h}$
25 °C	0.27±0.003	0.27±0.004	-0.42±0.04	0.27±0.06	-0.17±0.01
30 °C	0.40	0.38	-0.54	0.37	-0.23

*=based on dry cell mass **= based on $OD_{600nm.}$

2.4. Discussion

For the Herbert - Pirt equation, the average value of parameter a (based on experiments 1 and 2 was estimated a = - 0.42 [mol glycerol $\cdot$ (Cmol X)$^{-1}$] ± 0.07 and m_s = - 0.021 [mol glycerol consumed $\cdot$ (h $\cdot$ Cmol X present)$^{-1}$] ± 0.0004. The parameters from for experiment 3 (a = - 0.70 [mol glycerol $\cdot$ (Cmol X)$^{-1}$] ± 0.11 and m_s = -0.008 [mol glycerol consumed $\cdot$ (h $\cdot$ Cmol X present)$^{-1}$] ± 0.0027), contrasted to those related to the previous experiments, thus, not considered for average calculation. These values differ from those determined for growth of *E. coli* MG1655 using glycerol as substrate, namely a = - 0.47 mol S $\cdot$ (Cmol X)$^{-1}$ and m_s = - 0.0066 mol S $\cdot$ (h $\cdot$ Cmol X)$^{-1}$ [27]. For this strain, parameter b [mol glycerol $\cdot$ (mol P)$^{-1}$], related to the product formation was not estimated because the amount of glycerol consumed for santalene production was neglected in our experiments.

As seen in figure 5, significant variation was observed for the estimations of biomass accumulation for Experiments 1 and 2 around 78 h of fed-batch. This occurred due to considerable variations on cell dry weight determination for the last samples, which standard deviations ranged between 15.5 % and 13.6 % of average, respectively. Therefore, to take into consideration standard deviations per sample, all estimations of the Herbert - Pirt parameters were performed using the Solver in Excel for weighed regressions. This included the estimations for experiment 3. As seen from table 3, the resulting values for a and m_s were quite different between the first 2 and the third experiment, however, the average values were close to expectations from literature.

As seen in the results, section Exp 3 was the most successful for santalene production. One of the factors to be considered here is the higher specific growth rate, which resulted from a higher glycerol feed rate, as compared to the other experiments (see table 5 and figure 11). Additionally, antibiotics (66.5 mg $\cdot$ L^{-1} carbenicillin and 11.2 mg $\cdot$ L^{-1} chloramphenicol) were added to the feed solution, keeping the selection pressure that had been initially established by their addition to batch medium (17 mg $\cdot$ L^{-1} carbenicillin and 4.5 mg $\cdot$ L^{-1} chloramphenicol). Another relevant characteristic of this experiment was the volumetric IPTG volumetric concentration which dropped from 0.88 mM to 0.25 mM as the feed medium was added to the broth.

The effects of induction age and inducer concentrations over the protein expression efficiency and growth inhibition have been studied [38-40]. Toxicity and cost represent drawbacks for the utilization of IPTG (chemical inducer) for the production in large scale [41], while lactose is considered an alternative less expensive inducer with low toxicity [42].

For *Escherichia coli*, most chemical inducer concentrations found in literature did not exceed 2 mM. Still, for this IPTG concentration, lysis and lack of growth were described: a deadly effect had been associated to the overexpression of subtilisin, however, decreasing the inducer concentrations to 0.005 - 0.02 mM led to the best results [43]. According to Cho *et al* (1985), the maximum production of β-galactosidase (BG) occurred at 0.1 mM (IPTG) in steady state *E. coli* W3110 cells. Negligible β-galactosidase expression occurred for IPTG titers as low as 0.01 mM. For inducer

concentrations higher than 1 mM, the protein activity per cell had inferior performance, even lower for testing 10 mM [44].

In SDS-PAGE, 1.0 mM IPTG resulted in the best aminopeptidase (DmpA) expression, as compared to lower inducer concentrations (up to 0.5 mM) tested for *E. coli* BL21(DE3). A 3.42-fold higher aminopeptidase (DmpA) production rate was reported after 5 h induction at 1.0 mM, as compared to using 0.5 mM IPTG for induction [45]. A recombinant *Escherichia coli* BL21 (DE3) was used for the expression of amidase, remarkable for its thermostability properties. For the range tested (0.04 to 1 mM IPTG in batch operational mode), the concentration for which the maximum specific activity of amidase occurred was 0.4 mM [35].

The low santalene accumulation seen in figure 3 for Exp 2 could be related to a decrease of selection pressure in broth with time, since no antibiotics were used in the feed solution. This will be discussed in details in chapter 3, where a strategy involving antibiotics addition and product accumulation was tested. To the best of our knowledge, other genes encoding enzymes to compete for the general precursor FPP (farnesyl-diphosphate) and hinder product formation were not present. Literature describes other terpenes resulting from the santalene synthase activity. The enzyme from *Clausena lansium* (wampee), expressed in yeasts, led to the co-production of trans-α-bergamotene as a secondary product, as 12 % of all α-santalene [21].

2.5. Conclusion

Herbert-Pirt parameters estimated during the mentioned experiments presented similarity with literature for the bacterium *Escherichia coli* grown on glycerol. Those parameters could be used for Black-Box modeling. A 31.9 % lower batch specific growth rate was reported for Exp_s 1 and 2, which were performed at a lower temperature (25 °C, instead of 30 °C). Thus, the decreasing profile of specific rates versus time, typical of constant fed-batch fermentations, was likely more intense due to the temperature decrease.

Experiment 3, which used the same strain isolated in plates (referred to as SS*, as explained in table 2) had the best results of this chapter, either for product concentration or for specific productivity. However, the stress in plates described for paragraph 2.2.1.2 does not seem to be the main key factor here. Instead, a combination of intermediate inducer specific range, selection pressure in feed medium and early induction used in Exp 3 suggested improvements towards specific productivity.

Other experiments described here barely exceeded 10 % of the santalene accumulation for Exp 3 (nearly 0.7 g). For Exp 1, the strategy using continuous induction combined to antibiotics in feed had discrete impact on the sesquiterpene specific productivity: only around 43 - 45 h of fed-batch cultivation, as compared to Exp 2 (inducer injected in sterile conditions and lower concentrations through the septum).

Process steps likely to influence strain performance, such induction age and IPTG concentrations were studied here. However,

since the main goal of this chapter was to obtain Herbet -Pirt parameters, IPTG concentrations here were not studied in a systematic way to allow clear conclusions regarding the effect of such parameters over santalene productivity.

This chapter is the first step to understand the challenges for the biotechnological production of α-santalene using the available strain. Yet, the aspects discussed here do not address other process factors related to this strain. Metabolic burden and loss of selective pressure in broth, key aspect for the bioprocess yield, will be discussed in chapter 3.

2.6. Acknowledgements

2.7. Symbols

A_{600} = absorbance at λ=600 nm

a = stoichiometric parameter Herbert - Pirt [mol glycerol · Cmol X^{-1}]

b = stoichiometric parameter Herbert - Pirt [mol glycerol · mol P^{-1}]

bp = by-products

DCW = dry cell weight

C_s = substrate concentration [mol · m^{-3}]

CFU = colony-forming units

f = correction factor (complex samples)

Fs = feed rate [mol · h^{-1}]

GMOs = genetically modified organisms.

Exp or Exp_s = experiment or experiments (plural), respectively.

IPTG = isopropyl β-D-1-thiogalactopyranoside

ISPR = *in situ* product recovery

K_s = affinity constant for substrate [mol · m^{-3}]

LB = Luria-Bertani medium

m_{CS} = mass of tube with cleaned sample

m_{DS} = mass of tube with dry sample after 72 h at 70 °C

m_{DEP} = mass of dodecane added during extraction protocol [g]

m_{ET} = mass of empty tube [g]

m_{FS} = mass of frozen sample [g]

m_{HB} = mass of product in frozen sample with broth [mg]

m_{HES} = mass of product in dodecane extraction sample to be analyzed in GC [g]

m_s = [mol S consumed · (h · Cmol X present in the vessel)$^{-1}$]

m_{SD} = mass of sample diluted [g]

m_{STBD} = mass of sample to be diluted in the bottle [g]

m_{TS} = mass of tube with original sample [g]

m_{TOS} = mass of tube with original sample [g]

m_{TSD1} = mass of tube with sample and dodecane (first addition) [g]

m_{TSDR1} = mass of tube with sample and dodecane after first removal [g]

m_{TSD2} = mass of tube with sample and dodecane (second addition) [g]

M or m = mass [g or kg]

N_x = total moles biomass [mol]

OD_{600nm} = optical density (λ = 600 nm)

q_s = substrate specific rate [mol glycerol $\cdot$ (Cmol X $\cdot$ h)$^{-1}$]

q_p = product specific rate [mol P $\cdot$ (Cmol X $\cdot$ h)$^{-1}$]

R^2 = correlation coefficient

w = weight [g]

X = biomass

Greek

μ = biomass specific growth rate [Cmol X produced $\cdot$ (Cmol X present $\cdot$ h)$^{-1}$]

2.8. Appendix

2.8.1. Appendix A. Experiments: overview and identification

Table 5 presents an overview for experiments. Tables 6 and 7 list total and fed-batch cultivation ages for samples, respectively. Main steps per experiment are shown in table 8.

Table 5. Overview for experiments (all in 2 L bioreactors):

Exp	*PV	$v_{tip\ max.}$	Glyc. in feed	Air flow	Glyc. rate· $\cdot 10^2$	Max. conc. biomass	Max. product conc.$\cdot 10^2$	**AF
	$\dfrac{kW}{m^3}$	$\dfrac{m}{s}$	%	$\dfrac{nL}{min}$	$\dfrac{mol}{h}$	$\dfrac{g}{kg}$	$\dfrac{g}{kg}$	%
1	4.2	3.02	20	1.5	3.17	23.5 ± 3.5	3.9 ± 0.4	0.07
2	4.2	3.02	20	1.5	3.18	22.2 ± 3.0	2.7 ± 0.3	0.31
3	4.3	3.62	35	2.0	5.70	43.1 ±0.4	39.0 ± 1.0	0.04

* Average vol. power, calculated according to [46]/ ** AF = final concentration of anti-foam. Glyc: glycerol.

$v_{tip\ max:}$ maximum impeller tip speed.

Table 6. Sample total ages (h), per experiment:

Exp	2	3	4	5	6	7	8	9	10	11
1	21.1	37.6	40.2	41.9	46.6	60.8	65.6	88.8	-	-
2	20.1	37.6	40.1	41.9	46.6	60.7	65.8	88.8	-	-
3	13.7	16.8	17.8	20.8	36.6	41.1	44.8	61.1	67.4	84

Table 7. Fed-batch ages (h) for samples:

Exp	2	3	4	5	6	7	8	9	10	11
1	-1.6	14.9	17.5	19.2	23.9	38.2	42.9	66.1	-	-
2	-0.7	16.8	19.4	21.2	25.8	40.0	45.1	68.1	-	-
3	-1.1	2.0	3.0	6.0	21.7	26.2	30.0	46.2	52.6	69.5

Table 8. Key steps, per experiment. Standard santalene strain indicated as SS:

Exp	Strain	TUD.DIRC Code	Feed (h) Total age, since inoculation	Induction Fed-batch age	Dodecane Fed-batch age	End Fed-batch age
			h	h	h	h
1	SS	17.05.30	22.7	18.0	19.7	66.1
2	SS	17.05.30	20.7	19.5	21.2	68.1
3	SS*	16.12.05	14.8	5.0	6.0	69.5

Table 9. Remarks for off-gas data (or dissolved oxygen tension), per experiment:

Exp	Remark
1	Off-gas data was not available during the first 12 h, due to a failure in the channel of the gas analyzer.
2	Oscillations in both carbon dioxide and dissolved oxygen concentration profiles occurred.
3	Unfortunately, technical issues with the gas analyzer were detected for Exp 3. A strong oscillation occurred after 40 h for dissolved oxygen tension and carbon dioxide.

2.8.2. Appendix B. Calculations

Table 10. Calculations for off-line data (Chapters 2 to 4):

Description	Equations
	Eq. 1
CFU in sample	CFU·mL^{-1} = CFU in plates·dilution factor/plated volume (mL)
	Eq. 2 -5
Product calculations	$m_{FS} = m_{TS} - m_{ET}$ $m_{DEP} = (m_{TSD1} - m_{TS}) + (m_{TSD2} - m_{TSDR1})$ $[S_{QES}] * (m_{DS} + m_{DEP}) = m_{HES}$ $m_{HES} / m_{FS} = m_{HB}$
	Eq. 6
Dry Cell Weight (aqueous and bi-phasic)	$[(m_{DS} - m_{ET}) / (m_{TOS} - m_{ET})]·1000$
	Eq. 7
OD$_{600nm\ (aqueous)}$	$[(m_{SD} / m_{STBD}) ·A_{600}]$
	Eq. 8
OD$_{600nm\ (biphasic)}$	$[(m_{SD} / m_{STBD}) ·A_{600}] * f$
	Eq. 9
Correction for cleaning step (for OD$_{600nm\ CS}$)	$f = [(m_{CS} - m_{ET}) / (m_{TOS} - m_{ET})]$
	Eq. 10
Herbert Pirt	$q_s = \alpha.\mu + b.q_p + m_s$
	Eq. 11

Total biomass (constant feed)	$M_{x(t)} = \left(M_{x0} + \dfrac{F_s}{m_s}\right) \cdot e^{-\frac{m_s}{a} \cdot t} - \dfrac{F_s}{m_s}$
	Eq. 12
µ= Mx/ (dMx/dt)	$\dfrac{dM_{x(t)}}{dt} = -\dfrac{m_s}{a} \cdot \left(M_{x(t)} + \dfrac{F_s}{m_s}\right)$
	Eq. 13
Substrate uptake	$q_s = q_{s\ max} \cdot (C_s \cdot (K_s + C_S)^{-1})$

2.8.3. Appendix C. List of correlations used for data processing (chapters 2 to 4)

Table 11. On-line data processing calculations (Chapters 2 to 4):

	Eq.14
$$F_{g,in}\left[\frac{mol}{h}\right] = F_{g,in}\left[\frac{nL}{min}\right] \cdot \frac{1}{1000}\left[\frac{m^3}{nL}\right] \cdot \frac{1}{Vm}\left[\frac{1}{\frac{mol}{nm^3}}\right] \cdot 60\left[\frac{min}{h}\right]$$	
	Eq. 15
$$\text{Corr. factor} = \frac{xo_{2,in} \cdot 100}{PA_{O_2 \text{ value}(\%)}}$$	
	Eq. 16
$$x_{O_2,\text{ out}} = \frac{\text{Offgas}_{O_2,\text{value}(\%)}}{100} \cdot \text{Corr.factor}$$	
	Eq. 17
$$x_{CO_2,\text{ out}} = \frac{\text{Offgas}_{CO_2,\text{value}(\%)}}{100} \cdot \text{Corr.factor}$$	
	Eq. 18
$$F_{g,out}\left[\frac{mol}{h}\right] = F_{g,in} \cdot \frac{x_{N_2,in}}{1 - x_{O_2,out} - x_{CO_2,out}}$$	
	Eq. 19
$$R_{O_2}(t_i)\left[\frac{mol}{h}\right] = F_{g,out}(t_i) \cdot x_{O_2,out}(t_i) - F_{g,in}(t_i) \cdot x_{O_2,in}(t_i)$$	
	Eq. 20
$$R_{CO_2}(t_i)\left[\frac{mol}{h}\right] = F_{g,out}(t_i) \cdot x_{CO_2,out}(t_i) - F_{g,in}(t_i) \cdot x_{CO_2,in}(t_i)$$	
	Eq. 21
$$N_{O_2}(t_i)[mol] = R_{O_2}(t_i)\left[\frac{mol}{h}\right] \cdot (t_i - t_{i-1})[h] + N_{O_2}(t_{i-1})[mol]$$	
	Eq. 22
$$M_{O_2}(t_i)[kg] = N_{O_2}(t_i)[mol] \cdot MW_{O_2}\left[\frac{g}{mol}\right] \cdot \frac{1}{1000}\left[\frac{kg}{g}\right]$$	

	Eq. 23

$$R_{evap}^{(4°C)} = \frac{F_{g,out} \cdot P_v^{(4°C,1bar)}}{P_{atm}}$$

	Eq. 24

$$M_{evap}(t_i)[kg] = R_{evap}^{(7°C)}(t_i)[mol] \cdot MW_{H_2O}\left[\frac{g}{mol}\right] \cdot \frac{1}{1000}\left[\frac{kg}{g}\right]$$

	Eq. 25

$$M_{broth}^{total} = M_{feed} + M_{base} + M_{acid} + M_{AF} + M_{O_2} + M_{additions} - M_{CO_2} - M_{samples} - M_{evap}$$

	Eq. 26

$$N_{gly}^{batch\ med.}[Cmol] = M_{gly}^{batch\ med.}[kg] \cdot 1000\left[\frac{g}{kg}\right] \cdot \frac{1}{MW_{gly}} \cdot 3\left[\frac{Cmol}{mol_{gly}}\right]$$

	Eq. 27

$$M_x^{total}[kg] = M_{broth}^{total}[kg] \cdot DCW\left[\frac{g}{kg}\right] \cdot \frac{1}{1000}\left[\frac{kg}{g}\right] + M_x^{sample,cumm}[kg]$$

	Eq. 28

$$N_x^{total}[Cmol] = M_x^{total}[kg] \cdot 1000\left[\frac{g}{kg}\right] \cdot MW_x\left[\frac{Cmol}{g}\right]$$

	Eq. 29

$$M_{santalene}^{total}[g] = \frac{M_{broth}^{total}[kg] \cdot C_{product}^{broth}\left[\frac{mg}{g_{broth}}\right] \cdot 1000\left[\frac{g_{broth}}{kg}\right] + M_{product}^{sample,cumm}[mg]}{1000\left[\frac{mg}{g}\right]}$$

	Eq. 30

$$N_{product}^{total}[Cmol] = M_{product}^{total}[g] \cdot MW_{product}\left[\frac{mol}{g}\right] \cdot 15\left[\frac{Cmol}{mol}\right]$$

	Eq. 31

$$Carbon_{in}[Cmol] = N_{gly}^{batch\ med.}[Cmol] + N_{gly}^{feed}[Cmol]$$

	Eq. 32

$$Carbon_{out}[Cmol] = N_x^{total}[Cmol] + N_{CO_2}[Cmol] + N_{product}^{total}[Cmol] + N_{product}^{residual}[Cmol]$$

	Eq. 33

$$Carbon\ balance\ [Cmol] = Carbon_{in} - Carbon_{out}$$

	Eq. 34

$$Carbon\ Gap\ (\%) = \frac{Carbon_{in} - Carbon_{out}}{Carbon_{in}} \cdot 100$$

	Eq. 35

$$M_x(t) = M_{x0} \cdot e^{\mu \cdot t} [\text{Cmol}]$$

Eq. 36

$$\frac{dM_{O_2}^{(L)}}{dt} = OUR - OTR, \text{ and } \left(\frac{dM_{O_2}^{(L)}}{dt} \approx 0; \ OTR = \frac{dM_{O_2}^{(G)}}{dt}; \ OUR = q_{O_2} \cdot M_x \right)$$

Eq. 37

$$\frac{dM_{O_2}^{(G)}}{dt} = q_{O_2} \cdot M_x$$

Eq. 38

$$q_{O_2} = \mu \cdot \frac{M_{O_2}(t_{end}) - M_{O_2}(0)}{M_x(t_{end}) - M_{x_0}} \left[\frac{mol_{CO_2}}{Cmol \cdot h} \right]$$

Eq. 39

$$q_{CO_2} = \mu \cdot \frac{M_{CO_2}(t_{end}) - M_{CO_2}(0)}{M_x(t_{end}) - M_{x_0}} \left[\frac{mol_{O_2}}{Cmol \cdot h} \right]$$

Eq. 40

$$Y_{XS}^{batch} = \frac{Substrate_{consumed}\,[mol]}{Biomass_{produced}[Cmol]} = \frac{M_s(t_0) - M_s(t_{end})}{M_x(t_{end}) - M_{X_0}} = \frac{q_s}{\mu} \left[\frac{mol_s}{Cmol} \right]$$

Eq. 41

$$Y_{XO}^{batch} = \frac{Oxygen_{consumed}\,[mol]}{Biomass_{produced}[Cmol]} = \frac{M_{O_2}(t_{end}) - M_{O_2}(t_0)}{M_x(t_{end}) - M_{X_0}} = \frac{q_{O_2}}{\mu} \left[\frac{mol_{O_2}}{Cmol} \right]$$

Eq. 42

$$Y_{XC}^{batch} = \frac{CO_{2,produced}\,[mol]}{Biomass_{produced}[Cmol]} = \frac{M_{CO_2}(t_{end}) - M_{CO_2}(t_0)}{M_x(t_{end}) - M_{X_0}} = \frac{q_{CO_2}}{\mu} \left[\frac{mol_{CO_2}}{Cmol} \right]$$

Eq. 43

$$\text{Specific Productivity} \left[\frac{mg_{product}}{g_{x_{act}} \cdot h} \right] = \frac{M_{product}^{total}[g]}{M_x^{total}[g]} \cdot 1000 \left[\frac{mg}{g} \right]$$

Eq. 44

$$R_{NH_4^+} \left[\frac{mol}{h} \right] = -SLOPE \left(\frac{M_{NH_4OH}[kg]}{total.age[h]} \right) \cdot C_{base} \left[\frac{mol}{kg_{solution}} \right]$$

Eq. 45

$$N_{NH_4^+}(t_i)[mol] = N_{NH_4^+}(t_{i-1})[mol] + R_{NH_4^+}(t_i) \left[\frac{mol}{h} \right] \cdot (t_i - t_{i-1})[h]$$

Eq. 46

$$R_S \left[\frac{mol}{h} \right] = -SLOPE \left(\frac{M_{feed\ med.}[kg]}{total.age[h]} \right) \cdot C_{gly}^{feed} \left[\frac{kg_{gly}}{kg_{feed}} \right] \cdot 1000 \left[\frac{g}{kg_{gly}} \right] \cdot \frac{1}{MW_{gly}} \left[\frac{mol}{g} \right]$$

Eq. 47

$$R_x \left[\frac{mol}{g}\right] = - \frac{R_{NH_4^+}\left[\frac{mol}{h}\right]}{0.2}$$

	Eq. 48

$$N_x(t_i)[mol] = N_x(t_{i-1})[mol] + R_x(t_i)\left[\frac{mol}{h}\right]\cdot(t_i-t_{i-1})[h]$$

	Eq. 49

$$N_x\ diff[mol] = N_x(t_i)[mol] - N_x^{samples}(t_i)[mol]$$

	Eq. 50

$$q_i\left[\frac{mol_i}{Cmol\cdot h}\right] = \frac{R_x\left[\frac{mol_i}{h}\right]}{N_x[cmol]}$$

	Eq. 51

$$\mu\left[\frac{1}{h}\right] = \frac{R_x\left[\frac{Cmol}{h}\right]}{N_x[cmol]}$$

2.9. References

1.   Schempp, F.M., et al., *Microbial Cell Factories for the Production of Terpenoid Flavor and Fragrance Compounds.* Journal of Agricultural and Food Chemistry, 2018. **66**(10): p. 2247-2258.

2.   Sell, C., *Chemistry of Essential Oils*, in *Handbook of Essential Oils*. 2009, CRC Press. p. 121-150.

3.   Franz, C. and J. Novak, *Sources of Essential Oils*, in *Handbook of Essential Oils*. 2009, CRC Press. p. 39-81.

4.   Surburg, H. and J. Panten, *Common Fragrance and Flavor Materials: Preparation, Properties and Uses*. 2016: Wiley-VCH Verlag GmbH & Co. KGaA.

5.   Isobionics. *Sandalwood oil* [cited 2019 13-04-19]; Available from: http://www.isobionics.com/index-Sandalwood%20Oil.html.

6.   Berger, R.G., *Biotechnology of flavours—the next generation.* Biotechnology Letters, 2009. **31**(11): p. 1651-1659.

7.   Diaz-Chavez, M.L., et al., *Biosynthesis of Sandalwood Oil: Santalum album CYP76F cytochromes P450 produce santalols and bergamotol.* PloS one, 2013. **8**(9): p. 1-11.

8.   *Natural Raw Materials in the Flavor and Fragrance Industry*, in *Common Fragrance and Flavor Materials*, H. Surburg and J. Panten, Editors. 2016, Wiley-VCH Verlag GmbH & Co. KGaA. p. 193-264.

9.   Adams, D.R., Bhatnagar, S.P., Cookson, R.C., *Sesquiterpenes*

of Santalum album and Santalum spicatum. Phytochemistry, 1975. **14**(5/6): p. 1459-1460.

10. Wang, C. and S.-W. Kim, *Shaking up ancient scents: Insights into santalol synthesis in engineered Escherichia coli.* Process Biochemistry, 2015. **50**(8): p. 1177-1183.

11. Schalk, M., *Method for producing beta-santalene*, P.C. Treaty, Editor. 2010, Firmenich

12. Schalk, M., *Method for producing alpha-santalene* U.S.P.A. Publication, Editor. 2011: U.S.A. p. 37.

13. Welford, S.H., P. . *Evolva H118 results - Commercialisation on track*. 2018   [cited 2019 13-04-2019]; Available from: https://www.evolva.com/wp-content/uploads/2018/08/Edison-EVE-14Aug2018.pdf.

14. Howes, M.-J.R., M.S.J. Simmonds, and G.C. Kite, *Evaluation of the quality of sandalwood essential oils by gas chromatography–mass spectrometry.* Journal of Chromatography A, 2004. **1028**(2): p. 307-312.

15. Burdock, G.A., *Fenaroli's Handbook of Flavor Ingredients*. 2016: CRC Press.

16. Srivastava, P.L., et al., *Functional Characterization of Novel Sesquiterpene Synthases from Indian Sandalwood, Santalum album.* Scientific reports, 2015. **5**(10095): p. 1-12.

17. Jones, C.G., et al., *Quantitative co-occurrence of sesquiterpenes; a tool for elucidating their biosynthesis in Indian sandalwood, Santalum album.* Phytochemistry, 2006. **67**(22): p. 2463-2468.

18. Misra, B.B. and S. Dey, *Evaluation of in vivo anti-*

hyperglycemic and antioxidant potentials of α-santalol and sandalwood oil. Phytomedicine, 2013. **20**(5): p. 409-416.

19. Bommareddy, A., et al., *α-Santalol, a derivative of sandalwood oil, induces apoptosis in human prostate cancer cells by causing caspase-3 activation.* Phytomedicine, 2012. **19**(8): p. 804-811.

20. Jiang, M., G. Stephanopoulos, and B.A. Pfeifer, *Toward biosynthetic design and implementation of Escherichia coli-derived paclitaxel and other heterologous polyisoprene compounds.* Applied and environmental microbiology, 2012. **78**(8): p. 2497-2504.

21. Scalcinati, G., et al., *Dynamic control of gene expression in Saccharomyces cerevisiae engineered for the production of plant sesquitepene α-santalene in a fed-batch mode.* Metabolic Engineering, 2012. **14**(2): p. 91-103.

22. Scalcinati, G., et al., *Combined metabolic engineering of precursor and co-factor supply to increase α-santalene production by Saccharomyces cerevisiae.* Microbial Cell Factories, 2012. **11**(1): p. 1-16.

23. Laane, C., et al., *Rules for optimization of biocatalysis in organic solvents.* Biotechnology and Bioengineering, 1987. **30**(1): p. 81-87.

24. Chen, Y., et al., *Establishing a platform cell factory through engineering of yeast acetyl-CoA metabolism.* Metabolic Engineering, 2013. **15**: p. 48-54.

25. Tippmann, S., et al., *Production of farnesene and santalene by Saccharomyces cerevisiae using fed-batch cultivations with*

RQ-controlled feed. Biotechnology and Bioengineering, 2016.
113(1): p. 72-81.

26. Heijnen, J.J., *Black box kinetics model of microorganisms*, in *Metabolic Engineering (LB2771). Lecture notes*. 2012, Technische Universiteit Delft p. 1-50.

27. Taymaz-Nikerel, H., et al., *Genome-derived minimal metabolic models for Escherichia coli MG1655 with estimated in vivo respiratory ATP stoichiometry.* Biotechnology and Bioengineering, 2010. **107**(2): p. 369-381.

28. Wang, C., et al., *Metabolic engineering and synthetic biology approaches driving isoprenoid production in Escherichia coli.* Bioresource Technology, 2017. **241**: p. 430-438.

29. © DAB.bio, I. *FAST™ (Fermentation Accelerated by Separation Technology)*. 2024 Access date 21-03-2024]; Available from: https://dab.bio/technology.

30. Schalk, M., et al., *Toward a Biosynthetic Route to Sclareol and Amber Odorants.* Journal of the American Chemical Society, 2012. **134**(46): p. 18900-18903.

31. Schein, C.H. and M.H.M. Noteborn, *Formation of Soluble Recombinant Proteins in Escherichia Coli is Favored by Lower Growth Temperature.* Bio/Technology, 1988. **6**(3): p. 291-294.

32. Heijnen, J.J., *A thermodynamic approach to predict Black Box model parameters for microbial growth and product formation*, in *Fermentation Technology*. 2012, Delft University of Technology: Delft. p. 1-46.

33. Heijnen, J.J., *Design of fed batch fermentation processes*, in *Fermentation Technology & Environmental Biotechnology*

(LM3741). Lecture notes. 2012, Technische Universiteit Delft. p. 1-28.

34. Llenas, C.P., *Towards Integrated Production and Recovery of Sesquiterpenes: Impact of Fermentation Strategy*, in *Biotechnology.* 2017, Delft University of Technology: Delft. p. 112.

35. Olaofe, O.A., et al., *Improving the production of a thermostable amidase through optimising IPTG induction in a highly dense culture of recombinant Escherichia coli.* Biochemical Engineering Journal, 2010. **52**(1): p. 19-24.

36. Sigma-Aldrich. *IPTG (Isopropyl β-D-thiogalactoside)*. 29-04-2019]; Available from: https://www.sigmaaldrich.com/catalog/product/sial/i6758?lang=en&region=NL.

37. Tao, Z., et al., *Yeast Extract: Characteristics, Production, Applications and Future Perspectives.* J Microbiol Biotechnol, 2023. **33**(2): p. 151-166.

38. Hannig, G. and S.C. Makrides, *Strategies for optimizing heterologous protein expression in Escherichia coli.* Trends in Biotechnology, 1998. **16**(2): p. 54-60.

39. Lecina, M., et al., *IPTG limitation avoids metabolic burden and acetic acid accumulation in induced fed-batch cultures of Escherichia coli M15 under glucose limiting conditions.* Biochemical Engineering Journal, 2013. **70**: p. 78-83.

40. Schein, C.H., *Soluble protein expression in bacteria*, in *Upstream Industrial Biotechnology*, M.C. Flickinger, Editor. 2013, John Wiley & Sons Incorporated: Hoboken, New Jersey.

41.   Khani, M.-H. and M. Bagheri, *Skimmed milk as an alternative for IPTG in induction of recombinant protein expression.* Protein Expression and Purification, 2020. **170**: p. 105593.

42.   Gombert, A.K. and B.V. Kilikian, *Recombinant gene expression in Escherichia coli cultivation using lactose as inducer.* Journal of Biotechnology, 1998. **60**(1): p. 47-54.

43.   Bentley, W.E. and D.S. Kompala, *Optimal Induction of Protein Synthesis in Recombinant Bacterial Culturesa.* Annals of the New York Academy of Sciences, 1990. **589**(1): p. 121-138.

44.   Cho, S., et al., *Effect of iso-propyl-thio-β-D-galactoside concentration on the level of lac-operon induction in steady state Escherichia coli.* Biochemical and Biophysical Research Communications, 1985. **128**(3): p. 1268-1273.

45.   Heyland, J., L.M. Blank, and A. Schmid, *Quantification of metabolic limitations during recombinant protein production in Escherichia coli.* Journal of Biotechnology, 2011. **155**(2): p. 178-184.

46.   Riet, K.v.t. and J. Tramper, *Basic bioreactor design*. 1991, New York: Marcel Dekker.

Chapter 3

Plasmid dynamics and performance of an α-santalene producing *Escherichia coli* strain during fed-batch cultivation in the absence of ISPR

Abstract

This chapter focuses on the plasmid copy number dynamics during glycerol limited fed-batch cultivation of an α-santalene producing *Escherichia coli* BL21 (DE3) strain, as plasmid instability is known for influencing the performance of genetically modified organisms. Quantitative polymerase chain reaction (qPCR) was carried out to monitor the copy numbers of both plasmids of the strain during fed-batch cultivation in the absence of *in-situ* product recovery (ISPR).

The cultivation was carried out at a constant glycerol feed rate of $2.93 \cdot 10^{-2}$ mol $\cdot$ h^{-1}. After induction by IPTG, the specific α-santalene production rate increased asymptotically to a value of $2.2 \cdot 10^{-4}$ Cmol P $\cdot$ (Cmol X $\cdot$ h)$^{-1}$ after 144 hours of feeding.

During fed batch cultivation, the copy numbers of both the pACYCDuet^{TM}-1 and pETDuet plasmids increased with time and became more or less stable thereafter, showing that plasmid instability was not an issue in this strain.

Keywords: α-santalene production, *Escherichia coli* BL21 (DE3), fed-batch cultivation, plasmid copy number.

3.1. Introduction

3.1.1. Chemical stability of antibiotics: chloramphenicol and carbenicillin

A great stability has been described for chloramphenicol [1]. At ordinary temperatures, a very low sensibility to hydrolytic deterioration was described by [2] between 2 < pH < 7. For higher temperatures, as 100 °C, according to [3], only 14.2 % ± 0.11. of degradation occurred for this antibiotic in water after 1 h.

The chemical stability of carbenicillin, which is the *β*-lactam antibiotic used during this project, even for low temperatures (- 20 °C), is half of the value published for other antibiotics like tetracyclines and quinolones [4]. At 37 °C, stock carbenicillin solutions are considered stable during three days, while solutions with chloramphenicol are stable for five days [5, 6]. These two antibiotics were used to maintain selection pressure for each of the plasmids present in the santalene-producing strain.

3.1.2. Plasmid stability

It has been suggested that both the host strain and the type of plasmid used have an influence on the resulting copy numbers and plasmid stability [7]. Different stabilities were reported for three types of plasmids in combination with the commercial strain *Escherichia coli*

BL21(DE3), namely 63 %, 85 % and 97 % for pSVβ (6.9 kb), gWiz™(5.8 kb) and pQR150 (20 kb), respectively [7].

The key influence of plasmid stability and metabolic stress in the host strain on plasmid DNA yields is known [8]. The determination of plasmid copy number (PCN) is important to monitor plasmid segregational instability, a concerning factor for the productivity of plasmid DNA in fermentations [9]. Caused by uneven partitioning of plasmids into daughter cells during division, segregational instability leads to a loss of plasmids from a formerly plasmid-bearing population. Another type of instability of recombinant bacteria is structural, and is caused by deletions, mutations, or insertions [10].

Fed-batch fermentations with *E. coli* DH5 hosting the plasmid pVAX1-LacZ showed segregational instability, using either a constant or exponential feed. Plasmid copy numbers (PCN) decreased with 38.4 % ± 4.2 and 24.7 % ±1.7, respectively, at the end of each feeding strategy, compared to feed start. The heterogeneity of the population versus time was confirmed with DNA histograms and showed pronounced peak broadening profiles. Positive variations occurred for batch or constant feed fed-batch cultivations (3.2 g glycerol $\cdot$ (L $\cdot$ h)$^{-1}$), where the PCNs increased with 4.2 % [8].

Beyond the plasmid instabilities, further issues impact recombinant microorganisms for which protein expression depends on IPTG inducible promoters. This is due to the susceptibility of lac operon regulatory genes to modifications. Aiming at the high-level expression of β-lactamase in *Escherichia coli*, researchers indicated the presence of *lac*- mutants (Y$^-$ and I^s), which originated from

modifications in the host cell chromosome. Their presence in long term continuous cultures led to unexpected lower productivities [10].

Furthermore it has been shown that the presence of plasmids in high copy numbers affects the physiology of the host cells, resulting in decreased growth rates and biomass yields on substrate [9], [11].

3.1.3. Aim of this chapter

This chapter aims at the identification of factors that could have interfered with santalene production and the stability of the strain tested here and in chapter 2. For this, real-time PCR was used to quantify plasmid copy numbers during fed-batch cultivation in the absence of organic solvent (dodecane).

3.2. Materials and Methods

3.2.1. Strain and pre-culture medium

Escherichia coli BL21(DE3) (Novagen) was the basic biocatalyst used. The santalene-producing strain (SS) used during this project was built up with two plasmids and was kindly provided by an industrial partner. The plasmid pACYCDuet™-1 (built up with a gene for resistance against chloramphenicol) contained genes for the expression of typical enzymes of the mevalonate pathway [12], towards the production of farnesyl diphosphate (FPP or FDP, the precursor for all the sesquiterpenes). The other plasmid (pETDuet™-1), contained the gene for the final step, α-santalene synthase, converting FDP into the final product and a gene coding for resistance to the beta-lactam antibiotic ampicillin. The pre-culture preparation was performed as described in chapter 2.

3.2.2. Bioreactor set up

Aerobic fed-batch experiments under glycerol limitation were performed in jacketed 2 L reactors (Applikon, Delft, The Netherlands). The set up was equipped with mass flow controllers (Brooks, U.S.A.) for aeration ($1.5 \ nL \cdot min^{-1}$) and a single 6-blade Rushton impeller (diameter 45 mm) for stirring. Phosphoric acid (3 M) and Ammonium hydroxide (6 M) solutions were used for pH control (setpoint 7.0) and

supplied through the controller unit system BIOSTAT® BPlus (Sartorius). A Masterflex peristaltic pump (Cole Parmer, U.S.A) was used to supply the feed solution. For the dodecane free experiment presented here (Exp 5), a 10 % aqueous solution of Pluronic L-81 (Sigma-Aldrich) was used.

The pre-culture was prepared from glycerol stocks (25 % (w/v), frozen at - 80 °C), according to the reference article [13] [supporting info, section "Sclareol production in *E. coli*"] for antibiotic (and vitamin) types and concentrations. Round-bottom flasks (250 mL) containing 50 mL of LB (Luria-Bertani broth) (5 g · kg^{-1} bacto-tryptone, 10 g · kg^{-1} yeast extract and 10 g · kg^{-1} sodium chloride) were incubated (250 rpm, 37 °C) for approximately 5 h, then transferred to sterile flasks with 100 mL of fresh medium. The optical density in the flask was nearly 3 prior the transfer into the reactor, aiming for an initial broth with OD$_{600}$ = 0.2 after dilution.

3.2.3. Batch cultivation

For the batch phase, the bioreactor vessel contained around 0.8 kg of mineral "AM" medium, with a composition adapted from Schalk [13] (4.2 g · kg^{-1} KH$_2$PO$_4$, 11.98 g · kg^{-1} K$_2$HPO$_4$, 2 g · kg^{-1} (NH$_4$)$_2$SO$_4$, 1.7 g · kg^{-1} citric acid, 8.4 mg · kg^{-1} EDTA). The vessel with medium was autoclaved at 121 °C for 20 minutes after pH probe calibration (using buffers pH = 4 and 7). After cooling down to room temperature, filter-sterilized (0.2 μm) 100 mg · kg^{-1} carbenicillin, 17 mg · kg^{-1} chloramphenicol, and 4.5 mg · kg^{-1} thiamine·HCl and 10 mL of trace

metal solution (composition: 10 g · kg^{-1} Fe$_{(III)}$citrate, 0.25 g · kg^{-1} CoCl$_2$·6H$_2$O, 1.5 g · kg^{-1} MnCl$_2$·4H$_2$O, 0.118 g · kg^{-1} CuCl$_2$·2H$_2$O, 0.3 g · kg^{-1} H$_3$BO$_3$, 0.25 g · kg^{-1} Na$_2$MoO$_4$·2H$_2$O, and 1.3 g · kg^{-1}, Zn(CHCOO)$_2$·2H$_2$O, and 1.23 g · kg^{-1} MgSO$_4$·7H$_2$O) were added under sterile conditions.

Glycerol (30 g · kg^{-1}) was used as carbon source, and autoclaved separately (so was the yeast extract solution (5 g · kg^{-1})). Finally, sterile water was added to complete a total mass of 1 kg of medium prior the start of the batch phase. Subsequently the vessel was connected to the bioreactor under sterile conditions. Before inoculation, the pH was adjusted to 7.0 with 4 M NaOH and the temperature controller was set to 30 °C. After a stable temperature of 30 °C was reached a two-point calibration was carried out for the dissolved oxygen probe using nitrogen (0 %) and air (100 %).

3.2.4. Fed-batch cultivation

The composition of the feed solution was adapted from the previously cited article [13] and contained: 350 g · kg^{-1} glycerol, 24.6 g · kg^{-1} MgSO$_4$·7H$_2$O and 26 mg · kg^{-1} EDTA, 10 mL · kg^{-1} of trace metal solution (composition: 10 g · kg^{-1} Fe$_{(III)}$citrate, 0.25 g · kg^{-1} CoCl$_2$·6H$_2$O, 1.5 g · kg^{-1} MnCl$_2$·4H$_2$O, 0.118 g · kg^{-1} CuCl$_2$·2H$_2$O, 0.3 g · kg^{-1} H$_3$BO$_3$, 0.25 g · kg^{-1} Na$_2$MoO$_4$·2H$_2$O, and 1.3 g·kg^{-1} Zn(CHCOO)$_2$·2H$_2$O), 1.23 g · kg^{-1} MgSO$_4$·7H$_2$O) and filter-sterilized (0.22 μm) antibiotic and vitamin solutions to reach final concentrations of 0.1 g · kg^{-1} carbenicillin, 17 mg · kg^{-1} chloramphenicol, and 4.5 mg · kg^{-1}

thiamine·HCl. Based on literature reports on chemical stabilities, the antibiotic concentrations in the feed medium were the same as used for the batch phase. A constant feed rate was used ($2.93 \cdot 10^{-2}$ mol glycerol · h^{-1}).

The temperature setpoint was manually adjusted in the controller (from 30 to 25 °C) approximately 1 h before induction, and 5.9 h after feed start. Lower temperatures are expected to have positive effect over the quality of recombinant proteins [14] (in our case, not the final product, but the key enzymes of the biosynthetic pathway). For induction, a filter-sterilized IPTG (Isopropyl β-D-1-thiogalactopyranoside) solution was aseptically injected into the reactor just after the OD_{600} reached 40.8. The initial inducer concentration in broth was 0.14 mM.

In order to have more information about the reasons behind the instability of the santalene-producing strain, the experiment was carried out in absence of solvent. This was to avoid interference of dodecane with the PCR samples.

3.2.4.1. Preparation of samples for real-time PCR

For PCR experiments, duplicates from experiment 5 were kept in ice and transferred to the flow cabinet, after which 1 mL of sample was added under aseptic conditions to sterile *Eppendorf* tubes (as duplicates in DNA free, 2.5 mL tubes). These were centrifuged at 13000 rpm during 5 minutes and the cell pellets were kept at - 80 °C until the DNA extraction procedure. The DNeasy® Ultraclean®

Microbial Kit was used for extractions according to supplier instructions and samples were stored at - 20 °C.

Prior to amplification, the samples were diluted twice sequentially, using a 158-fold dilution factor per time.

3.2.5. On-line analyses

The software MFCShell /Win 2.1 (Sartorius Stedim Biotech S.A., France) was used to register pH, DOT, temperature and off-gas (CO_2 and O_2) composition. The gas stream leaving the system through a condenser kept at 4 °C and subsequently through a permapure dryer was passed through a combined O_2/CO_2 gas analyzer (Rosemount NGA-2000, Fisher Rosemount, Germany). Balances (Mettler Toledo, The Netherlands) registered the mass of bottles containing base and feed solutions every minute. Sensors (Applikon or Mettler Toledo, The Netherlands) for temperature, DOT and pH provided on-line data measurements in bench-reactor experiments.

3.2.6. Off-line analyses

3.2.6.1. Viable cell county

Broth samples (50 µL) were diluted sequentially four times (factor 100 per step). The population of viable cells per sample was estimated by plating (spread plate method) in Luria-Bertani-agar medium (free of antibiotics). Duplicates (150 µL) from the different

dilutions (10^{-7} and 10^{-8}) were placed at 30°C for 48 h in an incubator (Heraeus instruments), after which the colony-forming units (CFU) were counted. Samples with several dilution factors were prepared to estimate the CFUs (10^{-6}, 10^{-7}, 10^{-8} and 10^{-9}).

Viable cell count was expressed as the percentage of colony forming units (CFU) per g of dry cell weight (DCW), using as reference quantification before induction.

3.2.6.2. Other analyses

Sesquiterpene extractions and quantifications, chromatography methods, determination of Herbert-Pirt parameters, dry cell mass concentration, optical density, and specific productivities were performed as described in chapter 2 of this thesis. For santalene quantification related to both experiments described here, the number of replicate tubes was 3. For each of these tubes, the product extraction with dodecane was performed individually. The standard deviation for product accumulation versus time was calculated based on average of quantifications resulting from individual extractions (and two injections in Gas Chromatography per extraction sample).

3.2.7. Real-time PCR

3.2.7.1. Construction of the standard curves for PCN (plasmid copy number)

The plasmids pACYCDuet^{TM}-1 and pETDuet^{TM}-1 (Novagen) [15] were kindly provided by the laboratory of Biocatalysis section (Department of Biotechnology, Faculty of Applied Sciences, TuDelft). The concentrations of plasmids (ng · µL^{-1}) were measured using a HS-dsDNA quantification kit and a fluorometer Qubit 3.0 (Thermo Fisher Scientific, U.S.A). Plasmid copy numbers (PCN) were calculated as:

Standard copies = dsDNA input · 10^{-12} [ng] / dsDNA length [bp for plasmid or PCR product] · 660 [Dalton per bp of dsDNA molecule^{-1}] · 1.66057 · 10^{-27} (AMU in kg)

Ten-fold serial dilutions series ranging from 3.6·10^2 to 3.6·10^9 copies per total reaction were used as standard curves for both plasmids. The amplification for 16S ribosomal ribonucleic acid (rRNA) was carried out with the primer sets BAC 341-BAC907Rm (maximum 6.6·10^5 per total reaction). For data processing, the software qPCR soft version 3.2 (Analytik Jena AG, Jena, Germany) was used. The values for threshold cycle (C_t) per dilution were plotted against the logarithm of their template copy numbers for the standard curves based on linear regression. Unknows were calculated by determining the slope of the

Ct versus copy numbers. The PCR amplification efficiency (E) was obtained from the delay in cycles at Ct between standards, as follows:

E (%) = (10$^{-1/\text{cycles delay between standards at Ct}}$ -1) ·100 %

3.2.7.2. Primers sets testing for annealing temperatures

Seven primer sets (appendix D) were tested for annealing temperatures. A 45 minutes electrophoresis run (using 100 V) in agarose gel 3 % dissolved in Tris-borate buffer (TBE) and using Ficoll® as loading dye was carried out. The assay was carried out with PCR products resulting from different temperature settings: 48.5 °C, 51.5 °C, 55.5 °C, 59.5 °C, 63.3 °C and 64.9 °C for primers annealing temperature (Ta) selection. As negative control, *E. coli* K12 (Sigma-Aldrich) was used. The most stringent Ta was determined, melting curves and agarose gel electrophoresis were performed to verify the amplification product specificity and size (appendix D). All further amplifications as described in section 3.2.7.3 were performed using 59.5 °C as annealing temperature.

3.2.7.3. Real-time PCR amplification for the plasmids pET-duet and pACYC-duet

The assays were performed in a qTower^3 Real-time Thermal cycler (Analytic Jena) containing 96-well plates. For pET-duet plasmid DNA amplification, the following primers set was used: forward 5'-

CTTTCTTCCCTTCCTTTCT-3', and reverse 5'-GTTGAGTGTTGTTCCAGT-3' to amplify a fragment of 235 bp. For the pACYC-duet plasmid, the primers forward: 5'-ATGGTGTTTTTGAGGTG-3' and reverse 5'-CTTTTTTCTCCTGCCAC-3' were used to amplify a 187 bp product.

Every PCR reaction contained 7.5 µL SYBR® Green PCR mixture (Bio-Rad, U.S.A), 0.08 µL per primer and 2 µL of the specific template. PCR grade water was used to bring the total volume to 15 µL. After a 2 min pre-incubation at 98 °C, the DNA was amplified by 40 cycles of denaturation at 95 °C for 15 s, primer annealing (Ta) at 59.5 °C for 30 s and extension at 72 °C for 15 s. At 78 °C, a scan was performed for 10 s for the PCR product. Temperature annealing tests were shown in figure 11 (appendix D).

3.2.7.4. Protein analysis

Total protein measurements were carried out with the Bradford method (Sigma-Aldrich, 3.1 mL assay), expressed in bovine serum albumin (BSA) units. A calibration curve using $0.25 \text{ g} \cdot \text{L}^{-1}$, $0.5 \text{ g} \cdot \text{L}^{-1}$, $1.0 \text{ g} \cdot \text{L}^{-1}$ and $1.4 \text{ g} \cdot \text{L}^{-1}$ BSA was used. The absorbance was read at ($\lambda = 595$ nm) for supernatant samples diluted 5-fold. The centrifugation was performed using a Heraeus Biofuge Pico centrifuge at 13000 rpm for 5 minutes. Results shown in chapter 4, in comparison to humulene-producing strain.

3.3. Results

3.3.1. Bench scale bioreactor experiment

For this experiment the antibiotic concentrations in the feed medium (key for the maintenance of selection pressure) were the same as in the batch medium. Thus, if no degradation occurs, the antibiotic concentrations in the reactor were expected to be constant throughout the fed-batch fermentation.

Aiming at an overview between plasmid types per cell and viable cell count, the experiment was carried out without the organic phase to avoid interference with the qPCR. Appendix B presents an experiment overview in terms of maximum biomass and product concentrations, tip speed and ages (total and fed-batch).

Real-time qPCR was carried out in order to check the plasmid dynamics versus time (and search for indications of metabolic burden) by determining the plasmid. The lower inducer concentration used here relates to the high productivities reported for Chapter 4 for the humulene producing strain by using similar IPTG concentrations. This seemed to indicate that higher inducer concentrations were not required for sesquiterpene production in *E. coli*. Considering the contrasting productivities observed for the santalene-producing strain during this project, one of the research questions addressed is whether the plasmid types per cell change with time. For the strain used here, product formation depends on a good functionality of both plasmids.

Repeated foam-out events observed in previous dodecane-free fed-batch attempts that had foam control triggered by probe contact and higher glycerol rates. Therefore, the glycerol rate for the experiment reported here (exp 5 from table 5) was decreased in order to decrease the biomass formation. Furthermore, the foam control was increased by using cyclic anti-foam addition.
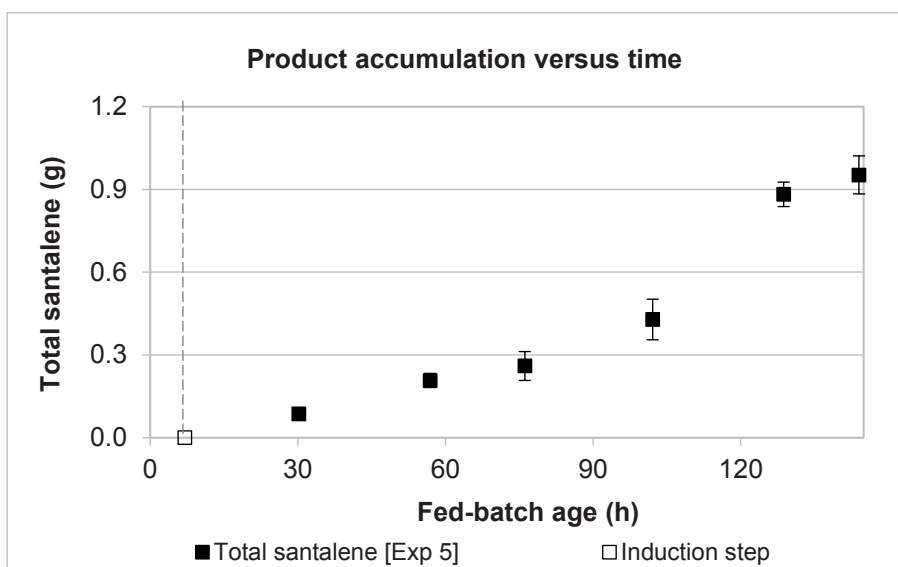

Figure 1. Santalene accumulation in the vessel during solvent free fed-batch cultivation (n = 3, black squares). The induction time is indicated by the open square and dotted line.

The highest cumulative amount of santalene noticed for this strain (including chapter 2) was reported here after a long process time: 128.7 h of fed-batch cultivation, estimated as 0.95 g (based on mass balance, figure 1).
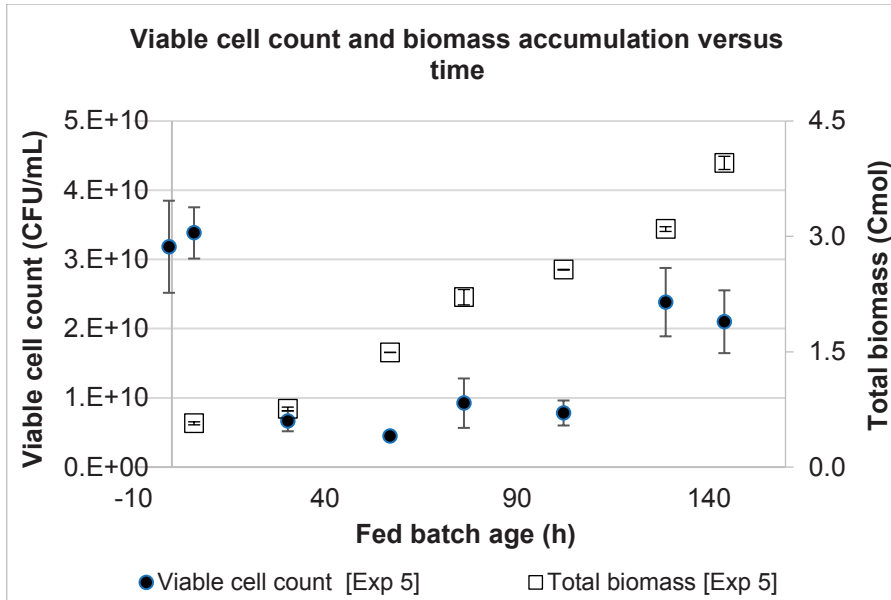
Figure 2. Viable cell count (left axis, black dots) and total biomass
(right axis, squares) experiment 5, versus fed - batch age. The
vertical bars indicate standard deviations (n = 2).

The contrast between viable cell count (right axis) and total
biomass (left axis) versus time is presented in figure 2, for the
percentage of viable cells in dilutions: D1 (dark blue circles) or D2 (light
blue triangles) for LB-agar (free of antibiotics). Viable cell count
reached a minimum after 56.8 h feed, recovering with time as the
(inducer free) feed medium was added to the broth. This trend could
represent sensitivity to IPTG addition performed at 7.0 h of feed phase
(even in lower volumetric concentrations as 0.14 mM). For samples
before this specific time, reliable CFU quantifications were possible
only in plates from less diluted tubes (10^{-6}), with the exception of the

first sample tested for the feed phase (before induction), when viable cell count was high.

For the last three samples taken during the experiment, viable cell count presents a discrete recovery until the end (figure 2), suggesting that the product increase with time (figure 1) does not indicate great inhibition over the cells. As will be addressed in the discussion section, log P values do not indicate toxicity of santalene over microorganisms.

3.3.1.1 Real-time qPCR

Figure 3 depicts the pET-duet and pACYC-duet plasmid copy numbers versus time for the santalene-producing strain (experiment 5, free of dodecane), indicating the presence of both plasmids throughout the fed-batch time. Their proportions, on the other hand, change with time. Initially, up to 30 h of fed-batch cultivation, the plasmid copy numbers per type were similar, while thereafter the copy number of the pET plasmid was always higher than that of the pACYC plasmid.

The maximum ratio of approximately 3 between pETDuet™-1 and pACYCDuet™-1 occurred after 102.1 h of fed-batch and a (pET/PACYC) proportion lower than 2 prevailed for other samples, contrasting to the range (3.33-4) reported in the Novagen user protocol [16].
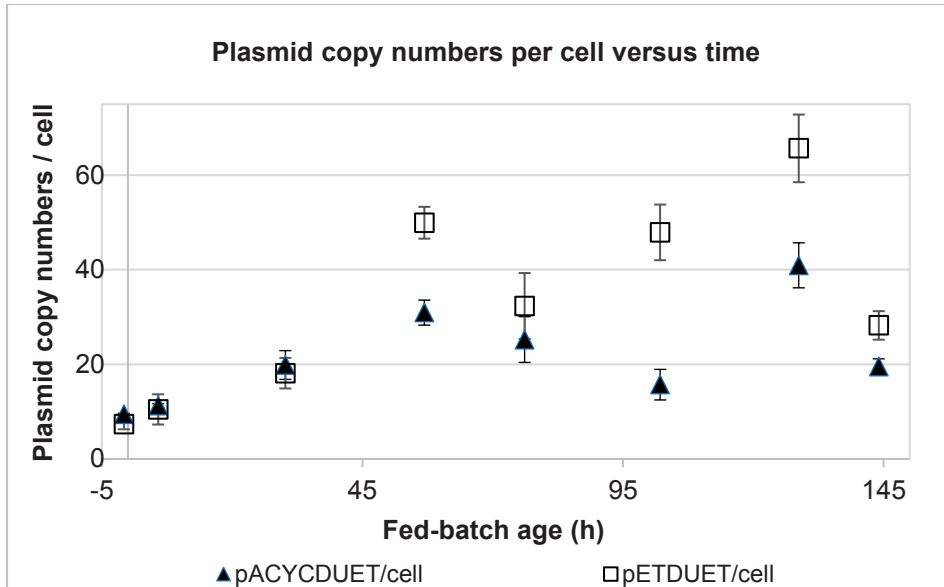
Figure 3. Plasmid copy numbers per cell for pET and pACYC versus time for solvent-free fed-batch cultivation, Exp 5 (SS strain). The error bars represent standard deviations (n = 2).

3.3.1.2. Overview for specific productivity and inducer concentrations

The specific productivities for the dodecane free experiment and experiment 3 which was carried out with dodecane (see chapter 2) are shown below (figure 4).

Specific santalene productivity rates (q_p) versus growth rates were presented in figure 4. As compared to Exp 3 (chapter 2 of this thesis), the maximum specific productivities reported here were still lower (up to $2.18 \cdot 10^{-4}$ Cmol P $\cdot$ (Cmol X $\cdot$ h)$^{-1}$ at the end of the fed-

batch). The inducer concentration shown in figure 6 was only 16 % of the initial concentration used in experiment 3 (chapter 2).
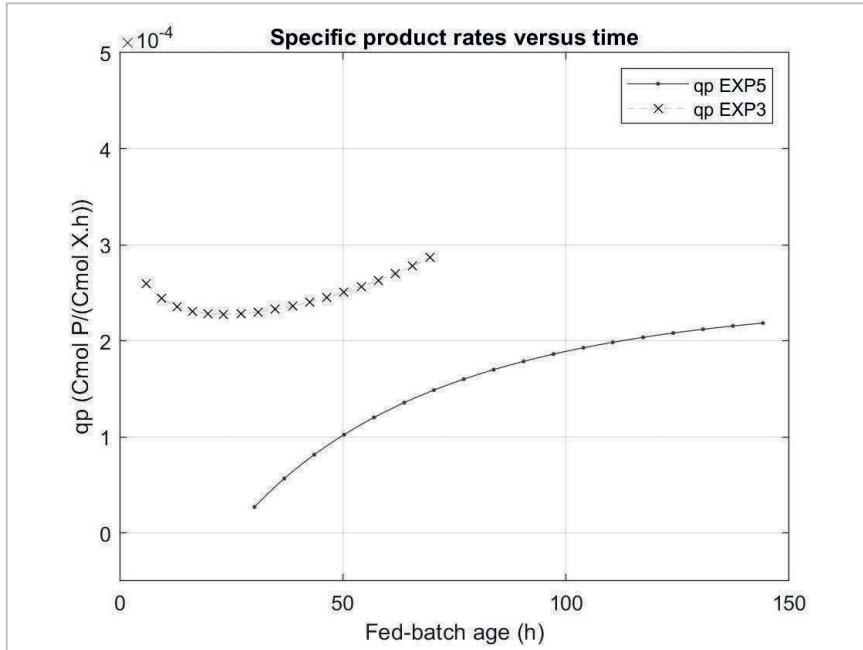

Figure 4. Specific santalene production rates rate (q_p) for solvent-free fed-batch cultivation, Exp 5 (current chapter) and solvent containing fed-batch cultivation, Exp 3 (chapter 2, induction at 5 h feed-phase age, with 0.9 mM IPTG).

The polynomial fit of specific santalene productivity rates (q_p) versus µ was hereby presented for experiment. 5 (figure 5). Within the growth rate (µ) ranges studied, lower µ values resulted in higher specific productivities.
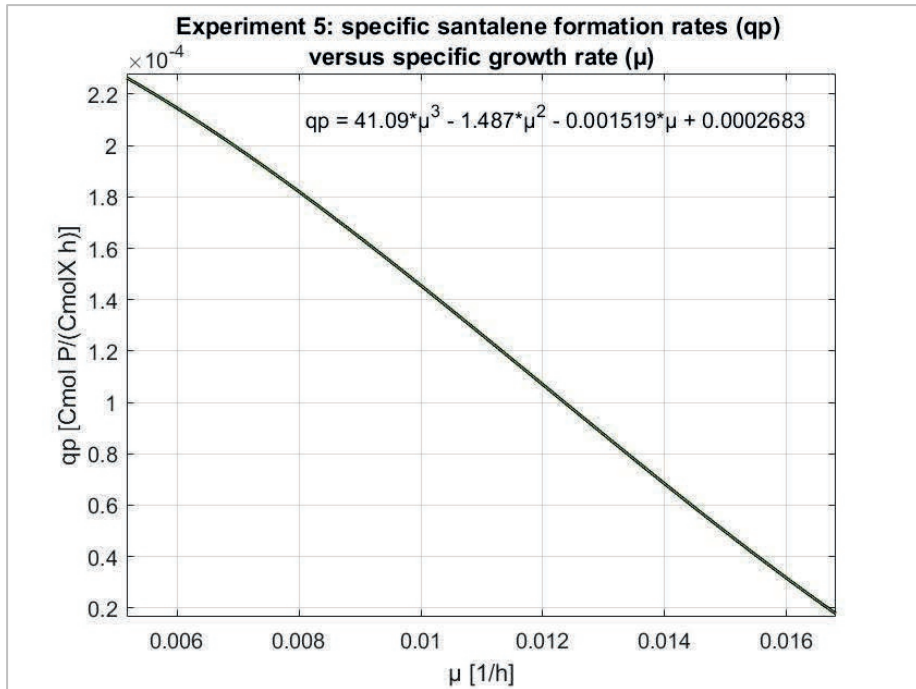
Figure 5. Plot of a polynomial fit of the specific santalene formation rate (q_p) versus specific growth rate (μ) for solvent free fed-batch cultivation Exp 5. Time interval: 30 h to 144 h of feed phase, R^2 = 0.99.
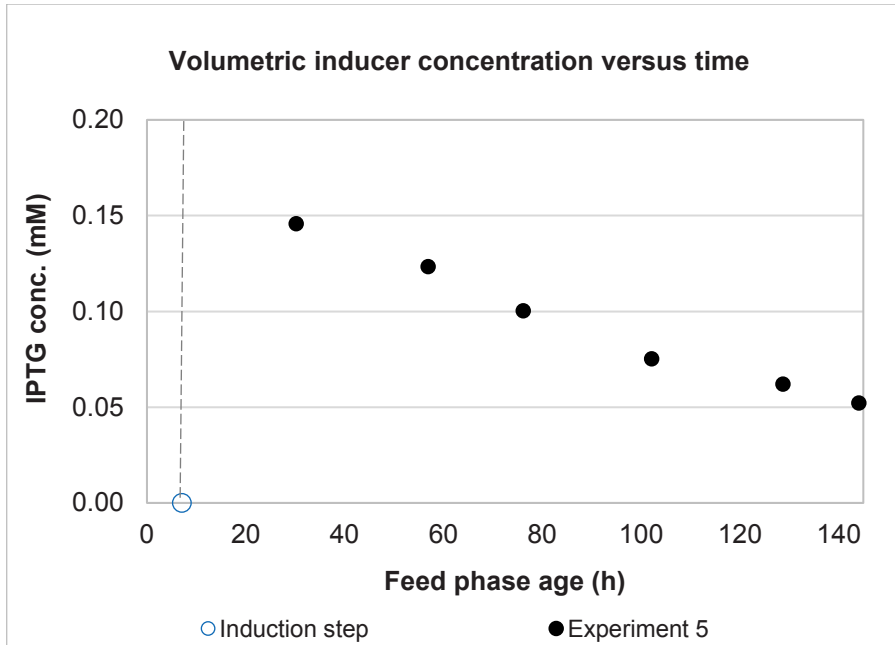
Figure 6. Estimation of the volumetric inducer concentration versus time for solvent free fed-batch experiment 5. Dotted line with open symbol indicates the induction time.

3.3.1.2. Herbert-Pirt parameters

As presented in figures 9 and 10 (appendix C), the specific growth rates were slightly different between experiments as the feed phase started, converging after 40 h of fed-batch cultivation. Table 1 presents a summary of the estimated values of the Herbert - Pirt parameters, based on the assumption that the amount of substrate consumed for santalene production is negligible. As exemplified by [17] (the product formation term was considered negligible when representing 2 % of the maintenance term), here the $b \cdot q_p$ term of the Herbert - Pirt correlation did not exceed 2.8 % of the maintenance term for the experiment with the best santalene production performance. Here, the b parameter estimated in appendix 4.8.4 (chapter 4) for humulene production was used for the calculation.

The amount of substrate (mol glycerol) required for the synthesis of 1 Cmol of biomass (parameter a) was more than two times higher than the value of 0.47 mol glycerol per Cmol biomass estimated for a non-transformed *E. coli* MG1655 strain [18] and also much higher than the values estimated from fed-batch experiments 1, 2 and 3 (chapter 2). This high substrate requirement for biomass formation, equivalent with a low biomass yield on substrate, might indicate that the presence of the two plasmids coding for the α-santalene biosynthesis pathway impose a metabolic burden upon the cells. Remarkably, the estimated value of the maintenance coefficient was equal to zero. Considering the observed nearly linear increase of the amount of biomass in time (Appendix E) during the constant feed fed-batch fermentation, this is

not a surprise. However, instead of a linear increase, an asymptotic increase is expected, because at an increasing amount of biomass during fed-batch cultivation, an increasing amount of the substrate is used for maintenance and thus a decreasing amount is available for cell growth. The reason for the observed linear increase of the biomass dry weight could have been the considerable requirement of anti-foam solution, of which the added amount had to be increased in time, leading to an overestimation of the biomass dry weight.

Table 1. Herbert-Pirt parameters, glycerol rate and initial μ at the feed phase:

	$M_{x(0)}$	a	m_s	rate glycerol $\cdot 10^2$	Initial μ $\cdot 10^2$
Exp	$Cmol_x$	$\dfrac{mol_{glycerol}}{Cmol_x}$	$\dfrac{mol_{glycerol}}{Cmol_x \cdot \text{h}}$	$\dfrac{mol}{\text{h}}$	$\dfrac{1}{\text{h}}$
5	0.75 ± 0.05	-1.12 ± 0.14	0.0000 ± 0.0014	2.68	3.18

Table 2. Overview for santalene production in this chapter:

Exp	Initial dodecane	Product Yield (Y_{PX})*	Overall productivity from induction time
-	% w/w	$\dfrac{mgP}{gDCW}$	$\dfrac{mgP}{gDCW \cdot h}$
5	absent	5.40	0.07

3.4. Discussion

In this chapter the biotechnological production of the sesquiterpene α-santalene was studied. The formation of α-santalene is derived from the universal sesquiterpene precursor farnesyl diphosphate (FPP) in a complex cyclization reaction catalyzed by santalene. synthases. The direct precursor FPP can either be synthesized through the methylerythritol phosphate (MEP) pathway or the mevalonate (MVA) pathway.

A possible reason for the low α-santalene specific productivities reported here could have been different expression levels of the synthase enzymes responsible for the conversion of FPP to the final product. It has been reported by a group that researched specific genes for sesquiterpene biosynthesis in *Escherichia coli* that the expression of cyclase enzymes could be a limiting factor for terpenes synthesis [19]. The formation of α-santalene is known for its complex kinetics. While comparing two types of santalene synthases different for product formation specificity, researchers suggested that the enzyme (SanSyn) known for higher proportion of α-santalene formation had a limited and more rigid cavity space, as compared to the less selective santalene synthase version (SaSSy).On the other hand, the more flexible conformational dynamics of the later type resulted in the formation of undesired intermediates such as exo-α-bergamotene [20]. In the same publication [20] the authors studied the specific mutagenesis of key amino acid residues affecting the conformational dynamics of intermediates to achieve a product distribution towards the maximization of α-santalene and β-santalene.

Another possibility could have been a lethal effect on cells harboring plasmids with the T7 promoter after the induction step for T7 RNA polymerase production. A high mortality of BL21(DE3) host cells has been observed during experiments aiming for the production of seven membrane proteins and ten globular proteins, highlighting limitations of the T7 RNA polymerase expression system [21]. A metabolic burden has been associated with the high activity of T7 RNA polymerase, potentially leading to mutations in the constructs and impacts on host physiology [22]. One hypothesis here is that factors like this could have affected the viable cell count with time (figure 2) and, to a certain extent, the α-santalene productivity.

Lastly, plasmid (in)stability could also have played a role in the lower productivity of the α-santalene producing strain. This was investigated in the current chapter, but was not identified as reason for the low productivity of this strain, as the plasmid copy number (PCN) did not decrease during the fed-batch cultivation and the PCN's for both plasmids were not lower than the expected values given in the Novagen manual.

After the experimental work on this chapter had been performed, relevant publications [23], [24] on α-santalene production in engineered *E. coli* appeared. After several metabolic engineering steps these authors succeeded to improve the final α-santalene titer of their strains from 0.4 to approximately 2.9 g · L^{-1}, which is about three times the value that we reached with our strain. This shows that rational metabolic engineering efforts can be successful in increasing the performance of sesquiterpene producing *E. coli* strains.

Apart from strain optimization also process optimization can be applied to increase the performance of the fermentation process. This can be done by increasing the cell density up to the limit of the oxygen transfer capacity of the bioreactor and by controlling the growth rate towards the value at which the maximum productivity is obtained. Controlling the growth rate at the desired value in fed-batch cultivations is achieved by using an exponentially increasing feed rate of the growth limiting substrate. For the strain used in this chapter this would be the specific growth rate that would lead to the best santalene productivities shown in figure 5 (approximately $2.2 \cdot 10^{-4}$ Cmol P $\cdot$ (Cmol X $\cdot$ h)$^{-1}$) for a μ of $5.7 \cdot 10^{-3} \cdot h^{-1}$.

Overall, HPLC has been tested for the quantification of glycerol in supernatant samples from cultivations of both strains described in this thesis. In samples originated from humulene producing strain, however, resolution problems were detected for the equipment hereby described, limiting the obtention of further data regarding glycerol quantifications. Therefore, for the later, the carbon gaps estimated per timepoint were slightly higher, as compared to processed data resulting from cultivations aiming at the production of santalene.

3.5. Conclusions

A constant feed fed-batch cultivation was performed with the α-santalene producing strain in the absence of ISPR with dodecane. During the cultivation in the absence of dodecane much more foam formation occurred than in the presence of the solvent, indicating that dodecane might act as a foam suppressor.

Although ISPR was not employed, the specific α-santalene productivity increased until the end of the fermentation, reaching a value of $2.18 \cdot 10^{-4}$ Cmol P $\cdot$ (Cmol X $\cdot$ h)$^{-1}$, which was about 25 % lower than the maximum productivity reached in the presence of dodecane (chapter 2). If this was due to the absence of ISPR remains to be investigated.

Quantification of the copy numbers, through qPCR, of both the pET and pACYC plasmids harboring the α-santalene biosynthesis pathway, showed that plasmid instability was not an issue during fed-batch cultivation of this strain.

Nevertheless, the current productivity is too low for commercial production of α-santalene and thus further optimization of the producing strain through metabolic engineering is required, e.g. focusing on targets such as:

- Avoiding imbalance of farnesyl diphosphate (FPP) synthesis and α-santalene synthase capacity, which could be due to absence or non-functionality of the pACYC plasmid for the expression of enzymes required for the synthesis of this precursor. Further studies would be necessary to elucidate the expression of specific key enzymes in this strain.

- Avoiding limitations in the conversion of the substrate FPP to α-santalene, due to problems with the expression of the synthase, encoded by the pET-duet plasmid in our strain. The proper formation of α-santalene has been already described as complicated due to the cyclization of the final molecule [25]. If the quality of this enzyme, responsible for the final bioconversion of FPP into α-santalene is compromised, inclusion bodies could be formed, minimizing or hindering the sesquiterpene formation

Given the limitations of either the antibiotics or microbial mechanisms of resistance against them, other strategies of microbial engineering, such as genome integration, could be considered for future strains.

3.6. Acknowledgements

3.7. Symbols

C_0 = initial concentration

CFU = colony-forming units

DCW = dry cell weight

DOT = dissolved oxygen tension

Exp = experiment

HS = humulene - producing strain

IB = inclusion bodies

Exp or Exp_s (plural) = short code of the experiment

IPTG = Isopropyl β-D-1-thiogalactopyranoside

ISPR = *in situ* product recovery

n = number of replicates

PL = plasmid

PCN = plasmid copy number

S = substrate (glycerol)

SS = santalene-producing strain

X = biomass

w = weight

AMU = atomic mass unit

3.8. Appendix

3.8.1. Appendix A. ISPR and intermediate inducer concentrations [experiment 4]

Dodecane was added after induction for *in situ* product recovery (ISPR). As mentioned previously, antibiotics were increased in feed medium, as compared to experiments from chapter 2. The reason for this relates to concerns regarding the decrease of selection pressure versus time (see section 3.1.1 on antibiotics stability and the discussion section). A constant feed of $3.84 \cdot 10^{-2}$ mol glycerol $\cdot$ h^{-1} was used. A high oscillation mainly for carbon dioxide off-gas occurred after 50 h (this could be due to malfunction of the off-gas analyser equipment or due to metabolic activity oscillations for this strain, as had been previously noticed). No oxygen limitation was observed.

The highest product accumulation, estimated as 0.31 g in the vessel occurred early: after 22.5 h of induction for an initial inducer concentration of 1.23 mM. Some of the samples for estimation of product extraction in tubes indicated high standard deviations (figure 7). Open symbol (square) and dashed line indicate induction time.

The IPTG concentration range used for Exp 4 (1.23 to 0.57 mM) was next, but slightly higher as compared to the used for Exp 3 (chapter 2, from 1 mM at induction step to 0.25 mM at the end) however, resulted in opposite product accumulation profiles versus time. It could be that a subtle inducer difference as 20 % increase (Exp

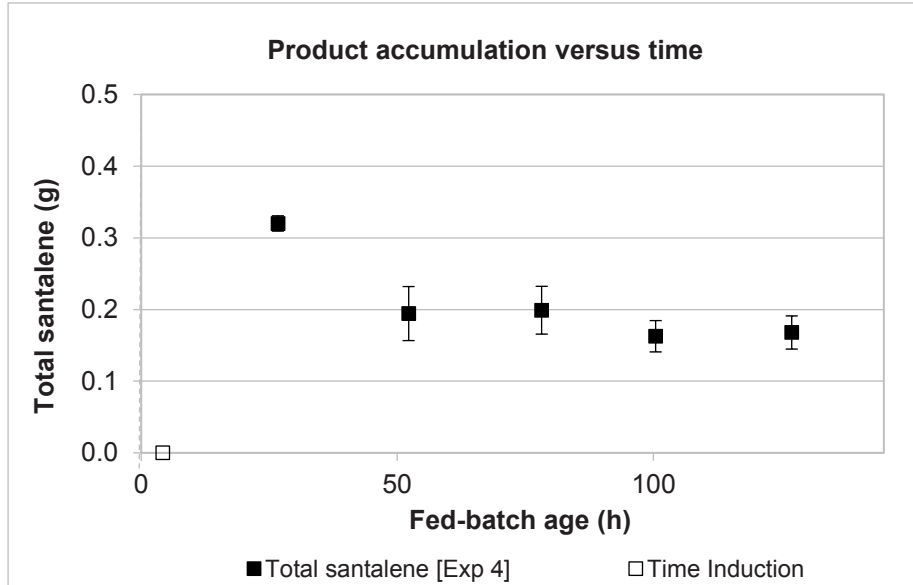4) could have resulted on inhibition or decrease of santalene production.

Figure 7. Sesquiterpene accumulation in the vessel (estimated from n = 3) versus time for experiment 4. Induction time is shown as empty square and dotted line. Error bars represent standard deviation for replicates.

For the experiment 4, the maximum optical density (OD_{600}) reached 85 ± 5.5. The standard deviation for maximum dry cell mass represented 5.3 % of average. Contrasting profiles occur between total biomass concentration and viable cell count (not shown). A decrease of viable cell counts as time advanced occurred, suggesting cell lysis. Plates with Luria-Bertani (dilutions 10^{-7} or 10^{-8}) presented very low numbers of colony-forming units to estimate their original

concentration in broth, not only after induction, as for sample 5 (feed phase age 52.2 h), but also at the end (after 127 h of feed).

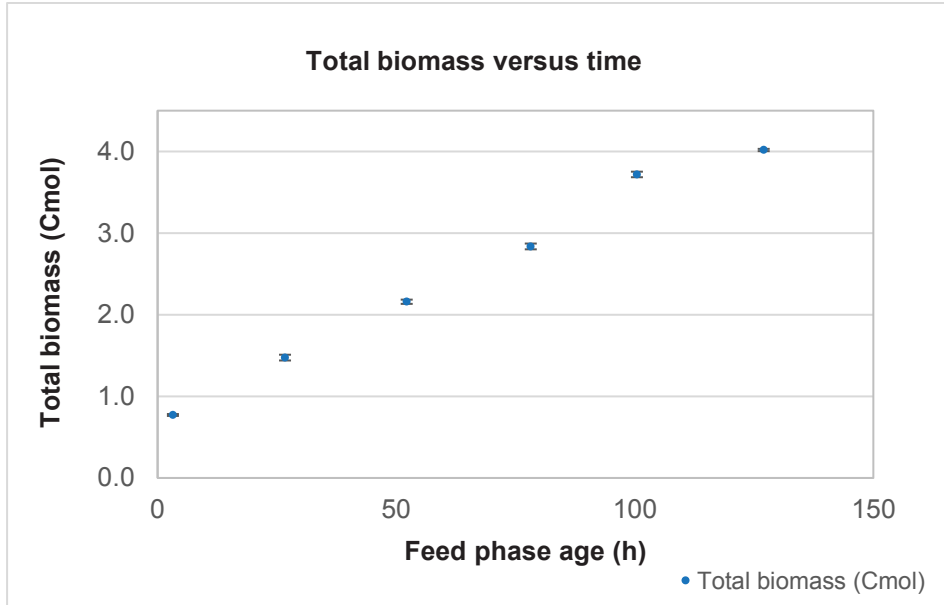**Figure 8.** Total biomass versus time, experiment 4.

Table 3. Herbert-Pirt parameters, glycerol rate and initial μ at the feed-phase:

	a	m_s	Rate glycerol $\cdot 10^2$	Initial μ $\cdot 10^2$
Exp	$\dfrac{mol_{glycerol}}{Cmol_x}$	$\dfrac{mol_{glycerol}}{Cmol_x \cdot h}$	$\dfrac{mol}{h}$	$\dfrac{1}{h}$
4	-1.046	-0.0024	3.84	7.45

Table 4. Overview for santalene production in this chapter:

Exp	Initial dodecane	Product Yield (Y_{PX})	Overall productivity from induction time
	% w/w	$\dfrac{mgP}{gDCW}$	$\dfrac{mgP}{gDCW \cdot h}$
4	13.25	3.52	0.02

The experiment combination of dodecane (in situ product recovery) and antibiotic concentrations (higher metabolic active fraction of the population) resulted in earlier santalene accumulation (experiment 4, figure 7). While the higher inducer concentrations for this experiment could have facilitated the heterologous protein expression towards terpene production, it could also have affected the viable cell count, as reported in literature related to IPTG effects [26].

A publication related to the chemical stability of pure α-santalene oil under ambient conditions reported a complex degradation mixture of eight components after two months [27]. Such article does not represent the interactivity of this terpene with other compounds of the broth in concentrations used in Exp 4. One hypothesis here is that such interactions resulted in degradation products, affecting the performance of the used strain.

Several papers were cited in chapter 6, with listed suggestions, including the effect of IPTG concentrations and temperature over the solubility of proteins of interest. Temperature and the solubility of proteins exert key influence here and should be further researched. Hydrophobic interactions in protein folding are closely dependent on

temperature [28]. Lower rates during the protein production can benefit a proper folding of the newly transcribed proteins [29].

Researchers recommended the protein expression in E. coli not exceeding 25 °C. When the formation of inclusion bodies is undesired, the range 15 - 25 °C was suggested, due to a correlation between decrease on temperature and protein quality [14, 29]. Sometimes, even using temperature decrease can compromise functionality, requiring improvements for expression methods [30].

As reported in chapter 2, inducer concentrations exert influence over viable cell count. For the production of protein ZZ (under control of lacUV5 promoter) by E. coli RB791 (bearing only the plasmid pRIT28NZZT). Lethality was described even under low inducer concentrations of IPTG (0.1 mM) raising suggestions towards replacement options [31]. Authors reported a strong decrease of the viable cell count after IPTG addition, combined with a decrease of the ribosome content of the cells, while a stable profile was described for non-induced bacteria [26].

3.8.2. Appendix B. Overview and sample ages per experiment.

Table 5 lists an overview of experiments. Ages for samples and other steps were placed in tables 6 and 7 (for total and feed phase age, respectively). The standard α-santalene-producing strain (SS) was used. The glycerol composition in feed was 35 % w/w.

Table 5. Overview for experiments:

Code	Exp	*PV	**$V_{tip\ max}$	Glyc. rate·10^2	Max. biomass ***conc.	Max. product conc.	AF ****
TUD DIRC		$\dfrac{kW}{m^3}$	$\dfrac{m}{s}$	$\dfrac{mol}{h}$	$\dfrac{g}{kg}$	$\dfrac{g}{kg}$	$\%\dfrac{w}{w}$
17.12.04 F#4	4	4.2	3.0	3.84	44.2±0.2	0.2±0.01	1.7
18.01.23 F#4	5	4.6	2.9	2.93	52.0±0.4	0.5±0.05	1.7

*PV = average volumetric power input [32].
**$V_{tip\ max}$: maximum impeller tip speed.
***conc.=concentration.
****AF=anti-foam final concentration.

Table 6. Total ages (h) for key steps and samples per experiment:

Exp	2	3	Ind.	Dod.	4	5	6	7	8
4	14.3	18.8	19.2	35.7	41.7	67.2	93.2	115.4	142.0
5*	13.0	19.6	20.8	-	44.0	70.7	89.9	115.9	142.5

Ind.: induction time / Dod.: dodecane addition time. *Experiment 5 had the later sample (ID = 9), taken at total age of 157.8 h.

Table 7. Feed phase ages (h) for keys steps and samples:

Exp	2	3	Ind.	Dod.	4	5	6	7	8
4	-0.7	3.2	4.2	20.7	26.7	52.2	78.2	100.4	127.0
5*	-0.8	5.8	7.1	-	30.2	56.9	76.1	102.1	128.7

Ind.: induction time / Dod.: dodecane addition time. *Experiment 5 had the later sample (ID = 9), taken at fed-batch age of 144.1 h.

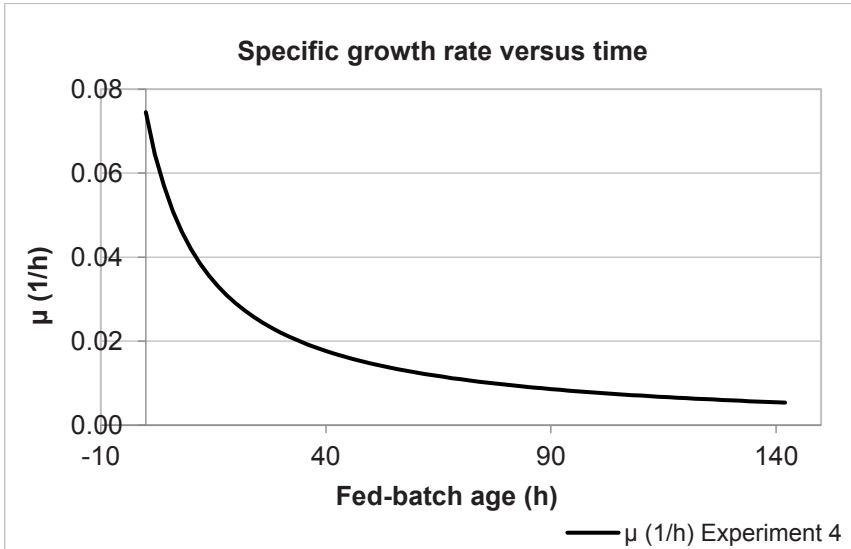### 3.8.3. Appendix C: Specific growth rates per experiment

Figure 9. Specific growth rate (μ) versus time for experiment using ISPR (Exp 4).
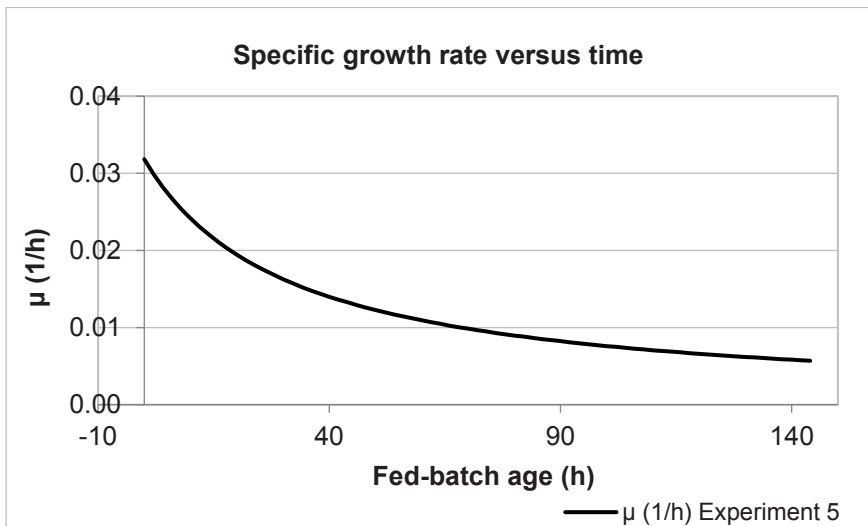

Figure 10. Specific growth rate (μ) versus time for dodecane-free experiment (Exp 5).

3.8.4. Appendix D. Selection of primers and annealing temperature (Ta):

Table 8. Complete selection of primers described during this project:

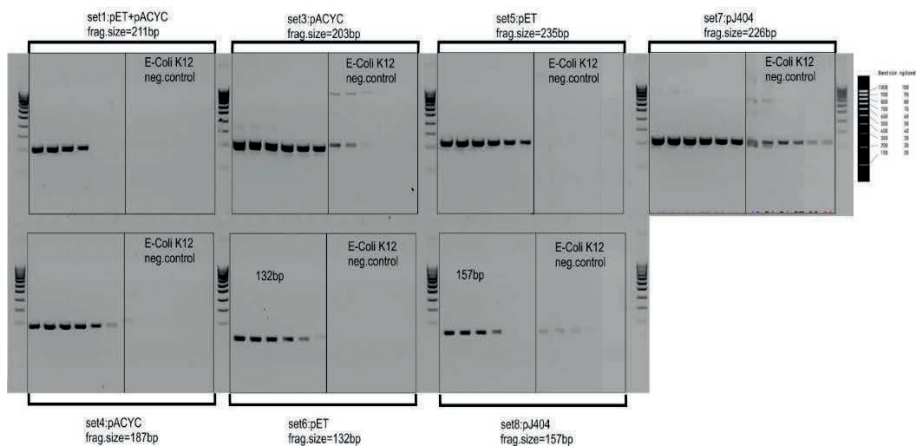| Set	Forward	Reverse	PL
1	CCATCACCATCATCAC	ATCTCCTTCTTATACTTAAC	1, 2
3	TGCGCTCTCCTGTTCCT	TTTGCATGTCTTTCCGGGTT	2
4	ATGGTGTTTTTGAGGTG	CTTTTTTCTCCTGCCAC	2
5	CTTTCTTCCCTTCCTTTCT	GTTGAGTGTTGTTCCAGT	1
5.2	CTTTCTTCCCTTCCTTTCT	GAACCATCACCCTAATCAA	1

PL= plasmid, 1 = pET, 2 = pACYC.

Figure 11. Test for annealing temperatures in agarose gel. For every set of primers presented above and described in table 8, temperature settings tested were respectively 48.5 °C, 51.5 °C, 55.5 °C, 59.5 °C (selected), 63.3 °C and 64.9 °C (from left to right).

3.8.5. Appendix E. Biomass accumulation

Biomass accumulation versus time [Exp 5]
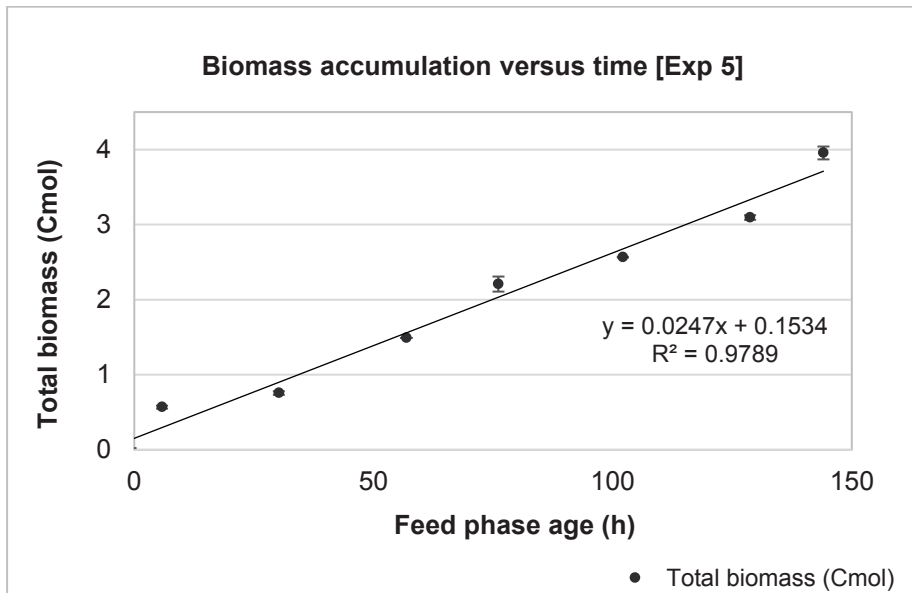
$y = 0.0247x + 0.1534$
$R^2 = 0.9789$

Figure 12. Biomass accumulation versus time: plateau was not observed at the end of feed phase. This profile could have been influenced by the anti-foam addition to the solvent-free fed-batch experiment (ID = 5).

3.9. References

1. Connors, K.A., et al., *Chemical Stability of Pharmaceuticals: A Handbook for Pharmacists*. 2nd ed. 1986, New York: John Wiley & Sons, Inc. 864pg.

2. Higuchi, T., C.D. Bias, and A.D. Marcus, *The Kinetics of Degradation of Chloramphenicol in Solution: II. Over-all Disappearance Rate from Buffered Solutions.* Journal of the American Pharmaceutical Association (Scientific Edition), 1954. **43**(3): p. 129-134.

3. Tian, L. and S. Bayen, *Thermal degradation of chloramphenicol in model solutions, spiked tissues and incurred samples.* Food Chemistry, 2018. **248**: p. 230-237.

4. Okerman, L., J. Van Hende, and L. De Zutter, *Stability of frozen stock solutions of beta-lactam antibiotics, cephalosporins, tetracyclines and quinolones used in antibiotic residue screening and antibiotic susceptibility testing.* Analytica Chimica Acta, 2007. **586**(1): p. 284-288.

5. Sigma-Aldrich. *Properties and description for carbenicillin disodium salt (89.0-100.5% anhydrous basis)*. [cited 2019 03/03/2019]; Available from: https://www.sigmaaldrich.com/catalog/product/sial/c1389?lang=en&region=NL.

6. Sigma-Aldrich. *Properties and description for chloramphenicol ≥98% (HPLC)*. [cited 2019 03/03/2019]; Available from: https://www.sigmaaldrich.com/catalog/product/sigma/c0378?lang=en&region=NL.

7.   Yau, S.Y., E. Keshavarz-Moore, and J. Ward, *Host strain influences on supercoiled plasmid DNA production in Escherichia coli: Implications for efficient design of large-scale processes.* Biotechnology and Bioengineering, 2008. **101**(3): p. 529-544.

8.   Silva, F., J.A. Queiroz, and F.C. Domingues, *Plasmid DNA fermentation strategies: influence on plasmid stability and cell physiology.* Applied Microbiology and Biotechnology, 2012. **93**(6): p. 2571-2580.

9.   Silva, F., et al., *Impact of plasmid induction strategy on overall plasmid DNA yield and E. coli physiology using flow cytometry and real-time PCR.* Process Biochemistry, 2011. **46**(1): p. 174-181.

10.   Fu, J., et al., *Escherichia coli Host Cell Modifications in Continuous Culture Affecting Heterologous Protein Overproduction: A Population Dynamics Study.* Biotechnology Progress, 1992. **8**(4): p. 340-346.

11.   Wang, Z., et al., *Effects of the presence of ColE1 plasmid DNA in Escherichia coli on the host cell metabolism.* Microb Cell Fact, 2006. **5**: p. 34.

12.   Wang, C., et al., *Metabolic engineering and synthetic biology approaches driving isoprenoid production in Escherichia coli.* Bioresource Technology, 2017. **241**: p. 430-438.

13.   Schalk, M., et al., *Toward a Biosynthetic Route to Sclareol and Amber Odorants.* Journal of the American Chemical Society, 2012. **134**(46): p. 18900-18903.

14.   Schein, C.H. and M.H.M. Noteborn, *Formation of Soluble*

Recombinant Proteins in Escherichia Coli is Favored by Lower Growth Temperature. Bio/Technology, 1988. **6**(3): p. 291-294.

15.   Merck-Millipore. *Information about pET-Duet plasmid*. 07/12/2018]; Information about pET-Duet plasmid]. Available from: http://www.merckmillipore.com/NL/en/product/pETDuet-1-DNA-Novagen,EMD_BIO-71146?ReferrerURL=https%3A%2F%2Fwww.google.nl%2F.

16.   Novagen, *User protocol TB340 (Duet Vectors) Rev F 0211JN*. 2011: Darmstadt, Germany. p. 1-12.

17.   Heijnen, J.J., *Design of fed batch fermentation processes*, in *Fermentation Technology & Environmental Biotechnology (LM3741). Lecture notes*. 2012, Technische Universiteit Delft. p. 1-28.

18.   Taymaz-Nikerel, H., et al., *Genome-derived minimal metabolic models for Escherichia coli MG1655 with estimated in vivo respiratory ATP stoichiometry.* Biotechnology and Bioengineering, 2010. **107**(2): p. 369-381.

19.   Martin, V.J.J., Y. Yoshikuni, and J.D. Keasling, *The in vivo synthesis of plant sesquiterpenes by Escherichia coli.* Biotechnology and Bioengineering, 2001. **75**(5): p. 497-503.

20.   Zha, W., et al., *Rationally engineering santalene synthase to readjust the component ratio of sandalwood oil.* Nature Communications, 2022. **13**(1): p. 2508.

21.   Miroux, B. and J.E. Walker, *Over-production of Proteins inEscherichia coli: Mutant Hosts that Allow Synthesis of some Membrane Proteins and Globular Proteins at High Levels.* Journal of Molecular Biology, 1996. **260**(3): p. 289-298.

22.   Kar, S. and A.D. Ellington, *Construction of synthetic T7 RNA polymerase expression systems.* Methods, 2018. **143**: p. 110-120.

23.   Wang, Y., et al., *Metabolic Engineering of Escherichia coli for Production of α-Santalene, a Precursor of Sandalwood Oil.* J Agric Food Chem, 2021. **69**(44): p. 13135-13142.

24.   Zhang, J., et al., *Sesquiterpene Synthase Engineering and Targeted Engineering of α-Santalene Overproduction in Escherichia coli.* J Agric Food Chem, 2022. **70**(17): p. 5377-5385.

25.   Tippmann, S., et al., *Production of farnesene and santalene by Saccharomyces cerevisiae using fed-batch cultivations with RQ-controlled feed.* Biotechnology and Bioengineering, 2016. **113**(1): p. 72-81.

26.   Dong, H., L. Nilsson, and C.G. Kurland, *Gratuitous overexpression of genes in Escherichia coli leads to growth inhibition and ribosome destruction.* Journal of bacteriology, 1995. **177**(6): p. 1497-1504.

27.   Ngo, K.-S. and G.D. Brown, *Autoxidation of α-santalene.* Journal of Chemical Research, 2000. **2000**(2): p. 68-70.

28.   Baldwin, R.L., *Temperature dependence of the hydrophobic interaction in protein folding.* Proceedings of the National Academy of Sciences of the United States of America, 1986. **83**(21): p. 8069-8072.

29.   Rosano, G.L. and E.A. Ceccarelli, *Recombinant protein expression in Escherichia coli: advances and challenges.* Frontiers in microbiology, 2014. **5**: p. 172-172.

30.   Schein, C.H., *Soluble protein expression in bacteria*, in *Upstream Industrial Biotechnology*, M.C. Flickinger, Editor. 2013, John Wiley & Sons Incorporated: Hoboken, New Jersey.

31.   Andersson, L., et al., *Impact of plasmid presence and induction on cellular responses in fed batch cultures of Escherichia coli.* Journal of Biotechnology, 1996. **46**(3): p. 255-263.

32.   Riet, K.v.t. and J. Tramper, *Basic bioreactor design*. 1991, New York: Marcel Dekker.

Chapter 4

Towards biotechnological α-humulene production from glycerol

Humulus Lupulus

Towards biotechnological α-humulene production from glycerol

Abstract

This chapter aims at the biotechnological production of α-humulene, a sesquiterpene produced by *Humulus lupulus* using genetically engineered *E. coli* BL21 (DE3) and glycerol as substrate. Furthermore, a fed-batch cultivation with a constant feed was used for the estimation of the Herbert-Pirt parameters for substrate requirements for biomass formation (a $= -\frac{1}{Y_{X/S}^{max}}$) and maintenance ($m_s$), respectively: - 0.65 mol glycerol $\cdot$ (Cmol X^{-1}) and m_s = - 0.01 mol glycerol $\cdot$ (h $\cdot$ Cmol X)$^{-1}$.

Fed-batch experiments with varying glycerol feed rate focused on the influence of dodecane as organic phase for *in-situ* product recovery (ISPR) on specific α-humulene productivity. ISPR resulted in higher specific productivities (maximum $4.3 \cdot 10^{-3}$ Cmol P $\cdot$ (Cmol X $\cdot$ h)$^{-1}$), as compared to the absence of ISPR, for which a maximum specific productivity of $2.8 \cdot 10^{-3}$ Cmol P $\cdot$ (Cmol X $\cdot$ h)$^{-1}$ was obtained at the end of the experiment. The experiment without ISPR resulted in excessive foaming and required cyclic addition of anti-foam solution for effective foam control.

The decrease of cell viability in long bioprocesses, as observed in this work, results in the release of proteins into the broth. The removal of the hydrophobic product via ISPR increases the process productivity and facilitates longer processes. However, transfer of released proteins to the organic phase used for ISPR may complicate product recovery due to gel formation. Such multi-factors dynamics in broth composition imposes challenges towards the production of sesquiterpenes. Despite such challenges, the competitive α-humulene

productivities reported here represent advancements in utilizing *E. coli* BL21 (DE3) as host in fed-batch processes, compared to results obtained with other microorganisms reported so far.

4.1. Introduction

4.1.1. α-Humulene

Like other sesquiterpenes, α-humulene ($C_{15}H_{24}$) is formed from three units of isoprene, the basic building block of terpenes. The chemical structure is presented in figure 1. The name is derived from *Humulus lupulus (hops)* [1] as α-humulene was first discovered in the essential oils of this plant [2].

Combined with its oxidative products, α-humulene contributes to the hoppy flavor of beers [1] and has a woody odor [3]. Its content in essential hop oils differs depending on the source. Prominent varieties are Vanguard and Sterling, with α-humulene contents as high as 51.2 % and 41.6 %, respectively, followed by Willamette (32.5 %), Hallertau #2 (28.0 %), Hallertau #1 (22.7 %), Saaz #2 and #3 (17.4 %), Northern Brewer (17.2 %), Saaz #1 (16.9 %), and Cascade (12.6 %) [4]. Amarillo hops contain between 19 and 24 % [5].
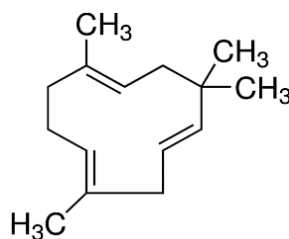

Figure 1. Alpha-humulene.

For the oxygenated α-humulene derivative, named zerumbone ($C_{15}H_{22}O$), a remarkable action against proliferation of colon cancer

cells has been confirmed [6]. Additionally, α-humulene has demonstrated anti-inflammatory [7-9], larvicide [10], insecticide [11] antitumor [12-15], antibacterial and antibiofilm properties [16], suggesting a strong potential for various applications.

Despite the great value of several terpenoids to industry, most of these compounds are naturally available in small quantities. Drawbacks such as the large consumption of environmental resources, impact of impurities and low yields have been reported for the extraction and purification of such substances from plants. Using engineered microorganisms is seen as an attractive alternative to both extraction and chemical synthesis [17], aiming at more economic and environmentally-friendly processes [18]. Regio- and stereoselectivity of enzymatic reactions are further advantages of biotechnological production of terpenoids [19].

Authors that worked on the characterization of α-humulene synthase described the biotechnological production of α-humulene from simple carbon sources as a possibility to supply this sesquiterpene in a steady and consistent manner, at reasonable costs [20]. Overall, a reduction of α-humulene production costs remains essential for its sustainable industrial production [21].

Table 1. ISPR strategies reported for α-humulene production from microorganisms:

ISPR material	Product titers	Ref.
n-dodecane (20 %)	2.0 g · L^{-1}	[22]
n-dodecane (20 %)	146 mg · L^{-1}	[23]
n-dodecane (20 %)	10.8 mg · L^{-1}	[24]
n-dodecane (10 %)	4.1 g · L^{-1}	[18]
Amberlite® XAD4	60.2 mg · L^{-1}	[25]
n-dodecane (20 %)	0.96 g · L^{-1}	[26]
n-dodecane (20 %)	0.83 mg · L^{-1}	[27]
n-dodecane (15 %)	1.6 g · L^{-1}	[28]
n-dodecane (10 %)	1.7 g · L^{-1}	[29]
n-dodecane (10 %)	1.3 g · L^{-1}	[30]

As seen from table 1, the main ISPR strategy reported for biotechnological production of α-humulene has been the utilization of solvent (dodecane), with the exception of [25] where hydrophobic resin was used for adsorption. Most publications reported fed-batch experiments for α-humulene production, however, batch [25] and shake flasks cultivations [26], [27] were also described.

Table 2. Achievements on biotechnological production of α-humulene:

Host	Product per present biomass	Volumetric *produc.	Specific *produc.	Ref.
	$\dfrac{mgP}{gDCW}$	$\dfrac{mgP}{L \cdot h}$	$\dfrac{mgP}{gDCW \cdot h}$	
Cupriavidus necator	36.4	5.8	0.1	[22]
Cupriavidus necator	17	0.06	0.1	[24]
Cupriavidus necator	16	4.6	1.8	[23]
Candida tropicalis	18.6	15.6	0.07	[18]
Escherichia coli	25.1	3.5	1.5	[25]
Escherichia coli	-	20.0	-	[26]
Methylotuvimicrobium alcaliphilum	0.75	0.01	0.01	[27]
Methylobacterium extorquens	55.0	13.8	0.46	[28]
Saccharomyces cerevisiae	110	10.2	0.65	[29]
Saccharomyces cerevisiae	67.3	9.3	0.48	[30]
Yarrowia lipolytica	230	30.7	1.2	[21]

*Produc.: productivity.

Several papers report the biotechnological production of α-humulene using *Escherichia coli* [25], [26]. Table 2 is an overview of productivities and yields for the biotechnological production of α-humulene. Most values were estimated from titers provided in original articles and further OD_{600nm} to biomass dry weight conversion factors described in literature per microorganism [31], [32], [33], [34].

This chapter aims at the development of the biotechnological production of α-humulene using *Escherichia coli* BL21 (DE3) in bench scale bioreactors, using dodecane extraction as the ISPR method. Different substrate feed rates were used, with manual control to avoid oxygen limitation. For one experiment, a constant glycerol feed was applied, to facilitate the estimation of the Herbert-Pirt parameters, which are required for scale-up studies (chapter 5).

4.2. Materials and Methods

4.2.1. Strain and pre-culture preparation

Escherichia coli BL21(DE3) (Novagen) was used as the host strain. The α-humulene producing strain (HP) contained genes from most of the mevalonate pathway integrated into the genome and one plasmid (pJ404, coding for alpha-humulene synthase expression) with an ampicillin resistance gene as selection marker.

The pre-culture was prepared according to the reference article [35] [supporting info, section "Sclareol production in *E. coli*"]. From frozen glycerol (25 % w·v^{-1}) stocks kept at - 80 °C, 500 µL was transferred to 10 mL of LB (Luria-Bertani medium) in baffled *Erlenmeyer* flasks (250 mL), glucose (10 g · L^{-1}) and carbenicillin (50 mg · L^{-1}). These flasks were incubated in an orbital shaker (Sartorius Stedim Biotech S.A., France), at 30 °C and 200 rpm. The first incubation lasted approximately 15 h, whereafter the culture was transferred to 200 mL of the same fresh medium and incubated under the same conditions for another 10.5 h in baffled *Erlenmeyer* flasks (500 mL). When the preculture reached and OD$_{600nm}$ between 5 and 8, it was used for reactor inoculation, aiming at an initial OD$_{600nm}$ of the bioreactor culture of around 0.2.

4.2.2. Experimental set up

Aerobic fermentation experiments under glycerol limitation were performed in fed-batch mode in jacketed stirred 2L bench reactors (Applikon, The Netherlands), equipped with a single 6-blade Rushton impeller (diameter 45 mm) and controlled by a BIOSTAT® Bplus system (Sartorius). Mass flow controllers (Brooks, U.S.A.) were used to control the aeration rate at 1.5 nL · min⁻¹. Phosphoric acid (3 M) and ammonium hydroxide (5 M) solutions were used for pH control. The substrate solution was fed using a Masterflex peristaltic pump (Cole Parmer, U.S.A), while each of the other integrated pumps of the Sartorius BIOSTAT controller was used for the addition of acid, base, dodecane and antifoam solution into the bioreactor. For experiments 6, 7 and 8, a sterile Erol-DF7911K (PMC Ouvrie, France) aqueous solution of 10 % w·w⁻¹ was used for foam control based on detection by a conductivity probe.

For Experiment 9, a 10 % w·w⁻¹ aqueous solution of Pluronic L-81 (Sigma- Aldrich) was used for cyclic addition of antifoam as Erol-DF7911K was not available anymore. From the inoculation, a 90 min interval was set between antifoam solution addition steps (1 second/pulse) decreasing to 60 min after induction. After induction (9.9 h of fed-batch cultivation) until 28.5 h of fed-batch cultivation, the interval was further decreased to 30 min. After 35.4 h of fed-batch cultivation the interval was decreased to 15 min. For every pulse during such cyclic addition, approximately 0.5 g of the 10 % w·w⁻¹ aqueous solution of Pluronic L-81 was added to the broth.

4.2.3. Batch phase

The bioreactor vessel with mineral "AM" medium (4.2 $g \cdot kg^{-1}$ KH_2PO_4, 12.0 $g \cdot kg^{-1}$ K_2HPO_4, 2 $g \cdot kg^{-1}$ $(NH_4)_2SO_4$, 1.7 $g \cdot kg^{-1}$ citric acid, 8.0 $mg \cdot kg^{-1}$ EDTA 1.3 $g \cdot kg^{-1}$ $MgSO_4 \cdot 7H_2O$) adapted from reference article [35] was autoclaved at 121 °C for 20 minutes after pH probe calibration. After cooling down to room temperature sterile water, yeast extract, glycerol solution, carbenicillin (to reach 5 $g \cdot L^{-1}$, 30 $g \cdot L^{-1}$ and 50 $mg \cdot L^{-1}$ final concentrations, respectively) and 1 % $v \cdot v^{-1}$ of trace elements solution (10 $g \cdot kg^{-1}$ $Fe_{(III)}$citrate, 0.25 $g \cdot kg^{-1}$ $CoCl_2 \cdot 6H_2O$, 1.5 $g \cdot kg^{-1}$ $MnCl_2 \cdot 4H_2O$, 0.15 $g \cdot kg^{-1}$ $CuCl_2 \cdot 2H_2O$, 0.3 $g \cdot kg^{-1}$ H_3BO_3, 0.25 $g \cdot kg^{-1}$ $Na_2MoO_4 \cdot 2H_2O$, and 1.3 $g \cdot kg^{-1}$ $Zn(CHCOO)_2 \cdot 2H_2O$) were added to obtain 1 kg of medium at the start of the batch phase. The carbenicillin solution was filter sterilized (0.22 µm), while the other solutions were autoclaved separately at 121 °C for 20 minutes.

After dissolved oxygen probe calibration, the pH and temperature were controlled at 7.0 and 30 °C respectively. For experiments 6, 7 and 8: respectively 110.2 g (10.0 % $w \cdot w^{-1}$), 44.1 g (4.3 % $w \cdot w^{-1}$) and 106.7 g (9.3 % $w \cdot w^{-1}$) of filter sterilized (0.22 µm) dodecane containing oil red O (50 $µg \cdot g^{-1}$ of organic phase) were pumped into the reactor just after inoculation for *in situ* product recovery. Experiment 9 was an exception, since no dodecane was used.

4.2.4. Fed-batch phase

Glycerol was used as carbon source for all experiments, with concentrations of 350 g · kg^{-1} feed was used for Exp$_s$ 6, 8 and 9 and 200 g · kg^{-1} feed for Exp 7. The composition of the feed medium was adapted from Schalk *et al* [35]. In brief EDTA (13 mg · kg^{-1}), MgSO$_4$·7H$_2$O (12.0 g · kg^{-1}) and glycerol were dissolved in approximately 900 mL of water and autoclaved at 121 °C for 20 minutes. After cooling down, 2 mL of a filter sterilized (0.22 µm) stock solution of thiamine hydrochloride (250 g · L^{-1}stored in the - 80 °C freezer) and 10 mL of a sterile trace elements solution (same composition as described in section 4.2.3) were added under sterile conditions. Finally, heat sterilized deionized water was added to obtain a final mass of 1 kg of feed medium.

The feed phase was started at 13.2 - 13.5 h after inoculation for all reactors (appendix A, table 5). After 8 to 12 hours of feeding, when the OD$_{600nm}$ reached a value of 60, the filter sterilized (0.22 µm) inducer IPTG (Isopropyl β-D-1-thiogalactopyranoside) solution was injected under sterile conditions into the reactor to reach an initial concentration of 0.1 mM. Prior to induction the temperature was decreased from 30 to 25 °C [35]. Inducer concentrations between experiments were comparable and trends for volumetric inducer concentrations versus time are available in Appendix B.

To achieve approximate dissolved oxygen ranges of around 30 % through most of the cultivation time, feed rates were manually controlled between 2.5·10^{-2} and 4.8·10^{-2} mol glycerol · h^{-1} for experiment 6, 2.8 ·10^{-2} and 5.5 ·10^{-2} mol glycerol · h^{-1} for experiment 7

and $1.0 \cdot 10^{-2}$ and $2.9 \cdot 10^{-2}$ mol glycerol $\cdot$ h^{-1} for experiment 9 (as shown in figure 2). The substrate feed rate was kept constant ($3.85 \cdot 10^{-2}$ mol glycerol $\cdot$ h^{-1}) for experiment 8. Usually, an automatic control of the dissolved oxygen was used according to the protocol used as reference, but technical limitations required a manual control.

Unfortunately, in experiment 7, the oxygen probe malfunctioned after 45.8 h (approximately 32 h into the feed phase). After this moment, the feed rate was manually set at a constant value of $2.8 \cdot 10^{-2}$ mol glycerol $\cdot$ h^{-1} to lower the oxygen demand until the end of this experiment (figure 2). For Exp$_s$ 6 and 7, carbenicillin was only supplied with the batch medium (0.05 g $\cdot$ L^{-1}, filter sterilized using 0.22 µm pore membrane) and was not added to the feed.

Antibiotic concentrations were expected to decrease with time due to, at least, dilution (degradation as mentioned in literature for previous chapters, also occurs).

In contrast to Exp$_s$ 6 and 7 for Exp$_s$ 8 and 9 carbenicillin (0.05 g $\cdot$ L^{-1}) was added to the feed medium to maintain the selection pressure during the feed phase as constant as possible.

During the fed-batch, the dodecane percentage decreased as the feed medium was continuously pumped into the vessel. Appendix A presents further information on the applied protocols in tables 5 and 6 (main features: feed start, dodecane addition, induction time). Tables 7 and 8 refer to information about ages (total and feed phase ages).

4.2.5. On-line analyses

Exhaust gas from the bioreactors was cooled to 4 °C by an in-line condenser and dried by a Nafion dryer (Permapure, Toms River, NJ, USA). The concentrations (% $v \cdot v^{-1}$) of carbon dioxide and oxygen in the dry exhaust gas were quantified with a Rosemount NGA-2000 gas analyzer (Fisher Rosemount, Germany) whereby the measurement data were stored using data acquisition software (MFCS/Win 2.1, Sartorius Stedim Biotech S.A., France). This software was also used to store the other data (pH, temperature and DOT, and masses of base and feed solutions versus time) obtained through probes (Mettler Toledo or Applikon, The Netherlands) or scales (Mettler Toledo, The Netherlands).

4.2.6. Off-line analyses

Sesquiterpene extraction and quantification, determination of cell dry weight and optical density and estimation of the Herbert-Pirt parameters were carried out as described in chapter 2. For gas chromatography, the method settings were exactly the same as described in chapter 2, however, α-humulene was detected at a retention time of 8.3 minutes.

4.2.6.1 Protein analysis and β-lactamase test (experiment 9, only)

Total protein measurements were carried out with the Bradford method (Sigma-Aldrich, 3.1 mL assay), expressed in bovine serum albumin (BSA) units. A calibration curve using 0.25 g · L^{-1}, 0.5 g · L^{-1}, 1.0 g · L^{-1} and 1.4 g · L^{-1} BSA was used. The absorbance was read at (λ = 595 nm) for supernatant samples diluted 25-fold. The centrifugation was performed using a Heraeus Biofuge Pico centrifuge at 13000 rpm for 5 minutes.

A colorimetric beta-lactamase activity assay kit (ab197008, Abcam) was used to detect the specific activity for that enzyme. The amount of beta-lactamase required to hydrolyse 1.0 µmol of nitrocefin per minute at pH 7.0 at 25 °C, defined as the unit, was calculated as mU · mL^{-1}. Samples from experiment 7 were submitted to multi assay plates according to the instruction of the supplier using 1.25, 2.5 and 5 as dilution factors. A Microplate Reader (Tecan Infinite Pro 200, λ = 490 nm), with the software Magellan version 7 was used.

4.2.6.2. Viable cell count assay

Samples (50 µL) from the original broth were four times sequentially diluted in 4.95 mL of sterile saline solution (0.9 % w·v^{-1} NaCl). Two different dilutions (usually 10^8 and 10^7) were prepared per sample (for experiment 9, this also included samples from a lower dilution factor: 10^6). Then, 150 µL of the dilution was plated in Petri dishes containing LB medium (5 g · kg^{-1} bacto-tryptone, 10 g · kg^{-1}

yeast extract, 10 g·kg^{-1} sodium chloride) with 1.5 % agar, free of antibiotics, using the spread-plate method. Plates were placed at 30 °C during 48 h in an incubator (Heraeus instruments, Germany). Then, the number of colony-forming units per mL of the original sample were calculated from the obtained CFU counts on the plates, provided that the CFU counts were between 20 to 250 per plate. The percentage of viable cells was calculated based on quantification of CFU per g of biomass (DCW) using as reference the value before induction for that dilution.

4.2.7. Specific growth rate and Herbert-Pirt parameter calculations:

The parameters a and m_s were estimated for the humulene-producing strain using the total biomass vs time data from experiment 8 according to the procedure described in chapter 2.

4.2.8. Determination of specific rate of product formation (q_p) versus time

For the determination of the specific rates of product formation, q_p, (Cmol P · (Cmol X · h)$^{-1}$), curve fitting was applied in Excel to the accumulation data of product (Cmol P) versus time. From the first derivatives of these curves the rate of product formation, R_p, (Cmol P · h^{-1}) versus time was obtained. Next, R_p fits were divided by the fits of biomass accumulation versus time Mx(t) (Cmol X) that had been obtained in Excel. Both the division and the plotting tasks were

performed in MATLAB using the fplot function defining (t) as variable. All product related accumulation or formation rates fits described here were used only for time ranges of between the first samples were α-humulene was detected up to the maximum amount of humulene reached.

4.2.9. Relation between specific product formation and specific growth rate

The specific growth rate (μ) values estimated during the feed phase were plotted versus the specific production rates (q_p) in MATLAB using the Curve Fitter app.

4.2.10. Chemicals

Alpha-humulene standard (≥ 96 %) and IPTG (Isopropyl β-D-1-thiogalactopyranoside) were purchased from Sigma-Aldrich (U.S.A).

4.3. Results

In this chapter, four experiments using the humulene-producing strain are described. This strain is known to have much higher sesquiterpene titers and productivities than the santalene producing strain (Chapters 2 and 3).

4.3.1 Higher dodecane fraction and long duration (experiment 6) versus lower dodecane fraction in feed and short duration (experiment 7)

Different glycerol concentrations in the feed were used for these experiments, respectively: 35 % w·w^{-1} for Exp 6 and 20 % w·w^{-1} for Exp 7 (see table 5, appendix A for an overview). For the longest experiment (Exp 6), a higher glycerol concentration in the feed was applied to limit the volume increase (maximum working volume should be ideally, 1.7 L).

Figure 2 presents the substrate feed rates in grey or black dashed lines for Exp 6 (0.025 - 0.048 mol · h^{-1}) and Exp 7 (0.027 - 0.055 mol · h^{-1}), respectively. Manual rate adjustments were performed in order to avoid oxygen limitation after a technical issue with the cascade control of the feed.

Experiment 6 lasted nearly 134 h. After 120 h, as occurred for other experiments, a strong oscillation occurred for carbon dioxide and dissolved oxygen (between 24.2 % < DOT< 74 %, no results shown). A more stable DOT profile (33.2 - 69.2 %) occurred for experiment 7, the shortest.
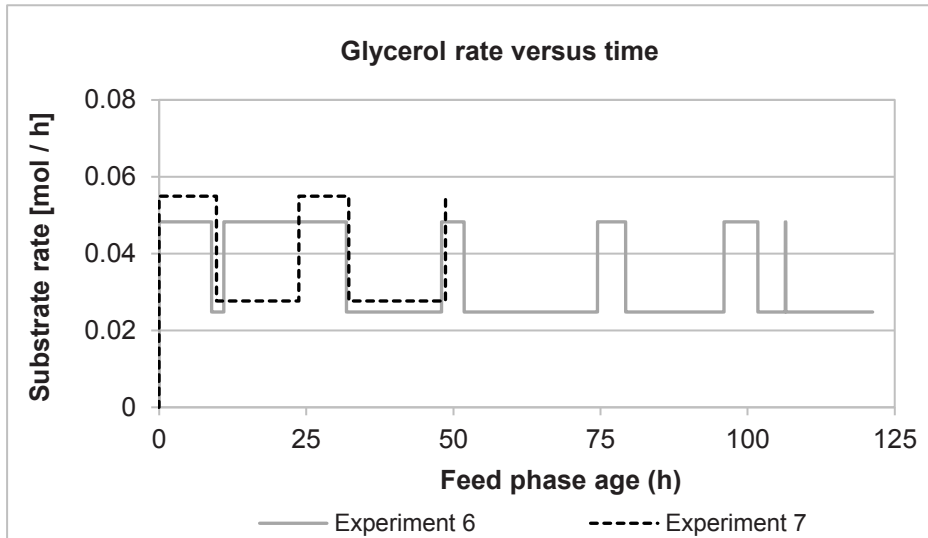
Figure 2. Substrate feed rate (mol glycerol · h⁻¹), per fed-batch experiment.

Figure 3 presents the α-humulene accumulation in broth with time. The total amount of humulene increased until 0.87 g at the end for the short experiment (Exp 7, performed with a lower initial dodecane concentration, 4.3 % w·w⁻¹), which was comparable to Experiment 6 up to this timepoint. Further, approximately 3.5-fold that amount was achieved around 118.8 h of feed for Exp 6 (long experiment with a higher initial dodecane concentration:10.0 % w·w⁻¹).
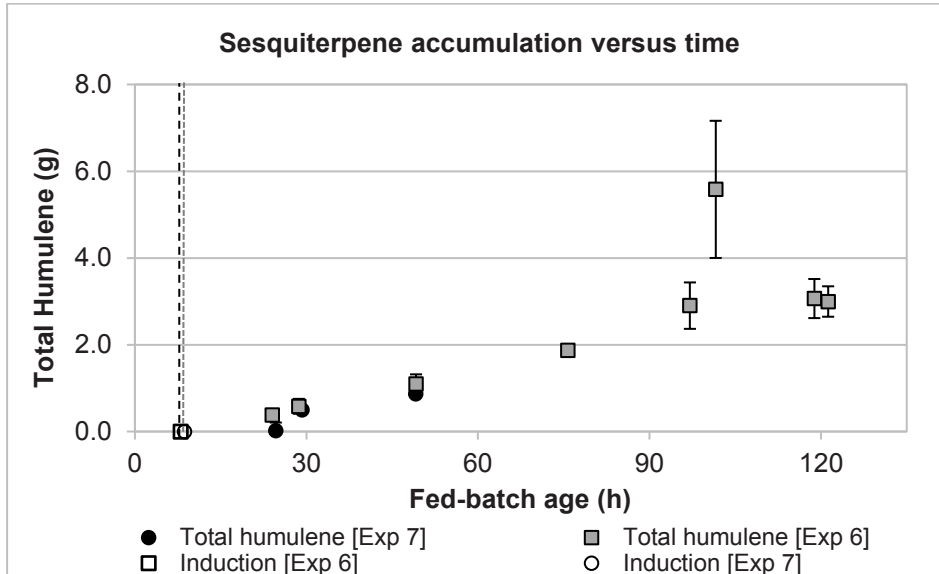
Figure 3. Total humulene accumulation: squares and circles for fed-batch Exp$_s$ 6 and 7, respectively. Open symbols with dashed lines indicate the time of induction.

Humulene accumulation at 102 h had a high standard deviation and was considered an outlier. Both experiments had high standard deviations for some samples (> 30 % of average) due to difficult product extraction. Bars represent standard deviations for 3 replicates for most samples, with the exception of those taken at 97.1 and 101.6 h of feed (n = 2) [Exp 6] (broken extraction tubes).
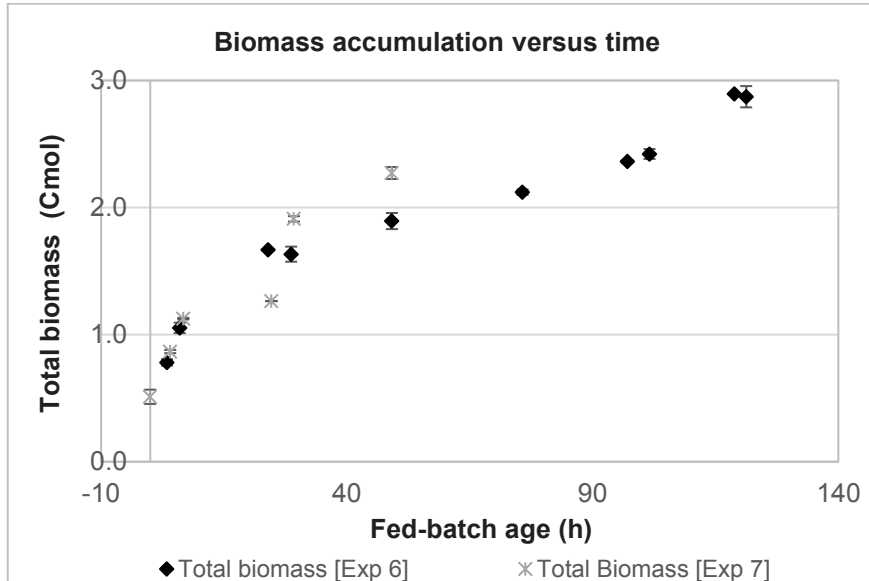
Figure 4. Total biomass accumulation during fed-batch cultivations Exp 6 and Exp 7. Vertical bars represent standard deviations (n = 2).

Figure 4 represents the biomass accumulation, calculated from the measured biomass concentration and calculated broth volume, for both experiments. Experiment 6 reached 2.90 Cmol X after 118 h of feeding, while Exp 7, which had a slightly higher average glycerol feed rate ($3.88 \cdot 10^{-2}$ mol $\cdot$ h^{-1} versus $3.33 \cdot 10^{-2}$ mol $\cdot$ h^{-1} for Exp 6), resulted in 2.27 Cmol X after 49.1 h of feed phase. Standard deviations for dry cell mass measurements did not exceed 11.4 % of average (maximum concentrations in table 5, appendix A).

The presence of dodecane appeared to be a source of variation for the viability assay by means of CFU counting, as the organic phase was not removed prior to the plating procedure. This resulted in high standard deviations.

4.3.2. Supply of antibiotics with the feed solution in the presence (experiment 8) and absence of organic solvent (experiment 9)

Contrasting to Exp_s 6 and 7 for this chapter, where the antibiotic concentrations in the culture decreased with time as a result of dilution/degradation, for Exp_s 8 and 9 the goal was to maintain the selection pressure as constant as possible, thus, the same concentration of carbenicillin (0.05 g $\cdot$ L^{-1}) was used for batch and feed medium preparations. The glycerol concentration in feed solution was the same for Exp_s 8 and 9 (35 % w$\cdot$w^{-1}). Experiment 9 differed from the other experiments with respect to the absence of dodecane.

4.3.2.1. Constant (theoretical) antibiotic concentration in the presence of dodecane (experiment 8) and constant glycerol feed rate

This experiment lasted nearly 120 h and the substrate feed rate was kept constant at 3.85$\cdot$10^{-2} mol glycerol $\cdot$ h^{-1}. A maximum biomass concentration of 38.49 ± 1.13 g X $\cdot$ (kg broth)$^{-1}$ was reached. No oxygen limitation was observed as the dissolved oxygen tension varied between 30.9 % and 72.2 %. Appendix A (tables 5 to 8) provides a detailed experiment overview, as well as ages for key steps and samples.

After 73.3 h of feed, the total maximum product accumulation of 4.55 g was reached (figure 5), which was almost 2.5-fold higher than what was reached in Exp. 6 after a similar period of fed-batch

cultivation. Open symbol with dashed line indicates when induction was performed. During the product extraction, gel formation occurred for sample 4 after dodecane mixing and centrifugation, decreasing the homogeneity expected for organic phase recovery. A high standard deviation was observed for that specific sample (32.5 h of feed). Proteins and their interaction with surface-active compounds (SACs) have possibly induced gel formation. Figure 6 shows the total biomass versus time profile.
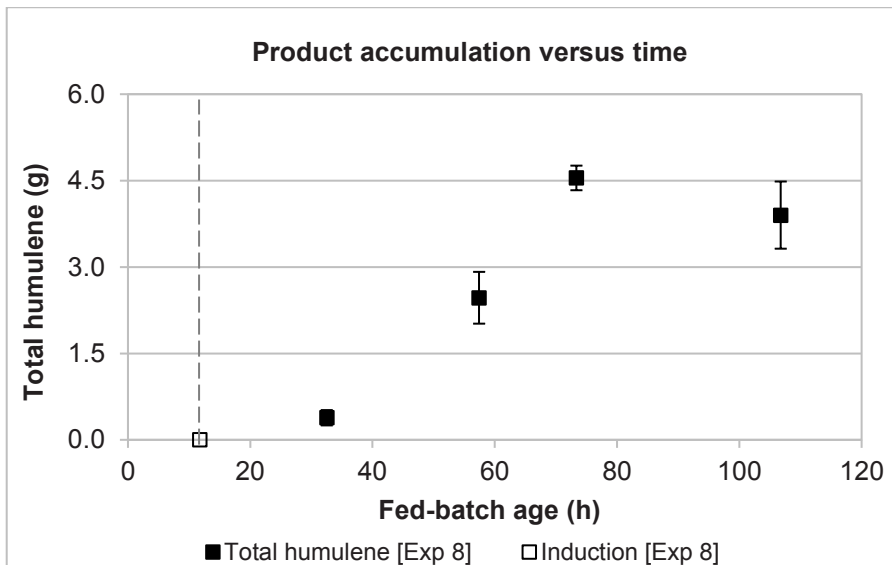

Figure 5. Product accumulation versus time in the vessel (squares) during fed-batch cultivation Exp 8. Bars represent for standard deviations for n = 3 (different extraction tubes).

Antifoam addition was controlled by probe contact and a final concentration of 0.98 % w·w^{-1} of broth was reached. Nevertheless, intense foaming occurred during this experiment. For previous experiments, foam formation had been observed mainly after

induction, at the moment of dodecane addition or just after this last step. Possibly the higher antibiotic concentration (due to the supply with the feed) could have triggered a stress response, resulting in increased cell lysis.
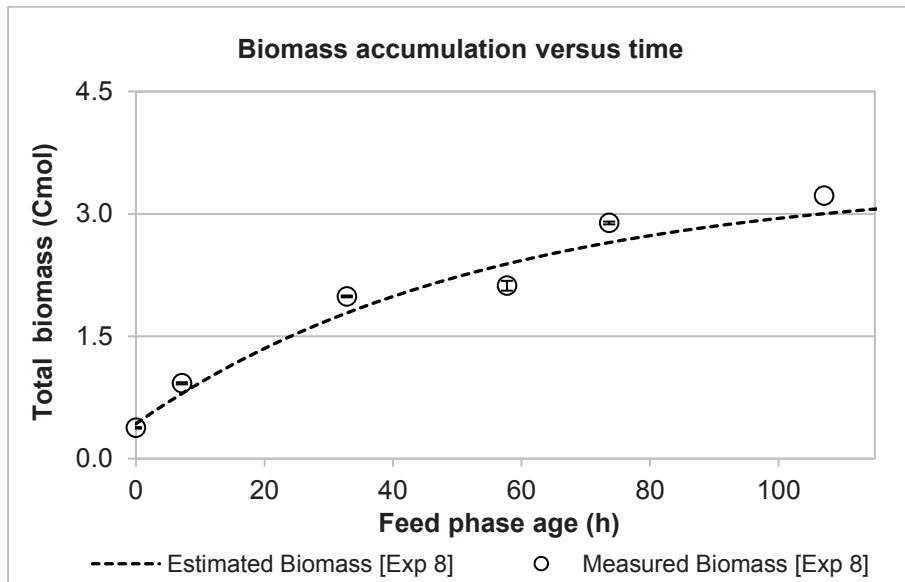

Figure 6. Experimental values of total biomass (dots) and fitted theoretical curve (dashed line) for the Herbert-Pirt parameters shown in Table 3. Error bars represent standard deviations (n = 2).

4.3.2.1.1. Herbert-Pirt parameters

In table 3, the estimated values of the Herbert-Pirt parameters based on the equation of total biomass (Cmol X), for a constant feed profile are shown (estimation procedure described in chapter 2). The absolute values of these parameters obtained here were slightly higher than those reported for *Escherichia coli MG1655* for growth on glycerol: a = - 0.47 mol glycerol $\cdot$ (Cmol X)$^{-1}$ and m_s = - 0.0066 mol glycerol $\cdot$ (h $\cdot$ Cmol X)$^{-1}$ [36], but closer to the parameters resulting from experiment 3 of this thesis: a = - 0.70 mol glycerol $\cdot$ (Cmol X)$^{-1}$ and m_s = - 0.008 mol glycerol $\cdot$ (h $\cdot$ Cmol X)$^{-1}$.

Table 3. Herbert-Pirt parameters during fed-batch phase for experiment 8. The term S indicates glycerol, hereby simplified for visualisation purposes:

a	m_s	Glycerol feed rate $\cdot 10^2$	$\mu_{initial}$
$\dfrac{mol_{glycerol}}{Cmol_x}$	$\dfrac{mol_{glycerol}}{Cmol_x \cdot h}$	$\dfrac{mol}{h}$	$\dfrac{1}{h}$
-0.62 ± 0.19	-0.011 ± 0.003	3.9	0.13

The specific growth rate versus time is presented in figure 7. An initial value of 0.13 $\cdot$ h^{-1} was estimated for μ, decreasing asymptotically with time, as expected for fed-batch experiments with a constant feed.
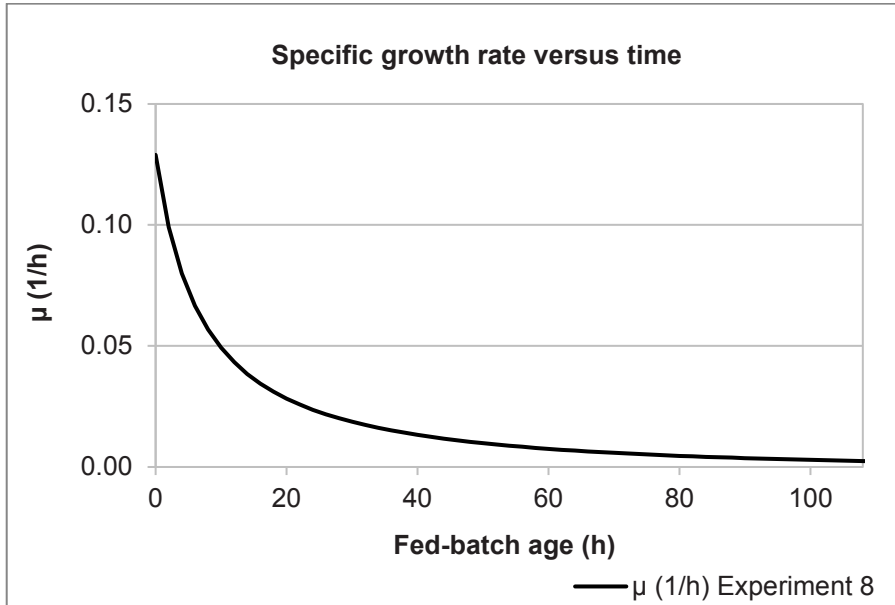
Figure 7. Estimated specific growth rate versus time for fed-batch experiment 8, calculated using equation 12 (Chapter 2, Appendix B).

4.3.2.2. α-Humulene production in the absence of organic solvent (Exp 9)

Contrasting to experiment 8, the absence of dodecane was tested (in situ product recovery was not performed in this reactor). The feed solution contained antibiotics prepared according to the values used for batch phase, to keep the concentration of carbenicillin (0.05 g · L^{-1}) as constant as possible.
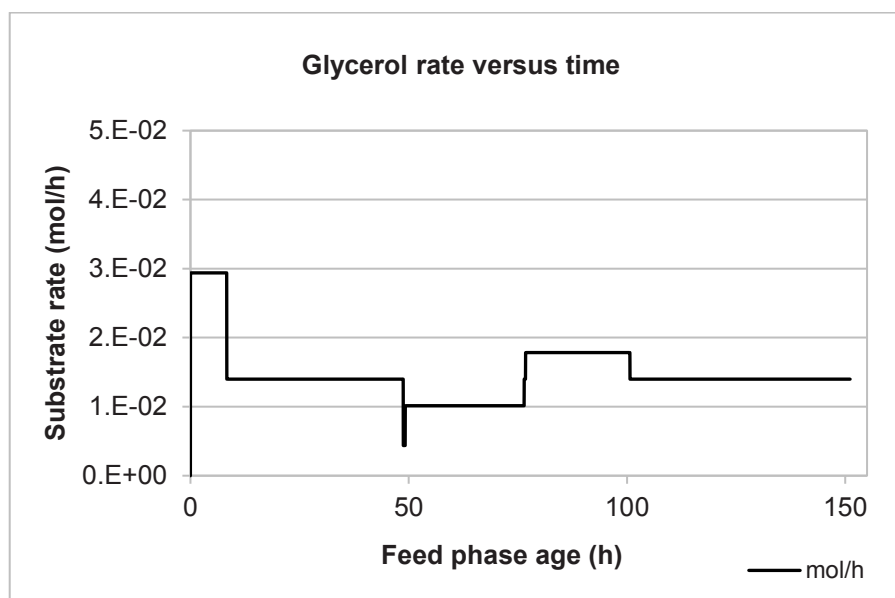
Glycerol rate versus time

Figure 8. Glycerol rate versus time for fed-batch experiment 9.

This experiment (Exp 9) demanded an intensive foam control. For previous experiments, the antifoam control had been based only on probe detection. During Exp 9, though, a cyclic addition of anti-foam

solution was necessary, in which the interval between antifoam additions was decreased in time (see section 4.2.2 for details).

The glycerol feed rate was manually controlled between $1.0 \cdot 10^{-2}$ and $2.94 \cdot 10^{-2}$ mol glycerol $\cdot$ h^{-1} (figure 8) whereby the average feed rate was $1.45 \cdot 10^{-2}$ mol $\cdot$ h^{-1}. Initially it was planned to use a constant feed rate of $2.94 \cdot 10^{-2}$ mol glycerol $\cdot$ h^{-1}, however, after the dissolved oxygen tension (DOT) approached 20 %, and manual control of the feed rate was required to avoid oxygen limitation and keep the DOT around 40 %.
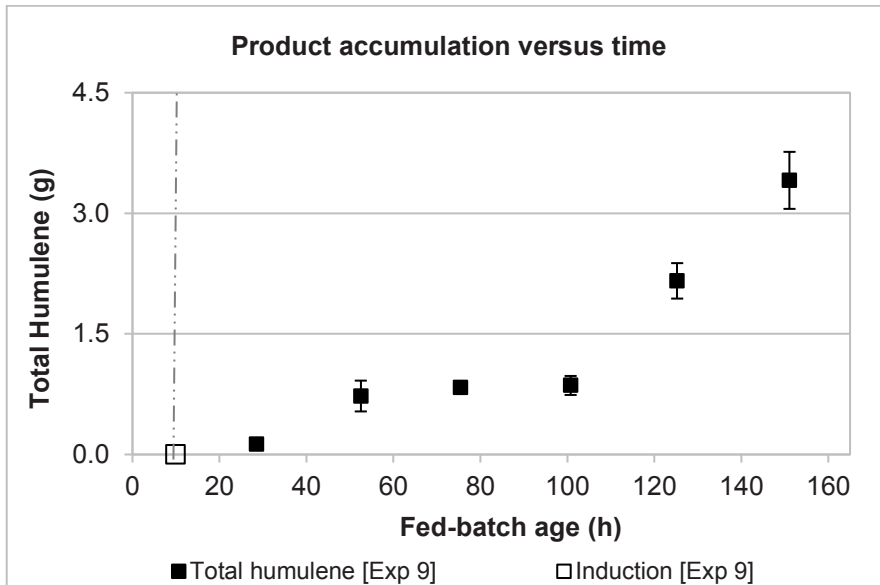

Figure 9. Total terpene accumulation for fed-batch Experiment 9 (dodecane-free). Bars represent standard deviation (n = 3).

For this experiment the α-humulene accumulation initially increased, levelled off between 50 and 100 h of cultivation and increased further thereafter (figure 9), reaching 3.41 g after 151 h of feed. This amount was significantly lower than the maximum amount of 4.55 g accumulated after 73 hours in experiment 8, which was carried out in the presence of ISPR. However, in contrast to what was observed for the dodecane free experiment, the total amount of product seemed to have levelled off in Exp. 8 after 73.3 h of feed (figure 5). For experiment 9, the total protein concentration in the culture supernatant was measured using the Bradford method (Figure 11), to serve as a second measure of cell lysis next to the relative viable cell count determination through CFU counts (Figure 10). For experiments carried out in the presence of dodecane, protein analysis was not possible due to interaction between surface-active compounds and the organic phase. Also, as has been mentioned above, CFU counts were not very reliable in the presence of dodecane.

As can be seen from figure 10, the relative viable cell count decreased significantly in time. After 52.5 h of fed-batch cultivation (42.6 h after induction), the relative viability reached a minimum value and partially recovered thereafter.

The specific protein concentrations for all supernatant samples from Exp 9 are shown in figure 11. The specific protein concentration increased in time, to level off after 75 hours of cultivation. Although the minimum relative viable cell count, reached after 52.5 h of cultivation did not correspond with the highest relative protein level, the measured

protein levels seem to confirm the decrease of the viable cell count with time.
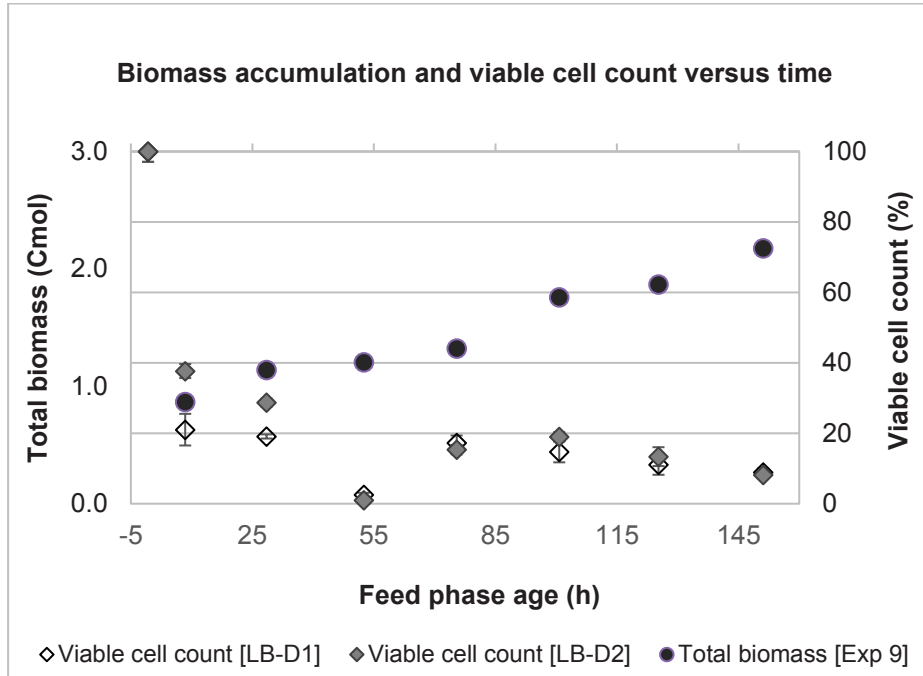
Figure 10. Total biomass (filled black circles) and the viable cell count (CFU $\cdot$ (g DCW)$^{-1}$ relative to CFU$\cdot$(g DCW)$^{-1}$ before induction), for two dilutions: D1 (empty diamonds); D2 (dilution 2, bright grey diamonds) for the dodecane free fed-batch experiment (Exp 9).

All samples for Exp 9 were submitted to the beta lactamase multi-assay test (see materials and methods) with different dilution factors (1.25, 2.5 and 5). No detection occurred for a dilution factor higher than 1.25. Differences in absorbances were barely observed for those. The quantification of the β-lactamase activity was only possible when the levels of protein detected were as high as 13.32 g $\cdot$ L^{-1}

(sample 9, 151.5 h of feed), indicating $3.33 \cdot 10^{-3}$ mU $\cdot$ mL^{-1} $\pm$ 0.3 %. Thus, the beta lactamases were only present in very low concentrations for most of the dilution factors used here and were near the detection limit. Unfortunately, due to time limitations, a repetition of this test for lower dilution factors was not possible.
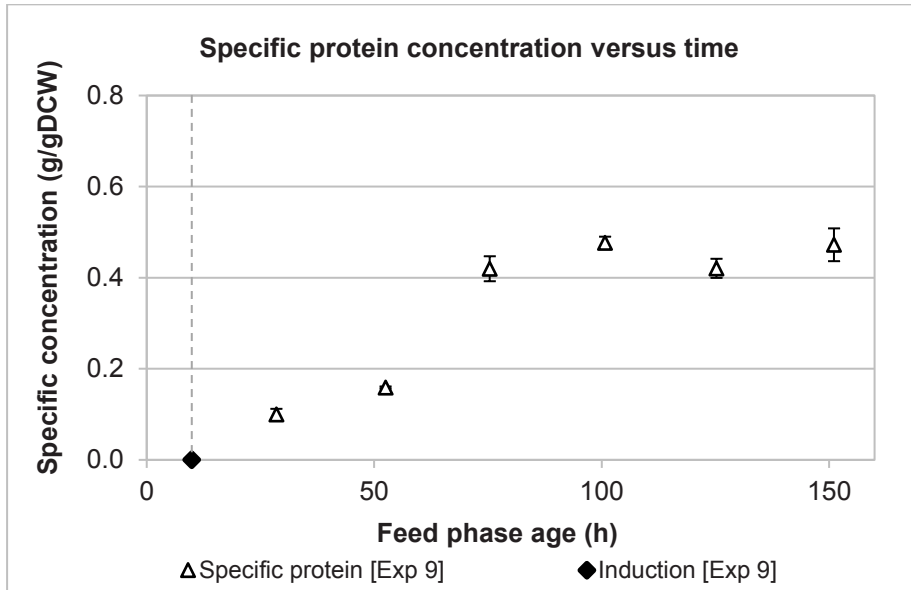
Figure 11. Specific protein concentration in broth during dodecane free fed-batch cultivation Exp 9. Bars indicate standard deviations for n = 2.

As indicated in figure 12, specific productivities reported for the solvent free experiment (Exp 9) ranged between $3.4 \cdot 10^{-4}$ Cmol P $\cdot$ (Cmol X $\cdot$ h)$^{-1}$ to $2.8 \cdot 10^{-3}$ Cmol P $\cdot$ (Cmol X $\cdot$ h)$^{-1}$ and reached the highest q_p only after 151.1 h of feed phase. Nevertheless, the product compartmentalization that occurred by using ISPR (Exps 6 and 8)

resulted in higher specific productivity ranges from the start of the feed phase, as compared to the experiment performed in the absence of dodecane. The highest specific productivity as compared to all other experiments was for Exp 8, reaching $4.35 \cdot 10^{-3}$ Cmol P $\cdot$ (Cmol X $\cdot$ h)$^{-1}$ at 74 h of feed phase.
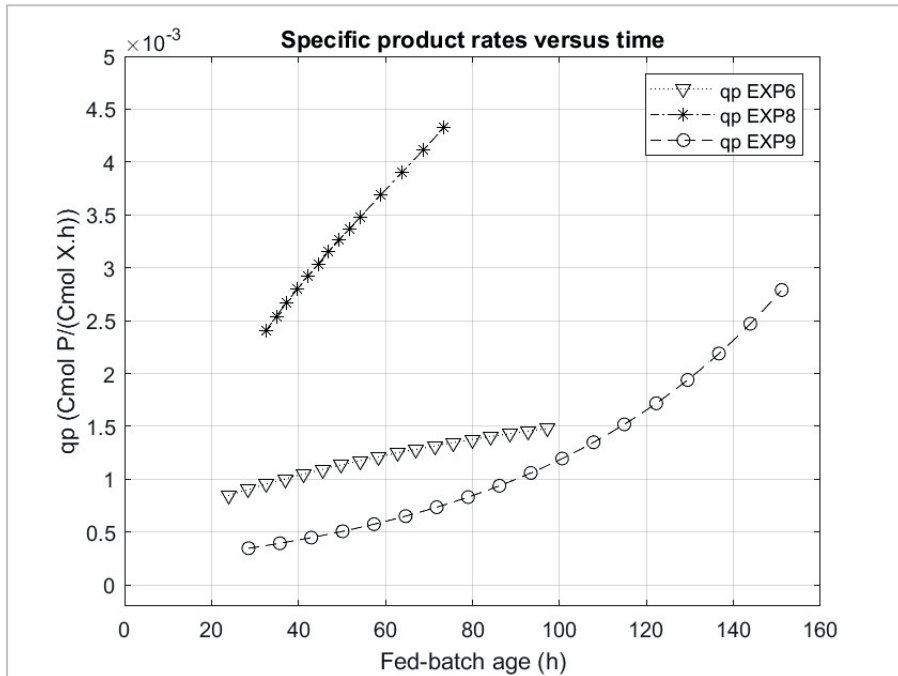
Figure 12. Calculated specific humulene formation rates (q_p) versus time for fed-batch experiments 6, 8, and 9.
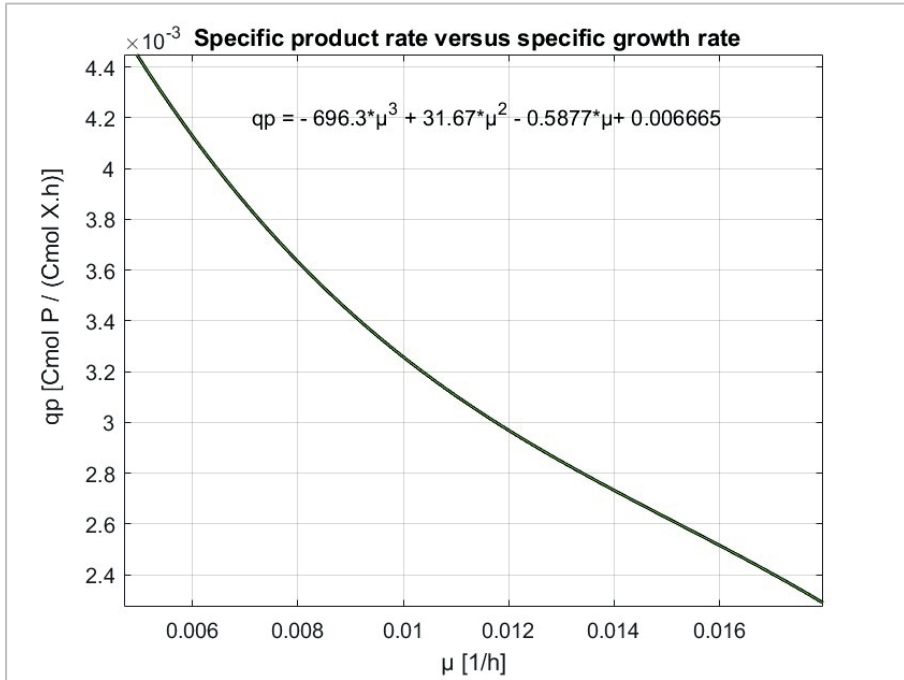
Figure 13. Polynomial fit of specific product rate **[Cmol P · (Cmol X · h)$^{-1}$]** versus specific growth rate (μ) for fed-batch experiment 8: 32 h to 74h of feed phase, $R^2 = 0.99$.

For experiment 8, a plot of specific productivity ranges versus specific growth rate is presented in figures 13 and 14. For the time range studied (32 to 74 h of fed-batch), the lower the growth specific rate reported, the higher was the specific productivity. A polynomial of grade 3 fit resulted in the best correlation coefficient.

Figure 14.Polynomial fit (used in Chapter 5) of specific product rate
[Mol P · (Cmol X · h)$^{-1}$] versus specific growth rate (μ) for fed-batch
experiment 8: 32 h to 74h of feed phase, R^2 = 0.99.

4.4. Discussion

Despite the fact that the same protein expression system (T7) was used, the santalene producing (SS) and humulene producing (HS) strains differed massively with respect to their specific terpene productivities. A 50 % lower α-santalene yield on biomass (as compared to farnesene yield) has been reported for a similar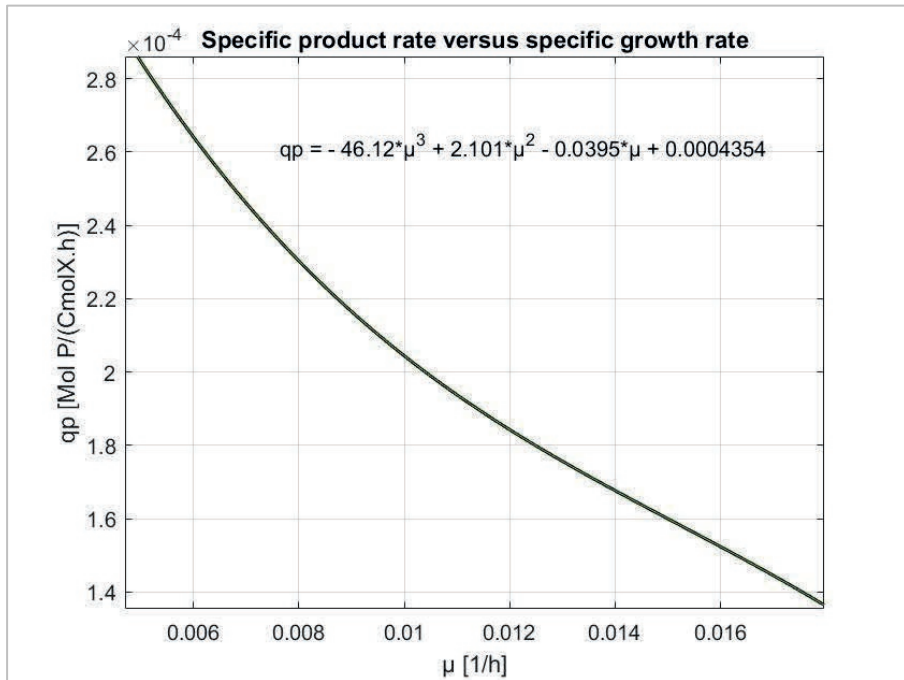 strain background. The authors [37] suggested as possible explanation for this difference, that the kinetics of the α-santalene synthase could be negatively influenced by the complexity of cyclization required for α-santalene formation.

A serious drawback of our *E. coli* fermentations was that a considerable extent of cell lysis occurred after induction, resulting in protein release into the broth. Decrease in cell viability has been reported before for *Escherichia coli* BL21(DE3), resulting from factors such as IPTG utilization, presence of plasmid DNA and metabolic burden related to the heterologous pathway [38]. Therefore, consequent challenges for the biotechnological production of sesquiterpenes such as loss of productivity and foaming (upstream processing) and gel formation (hindering coalescence and downstream processing) are expected.

Nevertheless, the product titers reported here exceeded the values previously reported for *E. coli* in literature [25], [26] for different cultivation strategies. However, α-Humulene titers of comparable magnitude were published for other bacterial hosts (*C. necator* [22], *M. extorquens* [28]) and yeasts (*C. tropicalis* [18], *S. cerevisiae* [30], [29] and *Y. lipolytica* [21]), see table 1.

Product yield on biomass for the three long fed-batches (Exp$_s$ 6, 8 and 9) reported in this chapter were at least 60 mg P · gDCW^{-1}, which exceeds published values estimated for *E. coli* [25] (table 2). When comparing with α-humulene production in other hosts, the products per present biomass achieved here were comparable to estimated values from data presented in [28] and [30], but lower than reported α-humulene yields on biomass for *S. cerevisiae* [29] and *Y. lipolytica* [21].

The specific humulene productivities achieved in experiments 6 and 8 (respectively 0.95 and 1.04 mg P · (g DCW · h)$^{-1}$) surpassed others from this chapter (table 8). Such productivities are greater than most related literature values shown in table 2, except for those reported for *Y. lipolytica* [21], *C. necator* [23] and *E. coli* [25]. It is possible that the decrease in viability (and lysis) reported [Exp 9] could have affected the specific productivity in the long term, as compared to batch with *E. coli* [25].

As seen in table 4 (appendix A), the addition of antifoam solution had to be increased in the last solvent free experiment (identified here as 9), which led to a final antifoam concentration of 2.1 % w·w^{-1}.

The absence of organic phase increased the demands for anti-foam (foam-out events occurred when a non-cyclic addition of antifoam was tested for similar feed rates to the used in Exp 8, using this same strain).

The utilization of a water immiscible organic phase to extract hydrophobic fermentation product *in situ* is a key strategy to improve performance in bioprocesses. The presence of dodecane (Exp$_s$ 6 and 8) not only led to the higher specific productivity ranges for the first

humulene extraction samples (figure 12) but overall minimized the foam formation, a disturbing factor in bioprocesses. The most logical explanation for both effects relates to the compartmentalization of α-humulene and proteins in the organic phase. However, these positive effects contrast to the negative interaction of the solvent with some surface-active compounds such as proteins Therefore, for this process, foaming problems are replaced or traded for emulsification challenges.

Even though the utilization of resin had not been the scope of our work, a related publication [25] compares α-humulene production in batch fermentations with and without ISPR using that strategy. The utilization of hydrophobic resin for ISPR increased the α-humulene volumetric concentrations by 2310 % in *Escherichia coli* BL21(DE3), as compared to a single-phase culture. The authors suggested that ISPR prevented the oxidative degradation of the produced α-humulene by the production strain and further utilization as energy source, after the depletion of other carbon sources, via the tricarboxylic acid cycle [25]. Oxidative degradation could be an explanation for the decrease in α-humulene accumulation observed in the current chapter (end of experiments 6 and 9).

4.5. Conclusion

The utilization of dodecane for ISPR in fed-batches, as reported for Exp 8 had great productivity ranges and product yield based on biomass (table 8). For this experiment, the Herbert-Pirt parameters: a = - 0.65 mol glycerol $\cdot$ (Cmol X^{-1}) and m_s = - 0.01 mol glycerol $\cdot$ (h $\cdot$ Cmol X)$^{-1}$ were estimated.

On the other hand, the solvent-free strategy (Exp 9) did not perform as well regarding foam formation and overall specific productivity (half of the achieved for experiment 8). The anti-foam concentration used for Exp 9 exceeded others (2.1 % w$\cdot$w^{-1}). The foam control was only possible using cyclic anti-foam solution addition. Late product accumulation occurred (3.41 g), though, impacting productivity. Regardless of the differences in productivities shown here, these are outstanding results for *E. coli* overexpressing foreign proteins for humulene production.

4.6. Acknowledgements

4.7. Symbology

B = Moles of hydrolysed Nitrocefin

BSA = Bovine serum albumin

CFU = Colony-forming units

D = Dilution factor

DCW = Dry cell weight

DOT = Dissolved oxygen tension

HS = Humulene-producing strain

Exp, or Exp_s (plural) = experiment, short experiment code

ISPR = *In situ* product recovery

LB = Luria- Bertani medium

Log P = Octanol-water-partition coefficient

MIC = minimum inhibitory concentration

OD_{600nm} = Optical density λ = 600 nm

P = Product , sesquiterpene of interest (α-humulene)

PV = Gassed volumetric power input [$kW \cdot m^{-3}$]

Ref = reference

t_2-t_1 = Time interval (minutes)

S = glycerol

SAC = Surface-active compounds

SS = Santalene-producing strain

w = weight

V = Volume of sample added (mL)

X = Biomass.

4.8. Appendix

4.8.1. Appendix A. Experiments: codes, properties, samples and main steps.

All experiments were performed using the humulene-producing *E. coli* BL21 (DE3). Table 5 presents the main features, table 6, total ages for main steps. Tables 7 and 8 refer to sample ages (from inoculation and since the feed start, respectively).

Table 4. General features of fed-batch experiments in this chapter:

Code	Exp	*PV	**$V_{tip\ max}$	Glyc. conc. in feed	Max. biomass conc.	Max. product conc.	***AF final conc.
TUD DIRC		$\frac{kW}{m^3}$	$\frac{m}{s}$	$\%\frac{w}{w}$	$\frac{g}{kg}$	$\frac{g}{kg}$	$\%\frac{w}{w}$
17.08.02 F#3	6	3.64	3.0	35	38.1 ± 0.0	3.6 ± 1.1	0.19
17.08.02 F#4	7	4.07	3.0	20	33.4 ± 0.9	0.5 ± 0.0	0.07
17.12.05 F#3	8	3.89	3.0	35	38.5 ± 1.1	2.6 ± 0.1	0.98
18.01.23 F#3	9	3.97	3.0	35	34.5 ± 0.2	2.5 ± 0.3	2.10

* P_g/V:Gassed volumetric power input (average), calculated according to [39].
**$V_{tip\ max}$: maximum impeller tip speed.
*** AF: anti-foam.

Table 5. Total ages (h) for key steps per experiment:

Exp	Dodecane addition	Feed start	Induction	End
6	0.2	13.2	21.2	134.4
7	0.2	13.2	22.4	62.9
8	0.15	13.3	25.1	120.1
9	0.02	13.5	23.4	164.6

Table 6. Total sample ages (h) per experiment using as reference inoculation time. After sample 9, fed-batch experiment 6 also had later samples: 10 (114.7 h), 11 (132.0 h) and 12 (134.4 h):

Exp	2	3	4	5	6	7	8	9
6	12.6	16.6	19.2	37.2	41.8	62.3	88.9	110.2
7	13.7	17.8	20.5	38.4	43.0	62.9	-	-
8	13.0	20.1	45.8	70.7	86.6	120.1	-	-
9	12.7	21.9	41.9	65.9	88.9	114.2	138.7	164.6

Table 7. Sample ages (h) per experiment, using as reference the feed start. After sample 9, fed-batch experiment 6 also had later samples: 10 (101.6 h), 11 (118.8 h) and 12 (121.2 h):

Exp	2	3	4	5	6	7	8	9
6	-0.6	3.4	6.0	24.0	28.7	49.2	75.7	97.1
7	-0.1	4.1	6.7	24.6	29.2	49.1	-	-
8	-0.3	6.8	32.5	57.4	73.3	106.8	-	-
9	-0.8	8.4	28.5	52.5	75.4	100.7	125.2	151.1

The yields of humulene from biomass for long fed-batches Exp_s 6, 8 and 9 (Y_{PX}, table 8 surpass the Y_{PX} calculated for the santalene-producing strain in chapter 3 (Exp 5: 5.40 mg P $\cdot$ gDCW^{-1} and Exp 4: 3.52 mg P $\cdot$ gDCW^{-1}).

Table 8. Overview for α-humulene yield on biomass (Y_{PX}). Calculations of fed-batch Exp_s 6 to 9 based on respectively 101.6 h, 49.1 h, 73.4 h and 151.1 h of feed-phase age:

Exp	Initial dodecane in broth	Product Yield (Y_{PX})	Specific productivity from induction time
	% w/w	$\dfrac{mgP}{gDCW}$	$\dfrac{mgP}{gDCW \cdot h}$
6	11.2	88.57*	0.95
7	4.4	14.85	0.30
8	10.6	64.21	1.04
9	absent	60.91	0.43

*high standard deviation for peak humulene accumulation.

4.8.2. Appendix B. Specific total protein concentrations in supernatant samples and volumetric IPTG concentrations versus time, per experiment
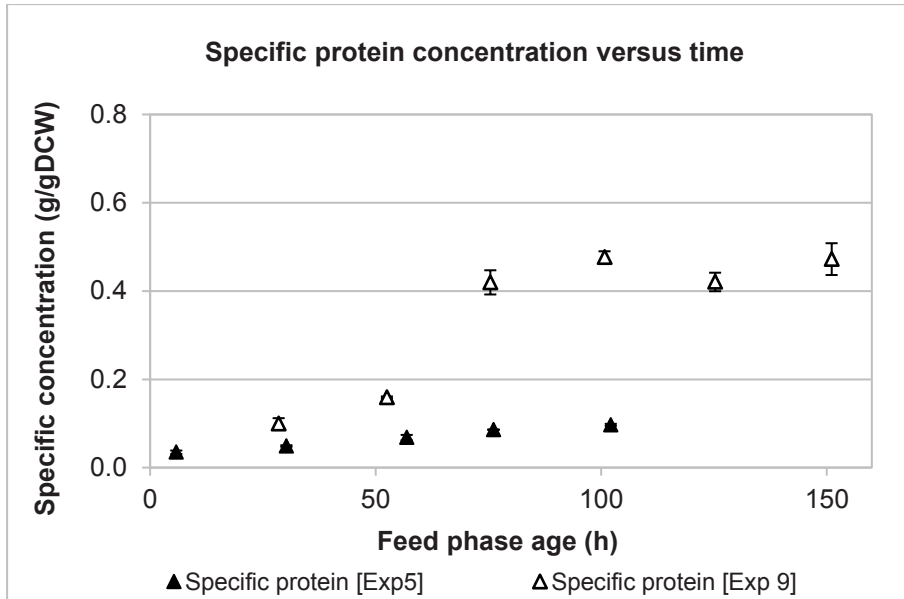

Figure 15. Specific protein concentrations (n = 2) for HS strain (in white [Exp 9], this chapter) and the α-santalene producing type (SS) (in black [Exp. 5], chapter 3).
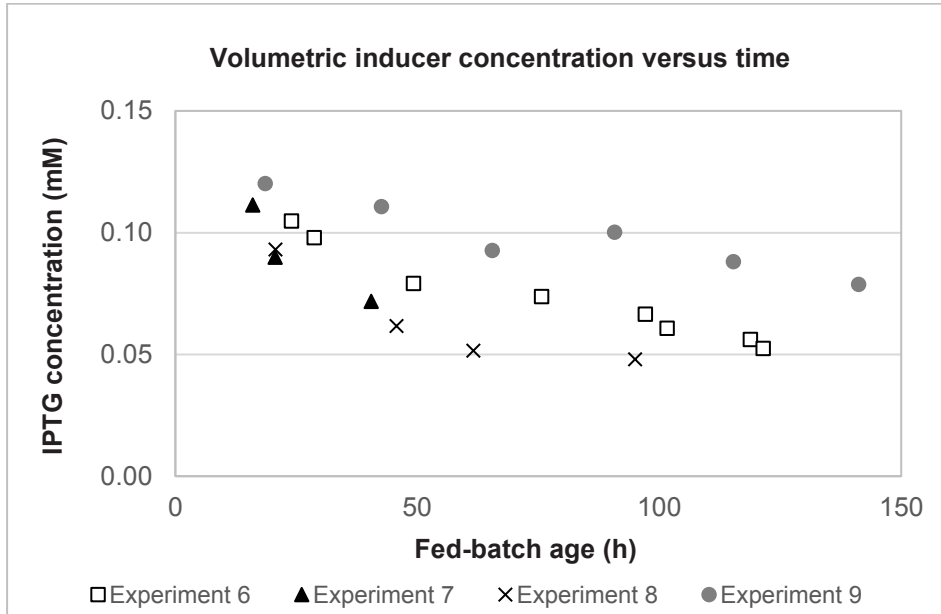
Figure 16. Calculated inducer concentrations for fed-batch experiments 6, 7, 8 and 9.

4.8.3. Appendix C. Facts to be considered in this thesis

The maximum specific protein concentrations for the two strains reached 0.01 g protein $\cdot$ (g DCW)$^{-1}$ ± 0.002 for the SS strain 0.48 g protein·(g DCW)$^{-1}$ ± 0.01 for the HS strain, both for dodecane free experiments. A simple comparison between the specific soluble protein concentrations versus time is presented (figure 15, using as reference for zero age the induction step).

A strong demand for a cyclic anti-foam addition occurred for a different solvent free experiment (Exp 5), performed with the santalene-producing strain in chapter 3.

The contrast between maximum overall specific productivities between this strain and the santalene-producing (SS) type is remarkable, leading to the humulene accumulation accomplished here (between 3.0 and 5.6 g) for long experiments (at least 75 h of feed phase).

As compared to experiments 6 and 7, experiments 8 and 9 had a stronger selection pressure, since the dilution of the antibiotic carbenicillin (added to batch medium) with feed medium addition did not occur. Both experiments 8 and 9 had antibiotics in feed medium prepared according to batch (0.05 g $\cdot$ L^{-1}) and their specific productivities profiles differed (figure 12).

Overall, negligible toxicity of the product here in scope is expected towards the host used in this work. Low antibacterial activity of sesquiterpenes (log P (partition coefficient) between 4 and 7.0) such as α-humulene was reported over *Escherichia coli* and *Staphylococcus aureus*, as compared to monoterpene alcohols,

aldehydes and such substances with intermediate ranges of log P (2 to 3) [40].

Considering that many solvents which are toxic to microorganisms are expected to have a log P between 1 and 5 [41], the log P of 6.6 for dodecane cited in literature [42], would suggest a negligible toxicity. According to [42], biocatalysis is expected to be high by using solvents with a partition coefficient greater than 4. Based only on partition coefficient criteria, the value reported for humulene (7.03) by [40] is unlikely to exert toxicity over microorganisms in general.

4.8.4. Appendix D. Rationale for Herbert-Pirt parameter on product formation (b)

The Herbert-Pirt parameter "b", was estimated by evaluating the mevalonate pathway as described in literature [43], considering incomes and outcomes of related individual steps, as well as the utilization of glycerol as substrate (details available in Chapter 1 of this thesis and in [36]).

-1 Glycerol +1 ATP+1 Acetyl-CoA + 3 NADH+ 1 CO_2

The complete combustion of glycerol yields 14 electrons [44], leading to 10.5 ATP having as reference [36] P/O (efficiency of oxidative phosphorylation in *E. coli*) of 1.5. From acetyl-CoA formation until the production of α-humulene ($C_{15}H_{24}$), the expected stoichiometry follows after the verification of carbon and electrons balances:

-9 Acetyl-CoA -6 NADPH -9 ATP +1 Humulene +3 CO_2
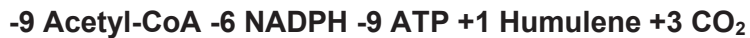
As a consequence, the product reaction below is expected, resulting in the energy balance of 31.5 ATP after NADH production and NADPH consumption. Next, the consumption of 18 ATP detailed in the same product reaction would lead to the net production of 13.5 ATP. The ratio between the net ATP production of the product reaction (13.5 ATP) and the ATP yield from the combustion of glycerol (10.5 ATP) would result in 1.29 mol glycerol, which deduction out of 9 mols

of glycerol would predict 7.71 mols of glycerol per mol of humulene ($b = -\frac{1}{Y_{P/S}}$), and thus, the corresponding yield of product on substrate ($Y_{P/S}$)= 1/7.71 = 0.130. These values were used in the modeling presented in chapter 5.

-9 Glycerol -18 ATP -6 NADPH+1 Humulene + 27 NADH+ 12 CO_2

4.9. References

1. Neuenschwander, U., B. Czarniecki, and I. Hermans, *Origin of Regioselectivity in α-Humulene Functionalization.* The Journal of Organic Chemistry, 2012. **77**(6): p. 2865-2869.

2. Nasiatka, K.J., et al., *Rapid Characterization of Hops (Humulus lupulus) Using DART-MS and Chemometrics.* Journal of the American Society of Brewing Chemists: p. 1-7.

3. Campelo, P.H., et al., *Modulation of aroma and flavor using dielectric barrier discharge plasma technology in a juice rich in terpenes and sesquiterpenes.* LWT, 2020. **130**: p. 109644.

4. Nance, M.R. and W.N. Setzer, *Volatile components of aroma hops (Humulus lupulus L.) commonly used in beer brewing.* Journal of Brewing and Distilling, 2011. **2**(2): p. 16-22.

5. Van Holle, A., et al., *The brewing value of Amarillo hops (Humulus lupulus L.) grown in northwestern USA: A preliminary study of terroir significance.* Journal of the Institute of Brewing, 2017. **123**(3): p. 312-318.

6. Singh, S.P., et al., *Zerumbone reduces proliferation of HCT116 colon cancer cells by inhibition of TNF-alpha.* Scientific reports, 2018. **8**(4090): p. 1-11.

7. Medeiros, R., et al., *Effect of two active compounds obtained from the essential oil of Cordia verbenacea on the acute inflammatory responses elicited by LPS in the rat paw.* Br J Pharmacol, 2007. **151**(5): p. 618-27.

8. Fernandes, E.S., et al., *Anti-inflammatory effects of compounds alpha-humulene and (−)-trans-caryophyllene isolated from the essential oil of Cordia verbenacea.* European

Journal of Pharmacology, 2007. **569**(3): p. 228-236.

9.   Rogerio, A.P., et al., *Preventive and therapeutic anti-inflammatory properties of the sesquiterpene alpha-humulene in experimental airways allergic inflammation.* Br J Pharmacol, 2009. **158**(4): p. 1074-87.

10.   Govindarajan, M. and G. Benelli, *α-Humulene and β-elemene from Syzygium zeylanicum (Myrtaceae) essential oil: highly effective and eco-friendly larvicides against Anopheles subpictus, Aedes albopictus, and Culex tritaeniorhynchus (Diptera: Culicidae).* Parasitology Research, 2016. **115**(7): p. 2771-2778.

11.   Benelli, G., et al., *Insecticidal activity of camphene, zerumbone and α-humulene from Cheilocostus speciosus rhizome essential oil against the Old-World bollworm, Helicoverpa armigera.* Ecotoxicology and Environmental Safety, 2018. **148**: p. 781-786.

12.   Legault, J., et al., *Antitumor activity of balsam fir oil: production of reactive oxygen species induced by alpha-humulene as possible mechanism of action.* Planta Med, 2003. **69**(5): p. 402-7.

13.   Legault, J. and A. Pichette, *Potentiating effect of beta-caryophyllene on anticancer activity of alpha-humulene, isocaryophyllene and paclitaxel.* J Pharm Pharmacol, 2007. **59**(12): p. 1643-7.

14.   Chen, H., et al., *α-Humulene inhibits hepatocellular carcinoma cell proliferation and induces apoptosis through the inhibition of Akt signaling.* Food Chem Toxicol, 2019. **134**: p. 110830.

15. El Hadri, A., et al., *Cytotoxic activity of α-humulene and transcaryophyllene from Salvia officinalis in animal and human tumor cells.* An R Acad Nac Farm, 2010. **76**(3): p. 343-356.

16. Jang, H.I., K.J. Rhee, and Y.B. Eom, *Antibacterial and antibiofilm effects of α-humulene against Bacteroides fragilis.* Can J Microbiol, 2020. **66**(6): p. 389-399.

17. Martin, V.J.J., et al., *Engineering a mevalonate pathway in Escherichia coli for production of terpenoids.* Nature Biotechnology, 2003. **21**: p. 796.

18. Zhang, L., et al., *Engineering the oleaginous yeast Candida tropicalis for α-humulene overproduction.* Biotechnol Biofuels Bioprod, 2022. **15**(1): p. 59.

19. Schempp, F.M., et al., *Microbial Cell Factories for the Production of Terpenoid Flavor and Fragrance Compounds.* Journal of Agricultural and Food Chemistry, 2018. **66**(10): p. 2247-2258.

20. Yu, F., et al., *Molecular cloning and functional characterization of α-humulene synthase, a possible key enzyme of zerumbone biosynthesis in shampoo ginger (Zingiber zerumbet Smith).* Planta, 2008. **227**(6): p. 1291-1299.

21. Guo, Q., et al., *High-yield α-humulene production in Yarrowia lipolytica from waste cooking oil based on transcriptome analysis and metabolic engineering.* Microbial Cell Factories, 2022. **21**(1): p. 271.

22. Milker, S., et al., *Gram-scale production of the sesquiterpene α-humulene with Cupriavidus necator.* Biotechnology and Bioengineering, 2021. **118**(7): p. 2694-2702.

23. Sydow, A., et al. *Autotrophic Production of the Sesquiterpene α-Humulene with Cupriavidus necator in a Controlled Bioreactor*. Bioengineering, 2023. **10**, DOI: 10.3390/bioengineering10101194.

24. Krieg, T., et al., *CO2 to Terpenes: Autotrophic and Electroautotrophic α-Humulene Production with Cupriavidus necator.* Angewandte Chemie International Edition, 2017. **57**(7): p. 1879-1882.

25. Alemdar, S., et al. *Bioproduction of α-humulene in metabolically engineered Escherichia coli and application in zerumbone synthesis*. Engineering in life sciences, 2017. **17**, 900-907 DOI: 10.1002/elsc.201700043.

26. Harada, H., et al., *Efficient synthesis of functional isoprenoids from acetoacetate through metabolic pathway-engineered Escherichia coli.* Applied Microbiology and Biotechnology, 2009. **81**(5): p. 915-925.

27. Nguyen, A.D., D. Kim, and E.Y. Lee, *Unlocking the biosynthesis of sesquiterpenoids from methane via the methylerythritol phosphate pathway in methanotrophic bacteria, using α-humulene as a model compound.* Metabolic Engineering, 2020. **61**: p. 69-78.

28. Sonntag, F., et al., *Engineering Methylobacterium extorquens for de novo synthesis of the sesquiterpenoid α-humulene from methanol.* Metabolic Engineering, 2015. **32**: p. 82-94.

29. Zhang, C., et al., *Harnessing Yeast Peroxisomes and Cytosol Acetyl-CoA for Sesquiterpene α-Humulene Production.* Journal of Agricultural and Food Chemistry, 2020. **68**(5): p.

1382-1389.

30. Zhang, C., et al., *Production of sesquiterpenoid zerumbone from metabolic engineered Saccharomyces cerevisiae.* Metabolic Engineering, 2018. **49**: p. 28-35.

31. Duman-Özdamar, Z.E., et al., *Tailoring and optimizing fatty acid production by oleaginous yeasts through the systematic exploration of their physiological fitness.* Microbial Cell Factories, 2022. **21**(1): p. 228.

32. Vancov, T., J. Palmer, and B. Keen, *Bioethanol production from Eucalyptus grandis using novel low-cost nutrient supplements in fermentation.* Biomass Conversion and Biorefinery, 2023.

33. Kim, T.-B., et al., *Increased xylitol production rate during long-term cell recycle fermentation of Candida tropicalis.* Biotechnology Letters, 2004. **26**(8): p. 623-627.

34. Xue, C., et al., *Efficient biotransformation of l-lysine into cadaverine by strengthening pyridoxal 5'-phosphate-dependent proteins in Escherichia coli with cold shock treatment.* Biochemical Engineering Journal, 2020. **161**: p. 107659.

35. Schalk, M., et al., *Toward a Biosynthetic Route to Sclareol and Amber Odorants.* Journal of the American Chemical Society, 2012. **134**(46): p. 18900-18903.

36. Taymaz-Nikerel, H., et al., *Genome-derived minimal metabolic models for Escherichia coli MG1655 with estimated in vivo respiratory ATP stoichiometry.* Biotechnology and Bioengineering, 2010. **107**(2): p. 369-381.

37.   Tippmann, S., et al., *Production of farnesene and santalene by Saccharomyces cerevisiae using fed-batch cultivations with RQ-controlled feed.* Biotechnology and Bioengineering, 2016. **113**(1): p. 72-81.

38.   Dvorak, P., et al., *Exacerbation of substrate toxicity by IPTG in Escherichia coli BL21(DE3) carrying a synthetic metabolic pathway.* Microbial Cell Factories, 2015. **14**(201): p. 1-15.

39.   Riet, K.v.t. and J. Tramper, *Basic bioreactor design*. 1991, New York: Marcel Dekker.

40.   Reichling, J., et al., *Antibacterial Activity and Irritation Potential of Selected Essential Oil Components – Structure-Activity Relationship.* Natural Product Communications, 2006. **1**(11): p. 1934578X0600101116.

41.   Dyrda, G., et al., *The effect of organic solvents on selected microorganisms and model liposome membrane.* Mol Biol Rep, 2019. **46**(3): p. 3225-3232.

42.   Laane, C., et al., *Rules for optimization of biocatalysis in organic solvents.* Biotechnology and Bioengineering, 1987. **30**(1): p. 81-87.

43.   Wang, J., Y. Li, and D. Liu, *Cloning and Characterization of Farnesyl Diphosphate Synthase Gene Involved in Triterpenoids Biosynthesis from Poria cocos.* 2014. **15**(12): p. 22188-22202.

44.   Heijnen, J.J. *Energy Conversion Pathways*. Study Material on "Fermentation Technology" 2012.

Chapter 5

A Black-box model to evaluate the biotechnological production of α-humulene

This chapter will be submitted as:

A Blackbox Model to evaluate the biotechnological production of α-humulene.

Abstract

Terpenes are an emerging category of versatile, hydrophobic molecules with a broad use in a range of industries, examples are flavors and fragrances, cosmetics, pharmaceuticals, chemical building blocks, solvents and fuel precursors.

In this chapter, fed-batch strategies are investigated for optimal production based experimental findings of high specific α-humulene production on glycerol at very low growth rate of the producing strain *Escherichia coli* BL21 (DE3), combined with positive effects of extractive fermentation for *in-situ* product removal and enhanced oxygen mass transfer.

In this work, measured oxygen mass transfer during actual extractive fermentations are presented and compared to relevant kLa correlations. A black box model as well as an oxygen mass transfer model were combined to design the fed-batch strategy and bioreactor dimensions for α-humulene biotechnological processes in larger scales, aiming at 1 m^3 and 10 m^3. This study focused on feed phase strategies using Exponential Feed (EF) or Constant Oxygen Consumption Rate (COCR) principles.

Considering the higher α-humulene productivities found at very low specific growth rates, a strategy of decoupling biomass production at high growth rates in smaller and cheaper seed reactors followed by α-humulene production at low growth rates was compared to operating a single bioreactor for both biomass and α-humulene production, all with exponential feeds. The 'decoupled'

strategy compared favorably in overall lower capital and operational costs with approximately 20 % shorter process times and 30 % higher volumetric productivities at 1 m^3 and 10 m^3 bioreactors, and potentially reduced separation costs due to higher cell viability.

5.1. Introduction

5.1.1. General considerations

To improve terpene fermentations, several manufacturing strategies have been proposed such as phase separated liquid product recovered by centrifugation [1], [2] or as condensate as volatile species from the off gas of a fermentation, or a mixture of both [3]. Alternatively, recovery by adsorption on apolar adsorption materials [4], or by different solvent based processes where the target product is extracted from the fermentation broth, lowering effectively its toxicity and volatility with subsequent recovery from the solvent phase which is recycled has also been proposed [5], [6] ,[7].

Various authors provide cost price estimates that range from an optimistic below $2/kg product [8], [2] to values in the range of 3-7 $/kg for commodity products and $50-500/kg or more for food, pharma specialty products [3], [9] for improved strains and fermentation systems. Capital cost related to the fermentation (bioreactors and compressors) dominate the equipment investment (60-75 %), while substrate cost dominate overall unit manufacturing cost due to the low (2-3 %) [10] carbon flux to the products [11], [3], ([9] (supplementing materials). Important industrial optimization strategies include improving carbon flux to terpene product as well as investment cost reduction of the fermentation systems [12].

Scales of manufacturing vary from 10s -1000s of tons for the higher added value products food, pharma and consumer products,

to 10…1007s of kilotonnes per year for commodity applications. This will translate in manufacturing plants with aerobic fermentors that range from the order of 1 (or few) m³ for high added value products and 10 to 100 m³ for the commodity products. For terpenes, a few applications are shown in the overview by [13] (Figure 1).

Figure 2. Terpenoid classifications and some examples of their commercial applications.

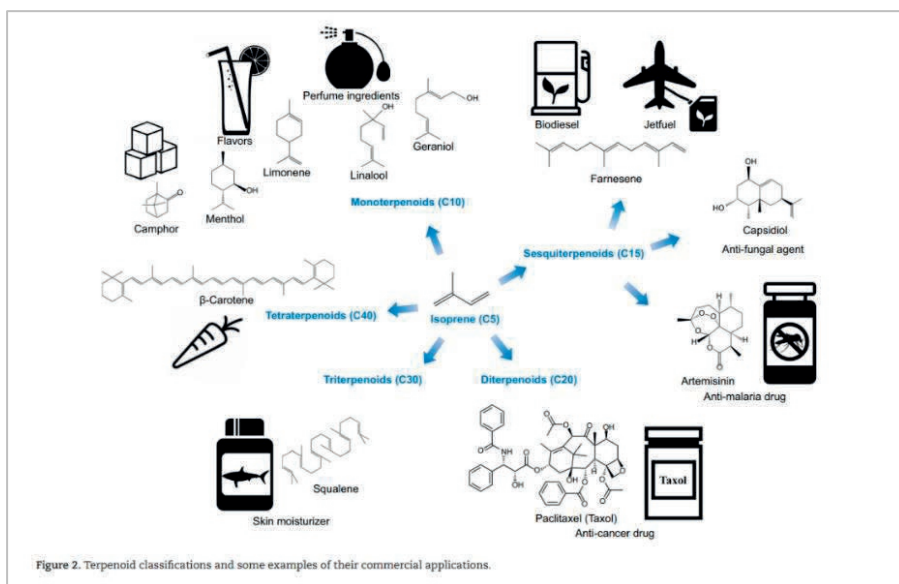**Figure 1.** Common applications for terpene compounds, after Zhang *et al* [13].

Product formation kinetics and other biological factors. In this work, we focus on the solvent-aided aerobic terpene fermentations, following earlier work by [9] and [6]. Both, however, did not take the impact of the specific product formation kinetics into account that generally show high biomass specific production rates

q_p at low growth rates [μ], which is decreasing with increasing growth rates (Chapter 4 of this thesis). Publications such as [14], [15], [16], [17] describe the formation of several compounds of interest under low or moderate specific growth rates in *Escherichia coli.*

It was also demonstrated (Chapter 4 of this thesis) that cell viability reduced with increasing (fed)batch time, resulting in cell lysis and protein release. The latter promoted increased foaming with fermentation age, resulting in enhanced antifoam use in solvent-free systems, whereas this effect was significantly less in solvent –aided systems. Here it however may lead to emulsification and reduced coalescence of the solvent as shown by [7].

Oxygen mass transfer. Another key aspect for design, scale-up and optimization of aerobic fermentations is oxygen mass transfer. A kLa range of 151 to 780·h^{-1} has been reported for *Escherichia coli* cultivations in 1 m^3 to 1.9 m^3 bioreactors [18]. Fundamental work has been done by Van t Riet [19], who underlined that oxygen mass transfer is considered a key, restrictive economic factor in aerobic industrial fermentations. The same author published earlier correlations [20] for overall oxygen mass transfer coefficients k_La in stirred non-coalescing, small bubble salt-containing solutions and for stirred, coalescing, large bubble water systems. More recently, Montes *et al* [21] provided an updated correlation for moderate salt containing, typical fermentation broths. For the overall mass transfer of oxygen stirred aqueous systems in the presence of antifoam agents, literature reports low [22] as well as from low to enhanced [23] (values subject to antifoam type and concentration). In

general, limited data have been published about actual oxygen mass transfer specifically in terpene fermentations which are mixed fermentation systems with typical salts, antifoams and phase separating organic molecules such as terpenes and organic solvents.

Various authors [24], [25] and [5] postulated potentially enhanced oxygen mass transfer by the presence of the organic solvents due to generally higher oxygen solubilities than aqueous fermentation broths. Therefore, there is a need to determine oxygen mass transfer characteristics in actual terpene fermentations with and without added organic solvent and antifoam during the fermentation processes.

In this chapter, we've measured oxygen mass transfer during actual extractive fermentations and compared to relevant k_La correlations. We also analyze the scale-up strategies in typical sesquiterpene fed batch fermentation taking the experimental system of α-humulene by *E. coli* as a benchmark for which we have both a metabolic model with the characteristic biomass specific declining q_p (μ) relation that we described above in conventional stirred aerobic fermentors with modest solvent content (5 - 10 vol %) comparable to the experimental systems studied here.

5.1.2. Metabolic model for the sesquiterpene-producing strains

The figure below summarizes schematically the simplified metabolic model including carbon and nitrogen sources for the production of α-humulene under aerobic conditions:

Stoichiometry of biomass and product formation using glycerol feedstock in an aerobic fermentation (see Appendix A for more details).

Biomass reaction for an α-humulene-producing strain

$-0.62 C_3H_8O_3 - 0.2 NH_4^+ - 1.12 O_2 + 0.86 CO_2 + 0.2 H^+ + 1 C_1H_{1.8}O_{0.5}N_{0.2} + 1.88 H_2O = 0$
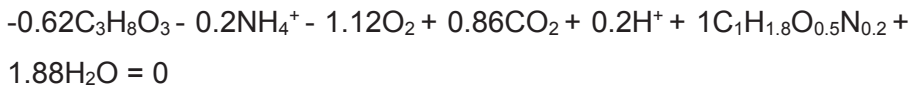
α-Humulene product formation reaction

$- 7.7\ C_3\ H_8\ O_3 - 5.95\ O_2 + 8.1\ CO_2 + 18.8\ H_2O + 1\ C_{15}\ H_{24} = 0$

Glycerol catabolic reaction:

$-1\ C_3H_8O_3 - 3.5\ O_2 + 3\ CO_2 + 4\ H_2O = 0$
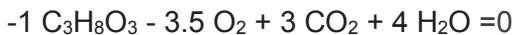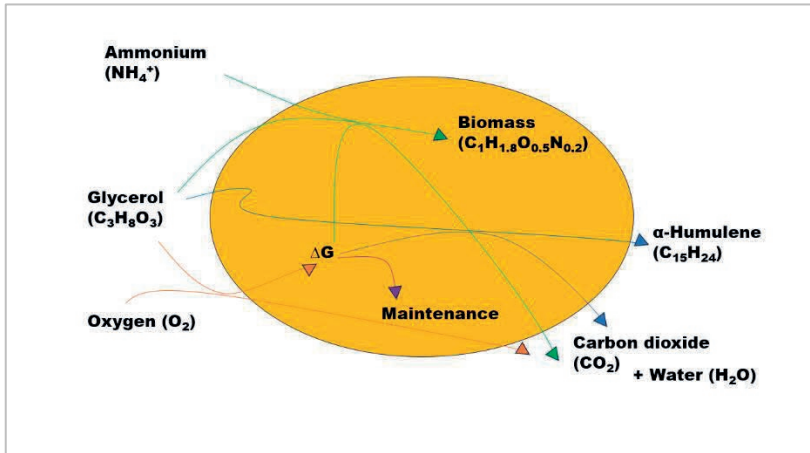
Figure 2. Schematic inputs and outputs for the aerobic production of α-humulene by *Escherichia coli* (adapted from [26]).

Kinetics

- Biomass and substrate using the Herbert Pirt model parameters from Chap 4.

$$-q_s = 0.62\,\mu + 7.7q_p + 0.01 \qquad \text{Eq. 5.1}$$

- product formation kinetics / q_p – μ relation (Chap 4, if polynomial grade 3 fit):

$$q_p = -46.12 \cdot \mu^3 + 2.101 \cdot \mu^2 - 0.0395 \cdot \mu + 4.354 \cdot 10^{-4} \qquad \text{Eq. 5.2}$$

- oxygen uptake (and CO_2, H_2O production) – from stoichiometry

$$q_{o_2} = 1.12\,\mu + 5.95\,q_p + 0.035$$

<div align="right">Eq. 5.3</div>

- CO_2 production, follows from stoichiometry:

$$q_{CO2} = 0.86\,\mu + 8.1\,q_p + 0.03$$

<div align="right">Eq. 5.4</div>

- H_2O production, follows from stoichiometry:

$$q_w = 1.88\,\mu + 18.8\,q_p + 0.04$$

<div align="right">Eq. 5.5</div>

5.2. Materials and Methods

5.2.1. Oxygen mass transfer in stirred aerobic fermentors.

5.2.1.1. k_La correlations

According to [27], for small scale vessels with single Rushton stirrer, k_La can be estimated respectively, for coalescing systems with large air bubbles in water [27] as a function of power input P_S/V_L and superficial air velocity v_{gs}:

$$k_La = 0.026 \left(\frac{Ps}{V_L}\right)^{0.4} \cdot \left(v_{gs}\right)^{0.5} \qquad \text{Eq. 5.6}$$

and for salt-containing, non-coalescing systems [28], with small and rigid bubbles:

$$k_La = 0.002 \left(\frac{Ps}{V_L}\right)^{0.7} \cdot \left(v_{gs}\right)^{0.2} \qquad \text{Eq. 5.7}$$

Real fermentation broths have been demonstrated to have mass transfer characteristics that are in between coalescing and non-coalescing behaviours. The following correlation was suggested by Montes *et al* [21] for such semi-coalescence behaviour:

$$k_L a = 0.032 \left(\frac{Ps}{V_L}\right)^{0.35} \cdot \left(v_{gs}\right)^{0.41} \qquad \text{Eq. 5.8}$$

5.2.1.2. Determination of experimental kLa

The steady state method, where the equilibrium between oxygen consumption and transport leads to the dissolved oxygen concentration, was used to determine the volumetric oxygen mass transfer coefficient ($k_L a$) [28]. For a pseudo steady state system, provided that oxygen concentrations are relatively stable, ($dC_w/dt \sim 0$) and the oxygen transfer rate (OTR approaches oxygen consumption rate R_{O2} (OTR ~ R_{O2}) [5, 29]. The dynamics of oxygen transfer ($k_L a$-associated) is expected to have a fast influence, as compared to oxygen consumption resulting from metabolic rates. Fed-batch fermentations for instance, when usually low growth rates occur in fed phase are examples for the utilization of this method [5].

The gas-phase analysis was performed to determine the difference between the molar flow rates of oxygen ($F_{O2}^{in} - F_{O2}^{out}$). The concentration of oxygen (C_L) in the aqueous medium was monitored. The calculation of $k_L a$ was carried out according to [29]:

$$kLa = \frac{[\ FO_2^{in} - FO_2^{out}]}{[V_{broth} \cdot (C^* - C_w)]}$$
Eq. 5.9

5.2.1.3. Mass transfer in scaled-up bioreactors

One of the reported scale-up strategies combine geometry similarity, constant kLa and constant tip speed [30]. Here, the strategy demonstrated by [31] was adapted for the kLa correlation (semi-coalescent gas behavior according to [21]) using as benchmark 1 m^3 bioreactors. The effect of 10-fold and 100-fold volume increase resulted in volumetric power 42.6 % and 18.2 % of the reference values. Additionally, to maintain a constant kLa, the demands over superficial gas velocities for 10 m^3 and 100 m^3 bioreactors would be respectively 2.5 - fold and 6.3 - fold the values required for 1 m^3 bioreactors.

As indicated by Junker [18] and Van 't Riet [19], aerobic bioreactors become oxygen mass transfer limited as the bioreactors volumes increase, and the volumetric power inputs by the stirrer(s) alone are insufficient. Moving from laboratory scale of several liters towards industrials scales in the range of 1 - 10 m^3, the common industrial strategy to maintain the $k_L a$ in the range of $0.05 \cdot s^{-1}$ by

increasing the superficial gas velocity and changing aspect ratio (height over diameter) of the reactor. Obviously, this strategy has also consequence on operational costs (OPEX) due to increased power consumption for gas input by the (larger) pressure drop over increasingly more column type reactors.

5.2.2. Fed batch fermentor: generic model

The generic model for fed-batch operation of the terpene fermentation is based on the differential mass balances for all species *i* involved: biomass, substrate, oxygen, carbon dioxide, water as well as the terpene product, with time dependent in and outflow terms F_i and conversion terms with biomass specific consumption and production rates q_i:

$$\frac{dM_i}{dt} = F_i + q_i \cdot M_x \qquad \text{Eq. 5.10}$$

For simple cases such as batch growth, consumption of production of species i the flow terms equals zero ($F_i = 0$), and analytical solutions can be found (Appendix F), but for the general case of coupled ordinary differential equations describing fermentation profiles of the 6 key species in the terpene fermentation (biomass (subscript X), substrate (S), oxygen (O_2), carbon dioxide (CO_2), water (W) and terpene product (P)), which requires a

numerical solution for the general case, but has an analytical solution for the case of exponential growth and feed strategy

5.2.3. MATLAB solutions

The software package MATLAB (version R2019b, MathWorks, Natick, MA, U.S.A) was used to calculate the time dependent biomass, substrate, oxygen, carbon dioxide and terpene product concentrations for the selected fed-batch fed strategies (EF and COCR). Figures displayed in Matlab using the fplot function. For the estimation of cumulative substrate and product at the end of cultivations, the "Trapz" function in Matlab was used for trapezoidal numerical integration using as reference vectors of the respective rates versus time at fed-batch.

Proposed feed strategies for the limiting substrate glycerol are Exponential Feed (EF) for fed-batch systems exponential increase at constant growth rate (for $\mu = 0.005 \cdot h^{-1}$)) or to maintain a Constant Oxygen Consumption Rate (COCR) at varying growth rate. Time dependent functions for the flow terms F_i .are shown in appendix C (EF) and appendix D (COCR), respectively.

EF: $F_{S,} = 0$ for $t < t_B$ (batch phase), and $F_S = F_{S,0}\ \exp(FB \cdot t)$ for $t \geq t_B$ with t_B is batch time.

5.2.4. Design of fed-batch processes

In this section, three strategies for substrate feed design are evaluated for biomass and product formation accumulation.

1. Strategy 1 is exponential feed (EF#1) was based on a low initial biomass of 107.3 Cmol X in the feed-phase, resulting from the inoculation of the bioreactor as performed in 2L bench bioreactors (0.2 biomass density, followed by a batch phase of approximately 10 h), and a significant production time of close to 500 h.

2. Strategy 2 is also exponential feed (EF#2) where the actual production phase is performed at higher initial biomass, which is preceded by a seed fermentor at 10 % volume of the main production bioreactor used for α-humulene production). For 1 m^3 bioreactors, the initial biomass in the production fermentor was 225 Cmol X, and a shortened feeding time considered 350 h. For 10 m^3 bioreactors, the initial biomass was 2250 Cmol X, for the same feeding time considered for 1 m^3 bioreactors.

3. The third strategy is based on a constant oxygen consumption rate (referred to as COCR). In this specific case, a limited time range was presented (up

to 70 h of feed, timepoint when the growth rate (μ) predictions would be close to $5.3 \cdot 10^{-3} \cdot h^{-1}$). This was due to limitations of experimental data (q_p versus μ) obtained in chapter 4. All fed-batch designs presented here were based on the correlations described in [6].

The strategies are evaluated with respect to the following KPIs:

(1) product accumulation (titer)
(2) efficiency in terms of product rate per biomass (q_p)
(3) efficiency in terms of product per substrate used, as well as
(4) oxygen requirements to explore robustness in terms of oxygen transfer capacity
(5) volumetric productivity, as an indication how well the capital investment in bioreactors (CAPEX) is used.

5.2.5. Equipment costs estimations

The overall process structure was adapted from [32] hereby referred to as "Base case" originally focused on farnesene production and designed for 10,000 metric tons (MT) per year. Here, however, more realistic costs for compressors are suggested (see table 4 for specifications). For the evaluation of process economic aspects, 8 bioreactors of 200 m^3 each (as commonly used in the ethanol industry). The 10,000 metric tons (MT) plant was based on the

individual cost of $ 432,000 per main bioreactor, which estimation leads to a total cost of $3,456,000 for this category. Here an important assumption is that one seed bioreactor (individual cost of $ 125,000) is expected to serve four main bioreactors. Using a similar rationale, such process was also downscaled (20-fold) to a 500 metric tons/year industrial plant (see table 5 for details). Furthermore, for the cost estimations of the fully installed plant having as reference the equipment costs, a Lang factor of 4.3 was used.

For compressors, the estimation of purchased equipment cost (C_e) was performed according to [33] and [34]. Here, "d" and "f" represent cost constants, and "n" (equipment specific exponent) which values specified for compressors were $580,000, $20,000 and 0.6, respectively. Additionally, "S" refers to size parameters (for compressor kW):

$$C_e = d + f \cdot S^n$$

5.3. Results

5.3.1. Benchmark: oxygen mass transfer experiments in 2 L bench bioreactors

Based on the experimental superficial gas velocities reported in table 1 and on the kLa correlations (described in section 5.2.1) for coalescing, non-coalescing and semi-coalescing systems were compared to the experimental kLa values (figure 19) reported in the appendix E. Reported volumetric power ranges (table 1). While kLa-values in extractive fermentation (ISPR) (figures 17 and 18) indicate a non-coalescing behavior, the kLa of solvent free fed-batch (figure 16) follows the coalescing correlation.

Table 1. Superficial gas velocities (v_{gs}) and power input ranges (2 L bioreactors):

Experiment	v_{gs} $[\frac{m}{s}]$	Pg/V $[\frac{kW}{m^3}]$ [35]
6	$3.21 \cdot 10^{-3}$	2.0-5.8 (3.6)
8	$3.68 \cdot 10^{-3}$	2.7-4.9 (3.9)
9	$3.19 \cdot 10^{-3}$	4.1-5.5 (5.1)

The solvent free experiment, identified as 9 in the tables above demanded more antifoam addition as compared to others, as mentioned in chapter 4. The addition of anti-foaming agents

facilitates the coalescence of bubbles, interfering on mass transfer rates [36], [37]. Alternatively, the presence of the solvent effectively increases the broth viscosity such that small bubbles have more difficulty (higher viscosity) to collide and coalesce. At 10 % dispersed phase such effect must be significant (effective viscosity one order of magnitude higher than aqueous viscosity [38].

5.3.2. Bioreactor results

For the calculations presented in the next sections, 1 m^3 and 10 m^3 bioreactors with tank and impeller dimensions that would result in a tip speed limit of 3 m $\cdot$ s^{-1}, airflow and stirrer speed according to [18] were selected. To fulfil such criteria, oxygen transfer rate (OTR) calculations according to [28] for 1 m^3 and 10 m^3 bioreactors resulted on 54.5 mol $O_2 \cdot h^{-1}$ and 606.2 mol $O_2 \cdot h^{-1}$, respectively.

Assumptions for such calculations were: for 1 m^3 an aspect ratio of 5 (D/T = 1/3) and for 10 m^3 an aspect ratio 6 (D/T = 1/4). Additionally, for maximal OTR calculations (Eq 5.19, Appendix A), both bioreactors were assumed to operate with 1 bar headspace, 75 % of nominal volume (after fed-batch end), aiming at the experimental average kLa (0.05 $\cdot$ s^{-1}) reported for 2 L bench-scale bioreactors in the absence of dodecane. Thus, the characteristic v_{gs} predicted for such bioreactor configurations were presented in figure 3.
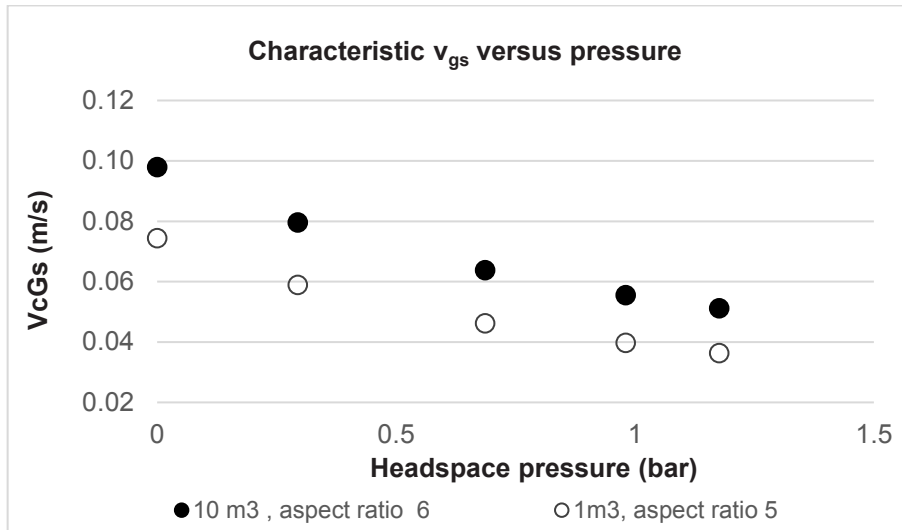
Figure 3. Increased V_{gs} requirements for scale-up in order to maintain the benchmark kLa reported for 2 L bioreactors.

For the estimations of broth volume increase due to feed medium addition, a concentration of 80 % glycerol was used, in order to allow the dilution of salts in feed medium, as well as minimally impact the total broth volume at the end of fed-batch. For calculations of biomass at the end of batch, the batch medium volume was assumed as 50 % of bioreactor nominal capacity.

5.3.2.1. Exponential feed (EF)

Using as reference the metabolic model presented in section 5.2 of the current chapter, figure 4 presents the glycerol (S) and oxygen (O_2) demands per mol of α-humulene (P) as function of specific growth rate (μ).

Based on the lower glycerol and oxygen demands expected for the lowest experimental μ ($5.3 \cdot 10^{-3} \cdot h^{-1}$) reported in experiment 8 (chapter 4, matching the highest q_p values reported), both exponential feed strategies reported in this chapter were developed based on the Process Reaction (PR) that followed from that specific growth rate (see appendix A, equation 5.12).
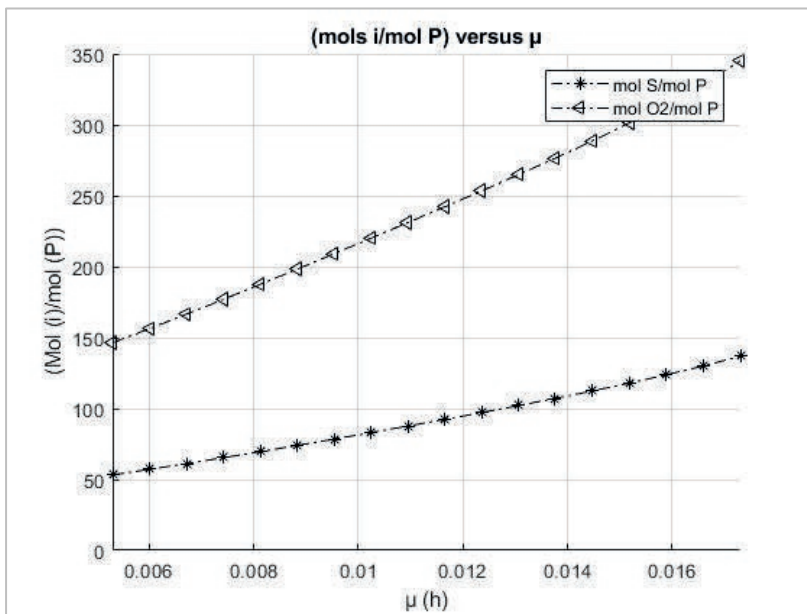
-53.29 $C_3H_8O_3$ -3.64 NH_4^+ -146.43 O_2 + 126.69 CO_2 + 3.64 H^+ + 18.19 $C_1H_{1.8}O_{0.5}N_{0.2}$ + 190.26 H_2O + 1 $C_{15}H_{24}$
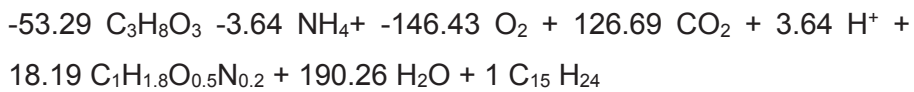

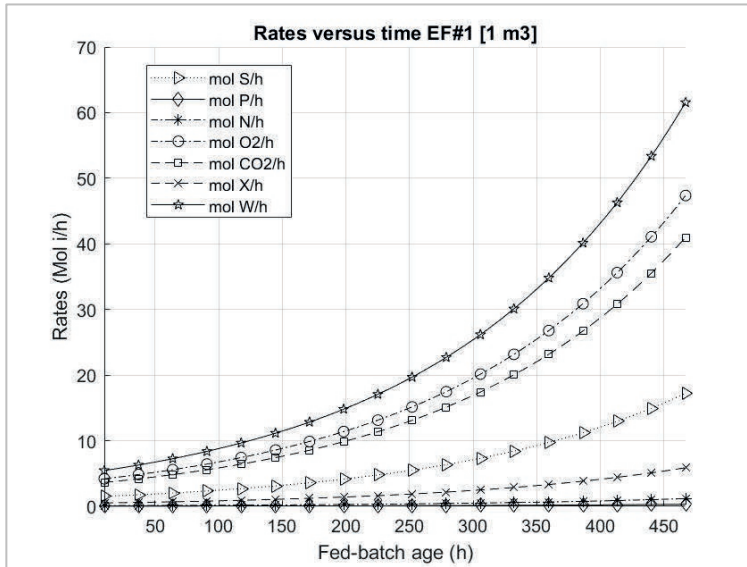**Figure 4.** Mol i / mol P ratios versus μ (experimental ranges, experiment 8, Chapter 4).

Figure 5. Molar rates versus time, exponential feed ($\mu = 5.3 \cdot 10^{-3} \cdot h^{-1}$, strategy 1).
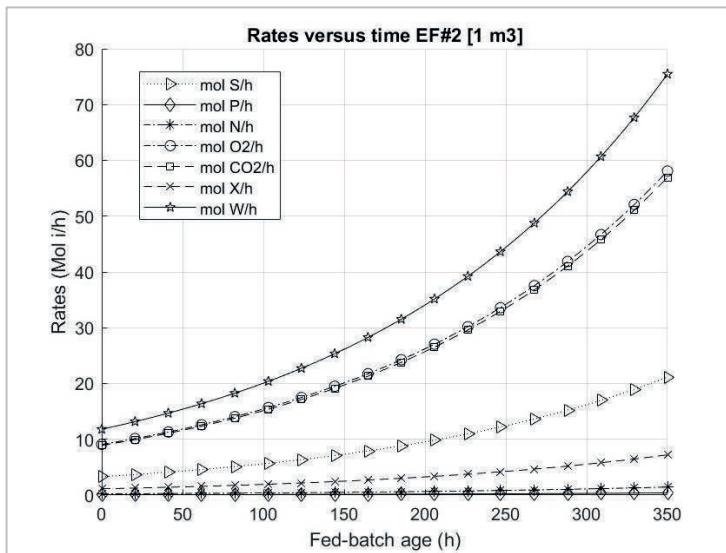
Figure 6. Molar rate versus time, exponential feed ($\mu = 5.3 \cdot 10^{-3} \cdot h^{-1}$, strategy 2).
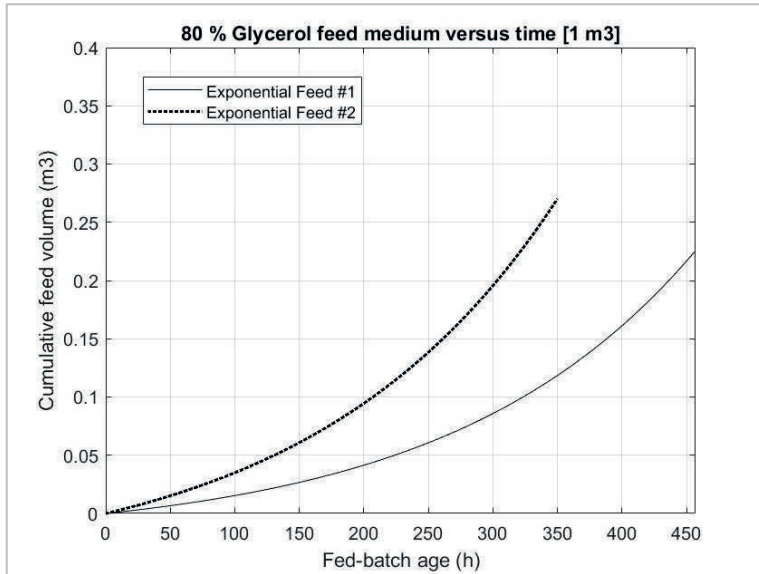
Figure 7. Volume increase versus time for feed (exponential feed, μ = 5.3·10⁻³ · h⁻¹).

5.3.2.2. Constant oxygen consumption rate (COCR)
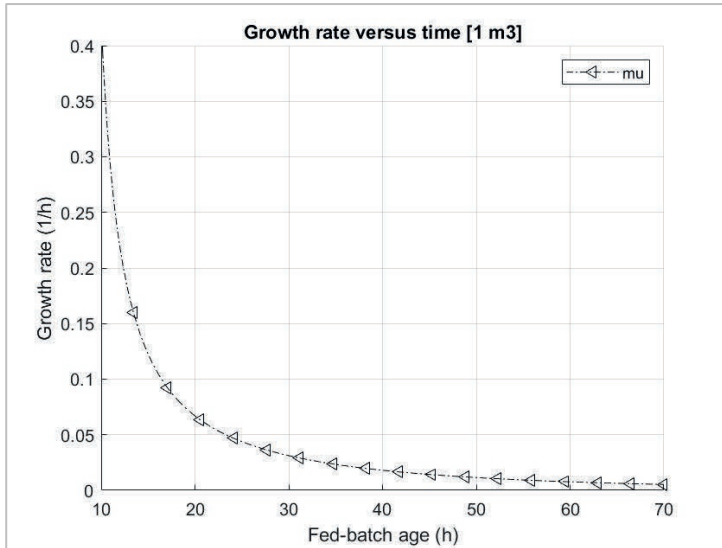
Figure 8. Growth rate versus time for constant oxygen consumption rate strategy.
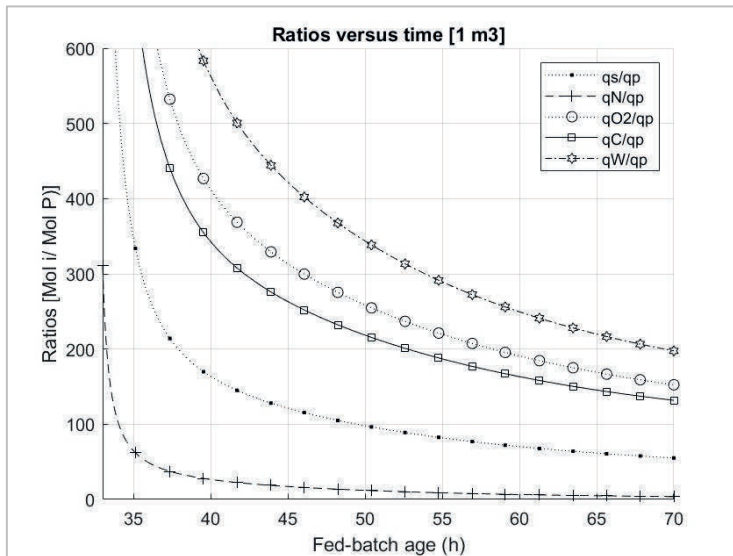
Figure 9. q_i/q_p ratios vs time for COCR feed strategy.
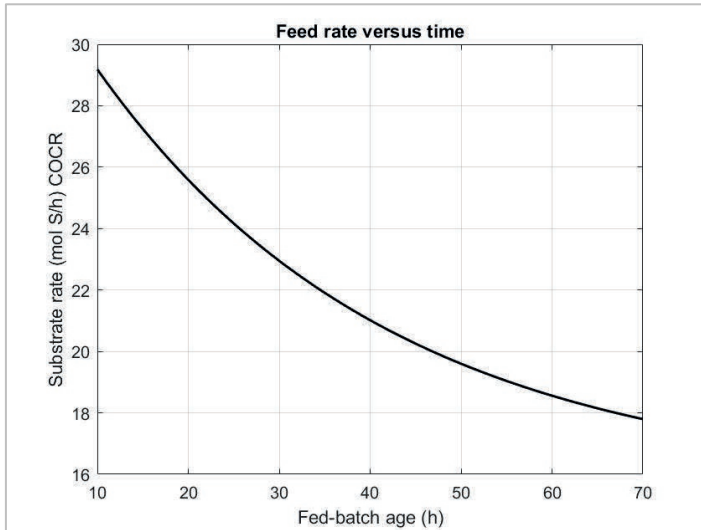
Figure 10. Feed rate for constant oxygen consumption rate (COCR), 1 m^3 bioreactors.
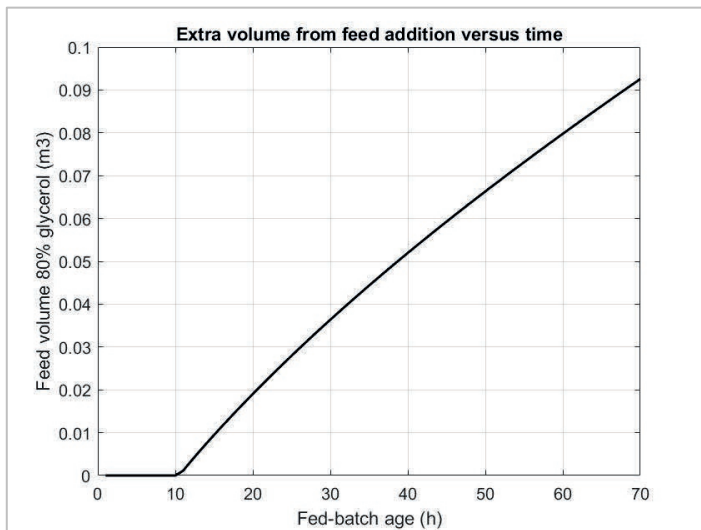
Figure 11. COCR (Constant oxygen consumption rate): expected volume increase in bioreactor versus time, due to medium addition after 70 h of fed - batch.
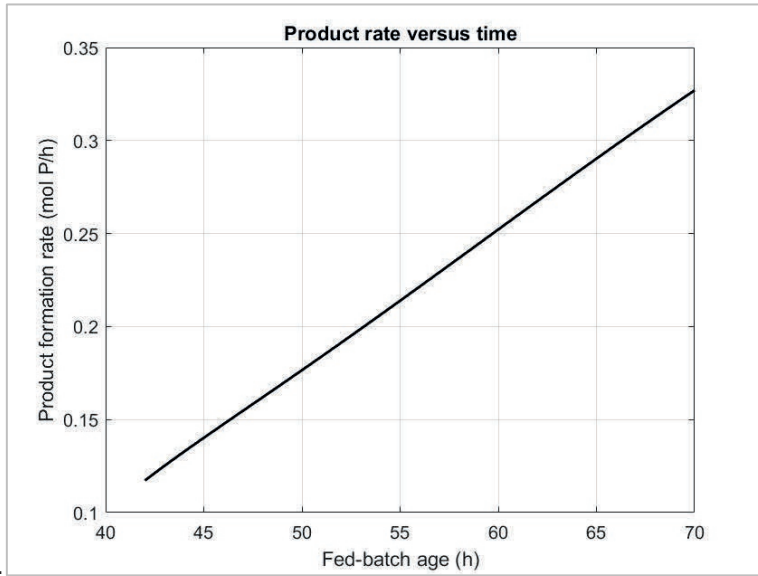
Figure 12. Product formation rate versus time: 1 m^3 (COCR).

5.3.2.3. Profile comparisons between exponential feed (EF) versus constant oxygen consumption rate (COCR)
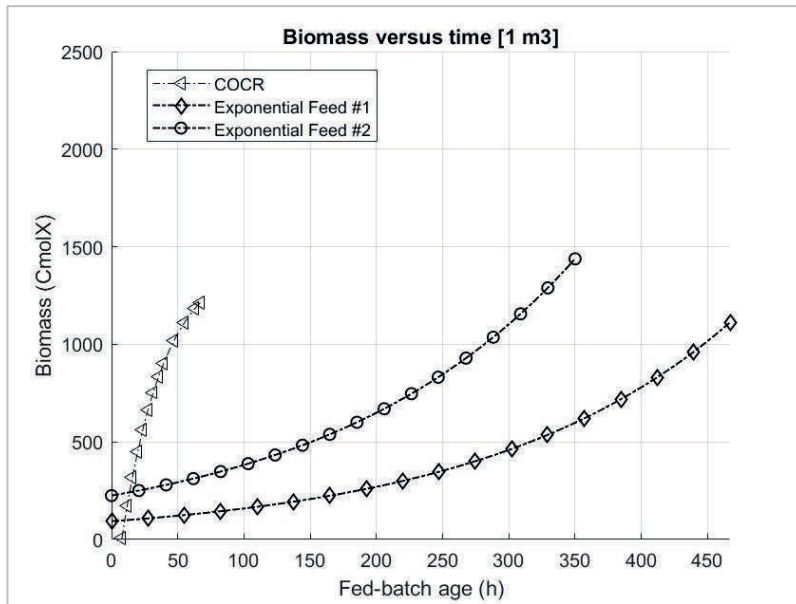
Figure 13. Predictions of biomass accumulation versus time using exponential feed strategy for 1 m^3, comparing fed - batch strategies.
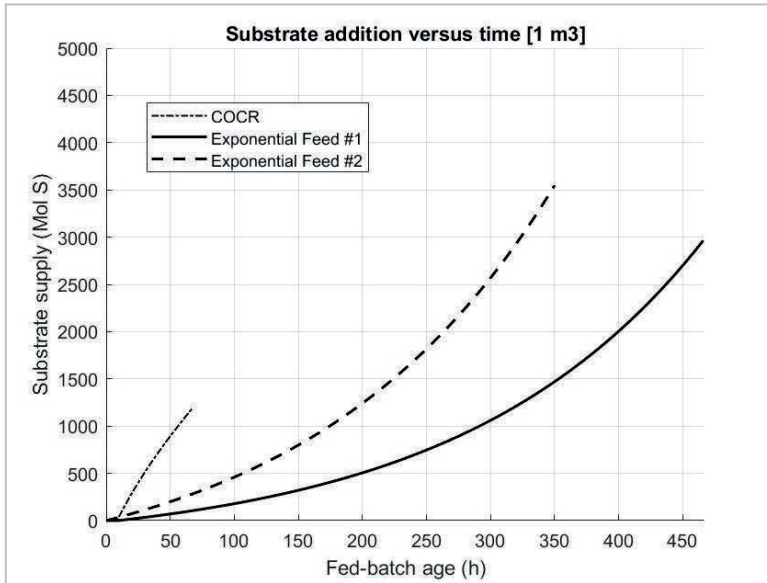
Figure 14. Substrate supply versus time, varying feeding strategies.
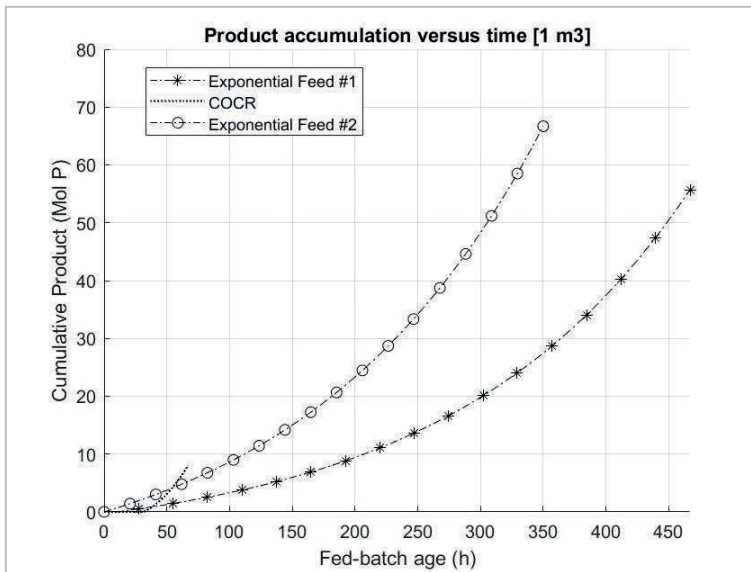
Figure 15. Product accumulation versus time for 1 m³ bioreactors (all strategies).

5.3.2.4. Summary of results between fed-batch strategies:

Table 2. Estimations for fed-batch modeling on 1 m^3 bioreactors:

	Unit	Exponential Feed#1	Exponential Feed#2	Maximal O_2 uptake rate
End time	$[h]$	457	350	70
Integral yield	$\left[\dfrac{Mol_{humulene}}{Mol_{glycerol}}\right]$	$1.9 \cdot 10^{-2}$	$1.9 \cdot 10^{-2}$	$7.0 \cdot 10^{-3}$
Integral productivity	$\left[\dfrac{Mol_{humulene}}{h}\right]$	0.13	0.19	0.15
Product concentration end	$\left[\dfrac{Mol_{humulene}}{m^3}\right]$	84.1	86.6	17.6
Final biomass	$[Cmol_X]$	1209.1	1438.1	1412.7
Product accumulation	$[Mol_{humulene}]$	60.7	66.7	10.7
Glycerol supply	$[Mol_{glycerol}]$	3222.3	3547.8	1533.1
Volumetric productivity	$\left[\dfrac{Mol_{humulene}}{m^3 \cdot h}\right]$	0.184	0.247	0.245

Table 3. Estimations for fed-batch modeling on 10 m^3 bioreactors:

	Unit	Exponential Feed#1	Exponential Feed#2	Maximal O$_2$ uptake rate
End time	$[h]$	457	350	70
Integral yield	$\left[\dfrac{Mol_{humulene}}{Mol_{glycerol}}\right]$	$1.9 \cdot 10^{-2}$	$1.9 \cdot 10^{-2}$	$5.0 \cdot 10^{-3}$
Integral productivity	$\left[\dfrac{Mol_{humulene}}{h}\right]$	1.47	1.91	1.59
Product concentration end	$\left[\dfrac{Mol_{humulene}}{m^3}\right]$	87.4	86.8	18.1
Final biomass	$[Cmol_X]$	13447	14401	14646
Product accumulation	$[Mol_{humulene}]$	673.6	668.1	114.6
Glycerol supply	$[Mol_{glycerol}]$	35837	35478	17528
Volumetric productivity	$\left[\dfrac{Mol_{humulene}}{m^3 \cdot h}\right]$	0.191	0.248	0.251

5.3.3. CAPEX estimations

Table 4. Capital Expenditures (CAPEX) for a 10,000 MT/year industrial plant:

	10,000 MT/year (Base case)		10,000 MT/year	
	Category cost ($)	Cost (%)	Category cost ($)	Cost (%)
Main bioreactors (8x)	3.456,000	42.8	3,456,000	39.1
Seed bioreactors (2x)	250,000	3.1	250,000	2.8
Compressor*	1,465,000	18.1	2,234,763	25.3
Others	2,904,000	36.0	2,904,000	32.8
Total equip	8,075,000	100	8,844,763	100
Fully installed plant	34,721,000	430	38,030,836,35	430
CAPEX $[\frac{\$}{MT \cdot year}]$	3,472.10		3,803.08	

* For compressor cost estimations, the power of 1571 kW was used. Additionally, the nominal values of each of the main bioreactors and seed bioreactors were respectively, 200 m^3 and 20 m^3.

Table 5. Capital Expenditures (CAPEX) for a 500 MT/year industrial plant:

	500 MT/year	
	Category cost ($)	Cost (%)
Main bioreactors (8x)	572,738	15.6
Seed bioreactors (2x)	41,431	1.1
Compressor*	854,232	23.3
Others	2,202,600	60
Total equip	3,671,000	100
Fully installed plant	15,784,619	430
CAPEX [$\frac{\$}{MT \cdot year}$]	31,569.24	

* For compressor cost estimations, the power of 78.5 kW was used. Additionally, the nominal values for each of the main bioreactors and seed bioreactors were respectively, 10 m^3 and 1 m^3.

5.4. Discussion

All used cases benefit from the most profitable fed-batch strategy. Contrastingly, tables 2 and 3 indicate similar volumetric productivities for fixed strategies if increasing scales. This relates to the higher oxygen transfer rate used for the 10 m^3 bioreactors (as compared to the 10-fold the value used for 1m^3 bioreactors), as a result of the pressure resulting from a higher aspect ratio (H_L/T = 6), as compared to 1m^3 scale (H_L/T = 5).

Overall, volumetric productivities reported for Exponential Feed (EF) strategy #2 and COCR were comparable for the time ranges studied, and exceeded for both bioreactor volumes the results reported for EF strategy #1.

As seen from tables 3 (1 m^3 bioreactors) and 4 (10 m^3 bioreactors), a considerable increase over the integral productivity resulted from modeling exponential feed strategy 2 (EF#2), as compared to strategy EF#1. The utilization of strategy EF#2 would demand 4-fold higher CAPEX costs related to full scale bioreactors (for 10-fold scale increase), as compared to bioreactors used for seed train preparations [39], as follows:

$$\frac{(CAPEX_{full\ scale})}{(CAPEX_{seed})} = \left[\frac{(Volume_{full\ scale})}{(Volume_{seed})}\right]^{0.6} \qquad \text{Eq. 5.11}$$

In terms of final product concentrations, the COCR strategy did not result in competitive results (for the time range studied), while comparable α-humulene volumetric concentrations were estimated for both EF strategies proposed (for EF#1 and EF#2, at least 4 - fold the values predicted for the COCR strategy would be expected).

The heterotrophic production of α-humulene by bacteria (*C. necator*) has been described by [10]. In that case, authors highlighted that a considerable percentage of the balanced carbon (source fructose) had been used for energy metabolism (72.3 to 73.7 % detected in off-gas as CO_2) and biomass formation (24.3 to 25.7 %), while only 2 % resulted in α-humulene production. Such result is comparable to observations from experiment 8 (chapter 4), where 2.4 % of the Cmols of glycerol supplied at the end of fed-batch were estimated by carbon balance as converted into α-humulene. As a consequence, the operational costs of the terpene fermentations are considerably high. Relevant references of techno-economic assessments describing operational costs on terpene processes are available from [2], [3] and [9].

Significant savings towards the industrial production of sesquiterpenes were proposed by [9], when considering the enhancement of the catastrophic (CPI) demulsification step efficiency, more specifically by the reduction solvent or product losses through aqueous streams of centrifuges, or the minimization of solvent demands. Additionally, the same authors suggested that the implementation of product recovery methods depending on less unit operations, or that allow product yield maximization are key

towards minimizing sesquiterpene production costs, which could also be achieved by lowering emulsifiers demands (solvents or surfactants).

As seen from table 4 and 5, the relative contribution of compressors for 10000 MT/year and 500 MT/year increases considerably as compared to the base case [32], representing 25.3 % and 23.3 % of the total equipment costs, respectively. Additionally, an 8.3-fold increase in CAPEX per unit production is expected as a consequence of a 20-fold volume scale-down. Therefore, as compared to having several bioreactors of small industrial scale, it would be preferable to have a lower number of fermentors of large industrial scale.

In summary, highlighting the importance of the utilization of main bioreactors dedicated for manufacturing the product of interest is a crucial consideration for industrial processes towards the production of sesquiterpenes. Furthermore, here we emphasize that the capital and operational costs that follow from the implementation of compressors in aerobic processes should not be neglected or underestimated.

5.5.   Conclusion

In this chapter, Black-box modeling was performed using parameters and stoichiometry resulting from chapter 4 for estimations of process time, yields and productivities for different fed-batch strategies using 1 m^3 and 10 m^3 bioreactors.

Overall, a very long process duration follows from high α-humulene productivities measured for very low specific growth rates, especially for strategy EF#1: exponential feed using a single bioreactor for the production of both biomass and α-humulene. Instead, decoupling biomass and α-humulene into two different bioreactors (EF#2) would lead to an attractive reduction of the process time in 20 %. Furthermore, a 30 % increase over volumetric productivities for EF#2 is estimated, as compared to (EF#1).

5.6. Acknowledgements

5.7. Symbols

A = bioreactor cross sectional area [m^2]

a or a_s = stoichiometric parameter Herbert - Pirt [mol S · Cmol X^{-1}]

a_o = stoichiometric parameter Herbert - Pirt [mol O_2 · Cmol X^{-1}]

b = stoichiometric parameter Herbert - Pirt [mol S · mol P^{-1}]

BR = Biomass reaction

CAPEX = Capital Expenditure

C_s = substrate concentration [mol · L^{-1}]

D = impeller outer diamater

Eq. = Equation

F_g = gas supply [m^3 · s^{-1}]

F_s = feed rate [mol · h^{-1}]

F_o = maximum oxygen supply rate [mol · h^{-1}]

ID = identification

K_s = affinity constant for substrate [mol · m^{-3}]

μ = biomass specific growth rate [Cmol X produced · (Cmol X present · h)$^{-1}$]

q_{CO2} = carbon dioxide specific rate [mol P· (Cmol X · h)$^{-1}$]

q_{O2} = oxygen specific rate [mol P · (Cmol X · h)$^{-1}$]

q_s = substrate specific rate [mol S · (Cmol X · h)$^{-1}$]

q_p = product specific rate [mol P · (Cmol X · h)$^{-1}$]

m_0 = maintenance term, oxygen consumption [mol O_2 · (h · Cmol X present)$^{-1}$]

m_s = maintenance term, substrate consumption [mol S · (h · Cmol X present)$^{-1}$]

MR = Maintenance reaction

M_x = total mols biomass [Cmol X]

$M_{x(t)}$ = biomass as a function of time [Cmol X]

M_{xf} = biomass at the end of batch [Cmol X]

M_{x0} = biomass at batch start [Cmol X]

P_g/V = volumetric power (gassed) [kW $\cdot$ (m^3)$^{-1}$], [W $\cdot$ (m^3)$^{-1}$]

PR = Process reaction

P_{so} = impeller power uptake under ungassed condition [kW]

P_{sg} = impeller power uptake under gassed condition [kW]

t_B = time of batch duration

T = bioreactor inner diameter

v_{gs} = superficial gas velocity [m $\cdot$ s^{-1}]

X = biomass

Y_{ij} = Yield, ratio of [q_j/q_i]

5.8. Appendix

5.8.1. Appendix A. General calculations

Table 6. General calculations used in this chapter:

Description	Equations	Eq.
Process reaction	(q_s/q_p) $C_3 H_8 O_3$ + (q_n/q_p) NH^{4+} + (q_o/q_p) O_2 + (q_c/q_p) CO_2 + (q_H/q_p) H^+ + (μ/q_p) $C_1 H_{1.8} O_{0.5} N_{0.2}$ + (q_w/q_p) H_2O + $(q_p/q_p=1)$ $C_{15} H_{24}$	5.12
Process reaction [PR]	$[PR] = \dfrac{\mu}{q_p} \cdot [BR] + \dfrac{q_p}{q_p} \cdot [HR] + (\dfrac{-m_s}{q_p}) \cdot [MR]$ For [BR] = biomass reaction; [HR] = humulene reaction; [MR] = maintenance reaction	5.13
Herbert -Pirt	$q_s = \dfrac{\mu}{Y_{xs,max}} + \dfrac{q_p}{Y_{ps,max}} + m_s$	5.14
Psg/P$_{S0}$ (Hughmark) [35]	$\dfrac{P_{sG}}{P_{s0}} = 0.10 \left(\dfrac{F_g}{NV}\right)^{-0.25} \left(\dfrac{N^2 D^4}{g H_s V^{\frac{2}{3}}}\right)^{-0.20}$	5.15
Biomass at end fed-batch (EF)	$M_{x \text{ (feed end)}} = \dfrac{F_o}{q_{O2 \text{ opt}}}$	5.16
Fed-batch duration (EF)	$t_{feed} = \ln\left(\dfrac{M_{x \text{ (feed end)}}}{M_{x(f=\text{end batch})}}\right) / \mu_{opt}$	5.17

Oxygen transfer rate (OTR) [28]	$OTR_{max} = k_L a \cdot V_L \cdot (\alpha_0 \cdot p^c \cdot X_o - C_{oL})$	5.18
Reactor cross sectional	$A = \pi \dfrac{T^2}{4}$	5.19
Superficial gas velocity	$v_{gs} = \dfrac{F_g}{A}$	5.20
Tank diameter	$T = \left[\dfrac{4 \cdot T}{H_L} \cdot \dfrac{V_L}{\pi} \right]^{\frac{1}{3}}$	5.21
Rate $_i$	$\dfrac{dM_i}{dt} = q_i \cdot M_x$	5.22

5.8.2. Appendix B. Parameters used for calculations of batch phase

Table 7. Batch specific rates (q_i) (product absent):

Description	Unit	Value
μ_{max}	$\dfrac{1}{h}$	0.397 ± 0.05
$-qs_{max}$	$\dfrac{mol_{glycerol}}{mol_x \cdot h}$	0.264 ± 0.06
$-qo_{2\,max}$	$\dfrac{mol_{O_2}}{mol_x \cdot h}$	0.508 ± 0.09
$qco_{2\,max}$	$\dfrac{mol_{CO_2}}{mol_x \cdot h}$	0.406 ± 0.07

5.8.3. Appendix C. Exponential feed: parameters and calculations

Table 8. Optimal specific rates and yields for exponential feed:

Index (Description)	Symbol	Unit	value
μ (biomass)	μ_{opt}	$\dfrac{1}{h}$	$5.3 \cdot 10^{-3}$
p (product)	qp^{opt}	$\dfrac{mol_{humulene}}{mol_x \cdot h}$	$2.91 \cdot 10^{-4}$
s (substrate	$-qs_{opt}$	$\dfrac{mol_{glycerol}}{mol_x \cdot h}$	$-1.55 \cdot 10^{-2}$
o₂ (oxygen)	$-qo_{2\,opt}$	$\dfrac{mol_{O_2}}{mol_x \cdot h}$	$-4.27 \cdot 10^{-2}$
c (carbon dioxide)	$qco_{2\,opt}$	$\dfrac{mol_{CO_2}}{mol_x \cdot h}$	$3.69 \cdot 10^{-2}$
w (water)	qw_{opt}	$\dfrac{mol_{H2O}}{mol_x \cdot h}$	$5.54 \cdot 10^{-2}$

Table 9. Analytic solutions for exponential feeding (EF) strategy:

Description	Equations	Eq. ID
Total biomass	$$M_x(t) = M_x(t_0)\exp(\mu \cdot t)$$	5.23
Total water mass	$$M_w(t) = M_w(t_0) + \frac{(\beta \cdot q_s + q_w)}{\mu} \cdot M_x(t_0)\exp(\mu \cdot t)$$	5.24
Total product mass	$$M_p(t) = M_p(t_0) + \frac{(q_p)}{\mu} \cdot M_x(t_0)\exp(\mu \cdot t)$$	5.25
Carbon dioxide formation rate	$$F_{CO2}(t) = q_c \cdot M_x(t_0)\exp(\mu \cdot t)$$	5.26
Feed rate	$$F_s(t) = q_s(\mu, q_p, m_s) \cdot M_x(t_0)\exp(\mu \cdot (t - t_B))$$	5.27
Total feed	$$\int_{t0}^{t} F_s(t) = \frac{q_s}{\mu} \cdot M_x(t_0)\exp(\mu \cdot t)$$	5.28
Oxygen uptake rate (OUR)	$$F_o(t) = q_o \cdot M_x(t)$$ $$= \left(1.12 \cdot \mu + 5.95 \cdot q_p + 3.5 \cdot m_s\right) \cdot \frac{M_x(t_0)}{\mu}\exp(\mu \cdot t)$$	5.29
Oxygen transfer rate (OTR)	$$OTR_{max} = k_L a \cdot V_R \cdot (C^* - 0)$$	5.30

β= ratio of water to substrate.

5.8.4. Appendix D. Calculations for the Constant oxygen consumption rate (COCR)

Table 10. General correlation (COCR):

Description	Equations	Eq. ID
$M_x(t)$	$$M_x(t) = M_{xEND} - (M_{xEND} - M_{xB}) \cdot \exp\left(-\frac{m_{O2}}{a_{O2}} \cdot (t - t_B)\right)$$	5.31
$\mu(t)$	$$\mu(t) = \frac{\left(\frac{F_{O2(max)}}{a_{O2}} - \left(\frac{F_{O2(max)}}{q_{O2(max)}} \cdot \frac{m_{O2}}{a_{O2}}\right)\right) \cdot \exp\left(-\frac{m_{O2}}{a_{O2}} \cdot (t - t_B)\right)}{M_{xEND} - (M_{xEND} - M_{xB}) \cdot \exp\left(-\frac{m_{O2}}{a_{O2}} \cdot (t - t_B)\right)}$$	5.32
$F_s(t)$	$$F_s(t) = \left(a_s \cdot \left[\left[\frac{\left(\frac{F_{O2(max)}}{a_{O2}} - \left(\frac{F_{O2(max)}}{q_{O2(max)}} \cdot \frac{m_{O2}}{a_{O2}}\right)\right) \cdot \exp\left(-\frac{m_{O2}}{a_{O2}} \cdot (t - t_B)\right)}{M_{xEND} - (M_{xEND} - M_{xB}) \cdot \exp\left(-\frac{m_{O2}}{a_{O2}} \cdot (t - t_B)\right)}\right] + m_s\right] \cdot M_x(t)\right)$$	5.33

$M_x(t)$ = Biomass versus time; $\mu(t)$ = Specific growth rate versus time; $F_s(t)$ = substrate rate versus time.

5.8.5. Appendix E. kLa correlations for coalescing, semi coalescing and non-coalescing systems per experiment (Chapter 4, α-humulene production)

kLa versus volumetric power [Exp 9]
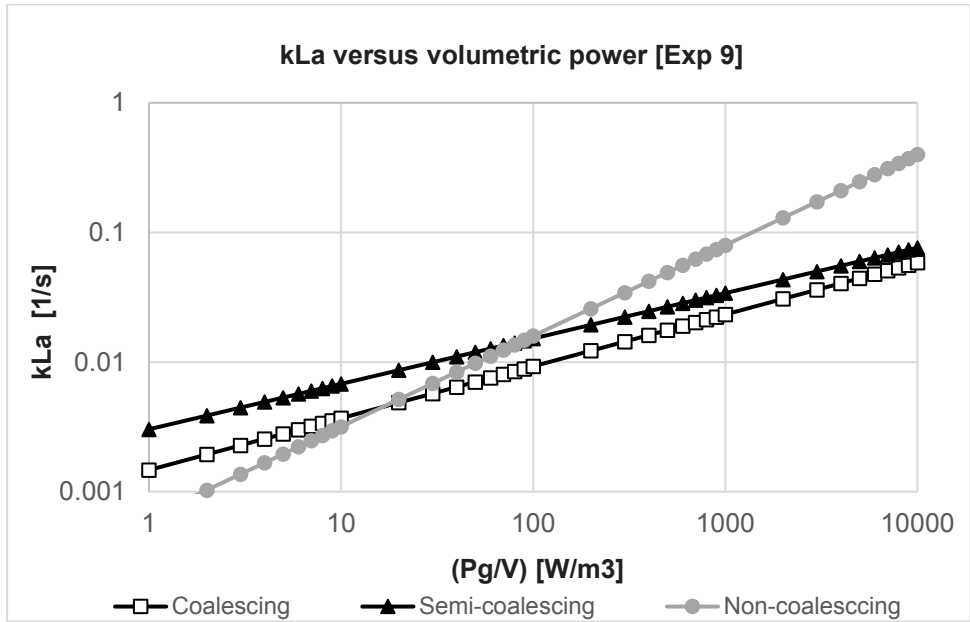
Figure 16. Experiment 9, (dodecane free, v_{gs} of $3.19 \cdot 10^{-3}$ m · s^{-1}) kLa models.
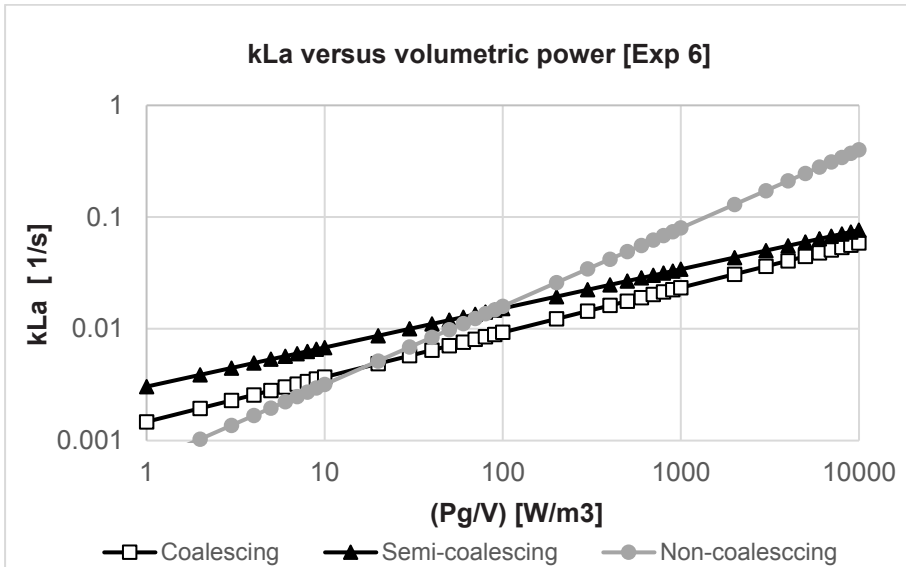
Figure 17. Experiment 6 (ISPR, v_{gs} of $3.21 \cdot 10^{-3}$ m · s^{-1}) kLa models.
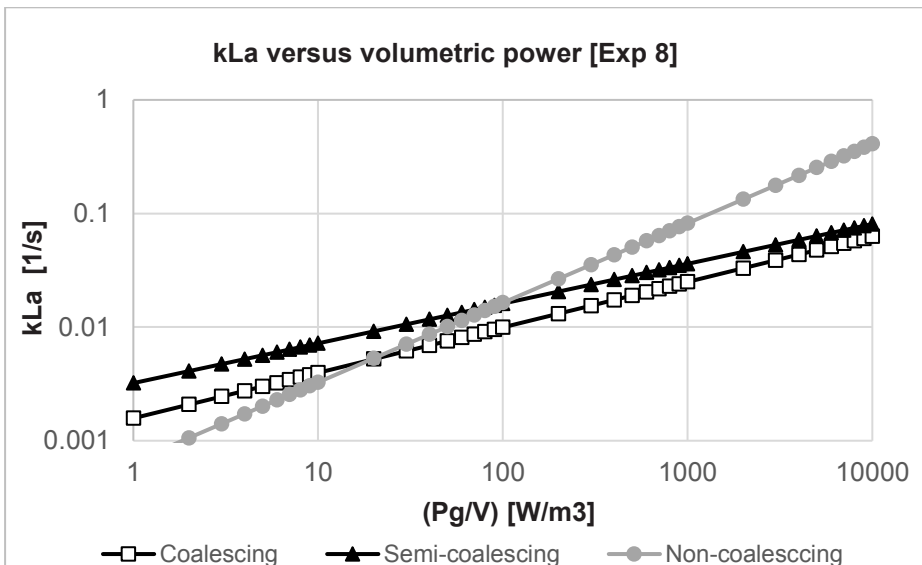
Figure 18. Experiment 8 (ISPR, v_{gs} of $3.68 \cdot 10^{-3}$ m · s^{-1}) kLa models.
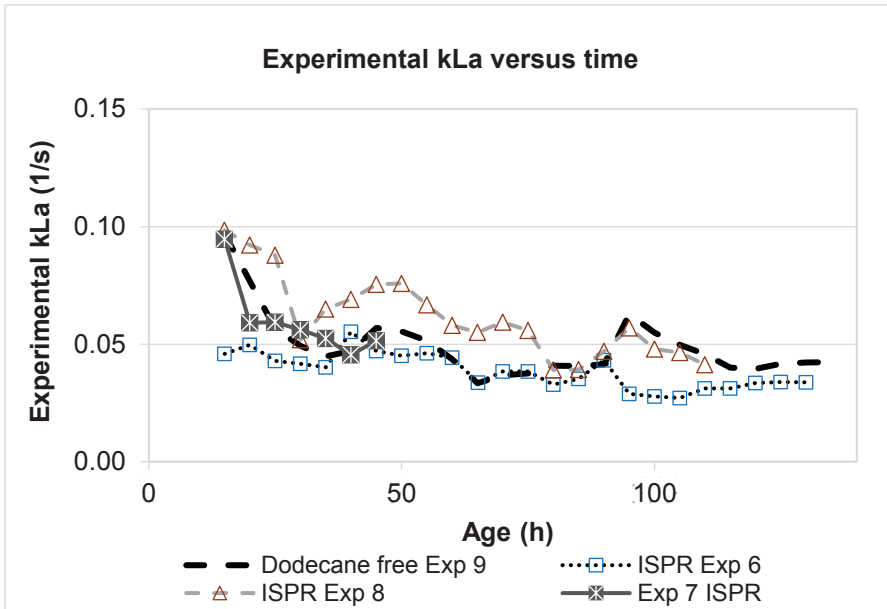
Figure 19. Experimental kLa values versus time for experiments using ISPR (6 (squares), 7 (asterisks), 8 (triangles)) and lacking ISPR (9, dashed line).

5.8.6. Appendix F. Additional information

Table 11. Dimensions informed by supplier [40] for the 2L jacketed bioreactors used in laboratory work, and of bioreactors considered for modeling (scale-up):

Total volume	Working volume	Internal vessel diameter [T]	Liquid height [H_L]	Internal height	Aspect ratio for working volume
(m^3)	(m^3)	(m)	(m)	(m)	
$2.2 \cdot 10^{-3}$	$1.7 \cdot 10^{-3}$	0.105	0.196	0.240	1.9
1	0.75	0.576	2.88		5
10	7.5	1.168	7.01		6

5.9. References

1.   Benjamin, K.R., et al., *Developing Commercial Production of Semi-Synthetic Artemisinin, and of β-Farnesene, an Isoprenoid Produced by Fermentation of Brazilian Sugar.* Journal of the Brazilian Chemical Society, 2016. **27**(8): p. 1339-1345.

2.   Ferreira, R. and D. Petrides, *Production of Farnesene (a Terpene) via Fermentation - Process Modeling and Techno-Economic Assessment (TEA) using SuperPro Designer.* 2020: Intelligen, Inc. 51p.

3.   Wu, W. and C.T. Maravelias, *Synthesis and techno-economic assessment of microbial-based processes for terpenes production.* Biotechnology for Biofuels, 2018. **11**(1): p. 294.

4.   Aguilar, F., T. Scheper, and S. Beutel, *Improved Production and In Situ Recovery of Sesquiterpene (+)-Zizaene from Metabolically-Engineered E. coli.* Molecules, 2019. **24**(18): p. 3356.

5.   Pedraza de la Cuesta, S., *(2019) Product emulsification in multiphase fermentations: The unspoken challenge in microbial production of sesquiterpenes. [Dissertation (TU Delft), Delft University of Technology].* https://doi.org/10.4233/uuid:a48e3fc9-5e7b-4872-9984-22e0eef6686

6.   Da Costa Basto, R.M., M.P.Casals, R.F.Mudde, L.A.M van der Wielen, Maria C. Cuellar., *A mechanistic model for oil*

recovery in a region of high oil droplet concentration from multiphasic fermentations. Chemical Engineering Science: X Volume 3 (2019),100033; https://doi.org/10.1016/j.cesx.2019.100033

7. Da Costa Basto, R.M., et al., *Impact of flocculant addition in oil recovery from multiphasic fermentations.* Food and Bioproducts Processing, 2020. **123**: p. 150-163.

8. AmyrisInc. *Amyris Achieves Record Low Cost Farnesene Production*. 2015 [Access date 21-03-2024]; Available from: https://investors.amyris.com/2015-10-12-Amyris-Achieves-Record-Low-Cost-Farnesene-Production.

9. Cuesta, S.P.-d.l., et al., *Techno-economic assessment of the use of solvents in the scale-up of microbial sesquiterpene production for fuels and fine chemicals.* Biofuels, Bioproducts and Biorefining, 2019. **13**(1): p. 140-152.

10. Milker, S., et al., *Gram-scale production of the sesquiterpene α-humulene with Cupriavidus necator.* Biotechnology and Bioengineering, 2021. **118**(7): p. 2694-2702.

11. Ferreira, R. and D. Petrides, *Production of Farnesene (a Terpene) via Fermentation - Process Modeling and Techno-Economic Assessment (TEA) using SuperPro Designer*. 2020.

12. © DAB.bio, I. *FAST™ (Fermentation Accelerated by Separation Technology)*. 2024 Access date 21-03-2024]; Available from: https://dab.bio/technology.

13.   Zhang, Y., J. Nielsen, and Z. Liu, *Engineering yeast metabolism for production of terpenoids for use as perfume ingredients, pharmaceuticals and biofuels.* FEMS Yeast Res, 2017. **17**(8).

14.   Riesenberg, D., et al., *High cell density cultivation of Escherichia coli at controlled specific growth rate.* Journal of Biotechnology, 1991. **20**(1): p. 17-27.

15.   Levisauskas, D., et al., *Model-based optimization of viral capsid protein production in fed-batch culture of recombinant Escherichia coli.* Bioprocess and Biosystems Engineering, 2003. **25**(4): p. 255-262.

16.   Gnoth, S., R. Simutis, and A. Lübbert, *Selective expression of the soluble product fraction in Escherichia coli cultures employed in recombinant protein production processes.* Applied Microbiology and Biotechnology, 2010. **87**(6): p. 2047-2058.

17.   Bäcklund, E., et al., *Fedbatch design for periplasmic product retention in Escherichia coli.* Journal of Biotechnology, 2008. **135**(4): p. 358-365.

18.   Junker, B.H., *Scale-up methodologies for Escherichia coli and yeast fermentation processes.* Journal of Bioscience and Bioengineering, 2004. **97**(6): p. 347-364.

19.   van 't Riet, K., *Mass transfer in fermentation.* Trends in Biotechnology, 1983. **1**(4): p. 113-119.

20.   Van't Riet, K., *Review of Measuring Methods and Results in Nonviscous Gas-Liquid Mass Transfer in Stirred Vessels.*

Industrial & Engineering Chemistry Process Design and Development, 1979. **18**(3): p. 357-364.

21.   Montes, F.J., J. Catalán, and M.A. Galán, *Prediction of kLa in yeast broths.* Process Biochemistry, 1999. **34**(6): p. 549-555.

22.   Warmoerskerken MCCG, S.J. *Surface contamination effects in stirred tank reactors. In: M Bruxelmanne, editor. . : Polytechnique de Mons. .* in *Proceedings of the International Symposium on Mixing in the Chemical Industry.* 1978. Mons, Belgium: Polytechnique de Mons.

23.   Morão, A., et al., *Effect of antifoam addition on gas-liquid mass transfer in stirred fermenters.* 1999. **20**: p. 165-172.

24.   Clarke, K.G. and L.D.C. Correia, *Oxygen transfer in hydrocarbon–aqueous dispersions and its applicability to alkane bioprocesses: A review.* Biochemical Engineering Journal, 2008. **39**(3): p. 405-429.

25.   Janssen, A.C.J.M., J.G.T. Kierkels, and G.F. Lentzen, *Two-phase fermentation process for the production of an organic compound*, in *WO/2015/002528.* 2015, Isobionics [NL], Janssen, A.C.J.M. (US), Kierkels, J.G.T. (US), Lentzen, G.F. (US).

26.   van Winden, W., *Personal Communications*. 2022.

27.   Riet, K.v.t. and J. Tramper, *Basic bioreactor design*. 1991, New York: Marcel Dekker.

28.   van der Lans, R., *Gas transfer*, in *Bioprocess Engineering Part 3. Design and Scal up of bioreactors*, J.J. Heijnen,

Noorman, H.J.; van der Lans, R.G.J.M, Editor. 2015, ECUST: Shangai p. 149-189.

29.   Garcia-Ochoa, F. and E. Gomez, *Bioreactor scale-up and oxygen transfer rate in microbial processes: An overview.* Biotechnology Advances, 2009. **27**(2): p. 153-176.

30.   Hubbard, D.W., *Scale-up strategies for bioreactors*, in *Biotechnology Processes: Scale-up and Mixing*, C.S. Ho and J.Y. Oldshue, Editors. 1987, American Institute of Chemical Engineers (AIChE): New York. p. pp 168-184.

31.   Ju, L.-K. and G.G. Chase, *Improved scale-up strategies of bioreactors.* Bioprocess Engineering, 1992. **8**(1): p. 49-53.

32.   Demetri Petrides and R.d.G. Ferreira, *Production of b-farnesene - Modeling and Evaluation with SuperPro Design* 2020, Intelligen, Inc. p. 1-51.

33.   [Access date: 28-April-2024]; Chemical Engineering and Process Engineering Resources]. Available from: https://www.cheresources.com/invision/topic/29270-estimation-of-gas-centrifugal-compressor-cost/.

34.   Sinnott, R. and G. Towler, *Chapter 6 - Costing and Project Evaluation*, in *Chemical Engineering Design (Sixth Edition)*, R. Sinnott and G. Towler, Editors. 2020, Butterworth-Heinemann. p. 275-369.

35.   Hughmark, G.A., *Power Requirements and Interfacial Area in Gas-Liquid Turbine Agitated Systems.* Industrial & Engineering Chemistry Process Design and Development, 1980. **19**(4): p. 638-641.

36.   Al-Masry, W.A., *Effects of antifoam and scale-up on operation of bioreactors.* Chemical Engineering and Processing: Process Intensification, 1999. **38**(3): p. 197-201.

37.   Pelton, R., *A review of antifoam mechanisms in fermentation.* J Ind Microbiol Biotechnol, 2002. **29**(4): p. 149-54.

38.   Van Der Wielen, L.A.M., M.H.H. Van Dam, and K.C.A.M. Luyben, *On the relative motion of a particle in a swarm of different particles.* Chemical Engineering Science, 1996. **51**(6): p. 995-1008.

39.   van der Wielen, L.A.M., S.I. Mussatto, and J. van Breugel, *Bioprocess intensification: Cases that (don't) work.* N Biotechnol, 2021. **61**: p. 108-115.

40.   *Applikon Biotechnology: cultivation systems from discovery to production*, Applikon, Editor. p. 16 to 19.

Chapter 6

Conclusions,   recommendations and outlook

6.1. Overview

This thesis is focused on the research of relevant factors towards the fermentative production of industrially relevant sesquiterpenes ($C_{15}H_{24}$). In chapter 1, biochemical pathways, definitions and relevance of sesquiterpenes was described, as well as challenges towards their biotechnological production using *Escherichia coli.* We briefly summarize our main findings and provide suggestions for follow-up research and development.

Metabolic model.

In Chapter 2, the santalene-producing *E. coli* was tested in bench reactor (2 L) experiments using dodecane for ISPR. Herbert-Pirt parameters for biomass formation and maintenance were estimated, while testing suitable induction strategies and varying feed rates.

Findings & short suggestions for next steps:

Herbert-Pirt parameters for biomass formation (a) and maintenance (m_s) were closer to literature values [1] for experiments that had in common low (and constant) feed rates and low α-santalene productivities, which decreased until the end of fed - batch. On the other hand, the experiment performed at a higher glycerol feeding rate and approximately 1 mM initial inducer concentration (added early in the process) was more successful, resulting in more stable specific

productivities with time. The Herbet-Pirt parameter "a" estimated for this specific experiment was slightly above the literature references value.

Stability considerations of α-santalene producing *Escherichia coli* strain

Plasmid instability critically influences the performance of genetically modified organisms. We studied in Chapter 3 the plasmid dynamics of an α-santalene producing *Escherichia coli* BL21 (DE3) strain during glycerol limited fed-batch cultivation. Quantitative polymerase chain reaction (qPCR) was carried out to monitor the copy numbers of both plasmids (pACYCDuetTM-1 and pETDuet) during fed-batch cultivation in the absence of *in-situ* product recovery (ISPR). The copy numbers of both plasmids mostly increased with time indicating that plasmid instability was not an issue in this strain.

Short suggestions for next steps:

The low specific productivities reported in this thesis for the santalene-producing strain does not seem to relate to segregational instability of plasmids. The recent literature on santalene synthases [2] suggests different specificities and therefore, efficiencies for those enzymes, whereas other authors highlight the complexity of α-santalene formation due to cyclization [3]. Therefore, the optimization of this specific synthase type seems to be a interesting and relevant

research line towards further improving α-santalene and other sesquiterpene yields.

Fermentative production in bioreactors.

For Chapter 4, the biotechnological production of the α-humulene, key sesquiterpene naturally available in *Humulus lupulus,* was explored. This alternative *E. coli* strain was compared for specific productivities testing different feeding strategies, absence (or presence) of ISPR and selection pressure variation in feed medium compositions. Herbert-Pirt parameters were obtained under a constant feed profile.

Findings & short suggestions for next steps:

Specific productivities in chapter 4 exceeded those reported in previous chapters of this thesis. Herbert-Pirt parameters estimated were comparable, but slightly higher as compared to literature, based on only one exploratory experiment. Therefore, elaborating this particular line of experimental research is be recommended. Here, the experimental work with the humulene producing strain was limited due to late access, considering thesis timelines. The next step following from this chapter was reported in chapter 5, due to the more successful specific productivities results, as compared to chapters 2 and 3.

Scale-up considerations.

Chapter 5 consists of scale-up studies using Black-box modeling, based on the kinetic parameters of the α-humulene producing strain. Measured oxygen mass transfer during actual extractive fermentations were presented and compared to relevant k_La correlations. Fed-batch strategies were investigated for optimal production based on experimental findings of high specific α-humulene production on glycerol at very low growth rate of the producing strain *Escherichia coli* BL21 (DE3).

An exponential feed strategy of decoupling biomass production at high growth rates in smaller and cheaper seed fermenters followed by α-humulene production at low growth rates was compared to the original exponential feed strategy of operating at a single bioreactor for biomass and α-humulene productions. The first option had a better outcome for overall lower capital and operational costs, with approximately 20 % shorter process times and 30 % higher volumetric productivities at 1 m^3 and 10 m^3 bioreactors.

Compact next steps:

Even though sesquiterpenes have been a strong focus of research, only a few of them (such as farnesene) are currently produced in industrial scale. As will be detailed in the next sections, further strain improvements in general seem essential to improve feasibility towards actual and robust industrial production.

6.2. Recent advances in strain engineering

Based on previous chapters of this thesis, a key demand is the improvement of sesquiterpene-producing strains. In the case of farnesene for instance, up to 160 $g \cdot L^{-1}$ have been reported when using *Saccharomyces cerevisiae* [4]. The next best titers for farnesene, 25.5 $g \cdot L^{-1}$ [5] and 22.8 $g \cdot L^{-1}$ [6] were reported for *Yarrowia lipolytica*, while for *Escherichia coli*, publications describing up to 10.3 $g \cdot L^{-1}$ of farnesene were found by the time of completion of this thesis [7].

Yeasts have been preferred production organisms in recent publications aiming at terpene production in view of their interesting biochemical features. Overall, high local concentrations of substrates and enzymes are expected, as well as low formation of by-products. Additionally, the high metabolic flux for the mevalonate pathway and the high availability of acetyl-CoA has been described for these microorganisms [8]. Several strategies have been published aiming at the optimization of terpenoids production:

- One of the limiting factors identified in terpene synthesis refers to the low expression of terpene synthases [9]. Thus, approaches such as the screening of terpene synthases from different origins have been widely tested, as well as increasing their expression by increasing their copy numbers and through the utilization of strong promotors [8]. In this context, one technique to improve expression efficiency consists of the computer-aided, artificial modification of amino-acids [8], which includes the expression of truncated enzymes

forms for their higher solubility and optimized catalytic potential [10], as exemplified in [11]. The PSIPRED platform [12] has been described as a tool for analyzing terpene synthases sequences for the further design of related truncated forms [13], [14].

- From a protein engineering perspective, the design of artificially fused enzymes has been proposed to maximize catalytic activity, stability and economic feasibility of processes [15]. The fusion of enzymes allows the proximity of their active sites, channeling therefore, the intermediates into target sites, minimizing the competition of substrates towards branch pathways [16].

Extensive research has focused on improving the regulation of terpene synthesis pathways. For instance, an expressive depletion of the NADPH pool results from the mevalonate pathway, affecting the intracellular redox homeostasis. Therefore, scientists have researched manners to increase the NADPH supply [8], [17]. Another example described the overexpression of rate-limiting enzymes such as the 3-hydroxy-3-methyl-glutaryl-coenzyme A (HMG), which directly impacts the availability of the intermediates isopentenyl diphosphate (IPP) and dimethylallyl diphosphate (DMAPP) [18], [19], [20].

6.3. Conclusion and perspectives

The sesquiterpene productivities differences between santalene-producing and humulene-producing strains were considerable. Still, the best productivities reported here for the humulene-producing strains demand improvements to increase the economic feasibility of the process. A diversity of factors could have influenced the results reported for chapters 2, 3 and 4, such as strain engineering details (not addressed in experimental chapters).

Here the expression of key enzymes and precursors was not investigated, due to limited time (and scope) of this work. It is known, though, that the simple deletion or overexpression of multiple enzymes in general could lead to metabolic burden or the accumulation of intermediates, indicating challenges regarding the regulation of terpene production pathways [8]. The utilization of biosensors for metabolites throughout the pathway is suggested as a strategy to promote a dynamic, balanced carbon flux between the formation of terpenes and cell growth [8]. Biosensors have been described for interactions with environmental stimuli and for their effective, precise and timely action mechanisms [16]. Specific types of biosensors, such as those described as transcriptional-factor based can be used as high throughput tools for screening the best performance strains [21].

In conclusion, the field of industrial manufacturing of sesquiterpene products through fermentation offers rich and relevant research opportunities along biological, bioprocess engineering and methodological dimensions. The above suggestions provide some guidance for future research work in this highly attractive domain.

6.4. References

1.   Taymaz-Nikerel, H., et al., *Genome-derived minimal metabolic models for Escherichia coli MG1655 with estimated in vivo respiratory ATP stoichiometry.* Biotechnology and Bioengineering, 2010. **107**(2): p. 369-381.

2.   Zha, W., et al., *Rationally engineering santalene synthase to readjust the component ratio of sandalwood oil.* Nature Communications, 2022. **13**(1): p. 2508.

3.   Tippmann, S., et al., *Production of farnesene and santalene by Saccharomyces cerevisiae using fed-batch cultivations with RQ-controlled feed.* Biotechnology and Bioengineering, 2016. **113**(1): p. 72-81.

4.   Meadows, A.L., et al., *Rewriting yeast central carbon metabolism for industrial isoprenoid production.* Nature, 2016. **537**: p. 694-697.

5.   Liu, Y., et al., *Engineering the oleaginous yeast Yarrowia lipolytica for production of α-farnesene.* Biotechnology for Biofuels, 2019. **12**(1): p. 296.

6.   Shi, T., et al., *Engineering the oleaginous yeast Yarrowia lipolytica for β-farnesene overproduction.* Biotechnol J, 2021. **16**(7): p. e2100097.

7.   Yao, P., et al., *Investigation of fermentation conditions of biodiesel by-products for high production of β-farnesene by an engineered Escherichia coli.* Environ Sci Pollut Res Int, 2020. **27**(18): p. 22758-22769.

8.   Yang, L., et al. *Recent Advances in Multiple Strategies for the Synthesis of Terpenes by Engineered Yeast*. Fermentation, 2022. **8**, DOI: 10.3390/fermentation8110615.

9.   Bohlmann, J., G. Meyer-Gauen, and R. Croteau, *Plant terpenoid synthases: molecular biology and phylogenetic analysis.* Proc Natl Acad Sci U S A, 1998. **95**(8): p. 4126-33.

10.   Williams, D.C., et al., *Truncation of limonene synthase preprotein provides a fully active 'pseudomature' form of this monoterpene cyclase and reveals the function of the amino-terminal arginine pair.* Biochemistry, 1998. **37**(35): p. 12213-20.

11.   Turner, G., et al., *Limonene synthase, the enzyme responsible for monoterpene biosynthesis in peppermint, is localized to leucoplasts of oil gland secretory cells.* Plant Physiol, 1999. **120**(3): p. 879-86.

12.   *PSIPRED Workbench*.   [cited 2024 08-May-2024]; Available from: http://bioinf.cs.ucl.ac.uk/psipred/.

13.   Chen, T., et al., *Metabolic engineering of Saccharomyces cerevisiae for pinene production.* CIESC Journal, 2019. **70**(1): p. p179-188.

14.   Jia, H., et al., *Collaborative subcellular compartmentalization to improve GPP utilization and boost sabinene accumulation in Saccharomyces cerevisiae.* Biochemical Engineering Journal, 2020. **164**: p. 107768.

15.   Elleuche, S., *Bringing functions together with fusion enzymes--from nature's inventions to biotechnological applications.* Appl Microbiol Biotechnol, 2015. **99**(4): p. 1545-56.

16. Fordjour, E., et al., *Toward improved terpenoids biosynthesis: strategies to enhance the capabilities of cell factories.* Bioresources and Bioprocessing, 2022. **9**(1): p. 6.

17. Liu, Y., et al., *Progress and perspectives for microbial production of farnesene.* Bioresource Technology, 2022. **347**: p. 126682.

18. Stermer, B.A. and R.M. Bostock, *Involvement of 3-hydroxy-3-methylglutaryl coenzyme a reductase in the regulation of sesquiterpenoid phytoalexin synthesis in potato.* Plant Physiol, 1987. **84**(2): p. 404-8.

19. Zhao, Y., et al., *High-efficiency production of bisabolene from waste cooking oil by metabolically engineered Yarrowia lipolytica.* Microb Biotechnol, 2021. **14**(6): p. 2497-2513.

20. Matthäus, F., et al., *Production of lycopene in the non-carotenoid-producing yeast Yarrowia lipolytica.* Appl Environ Microbiol, 2014. **80**(5): p. 1660-9.

21. Yu, H., et al., *Establishment of BmoR-based biosensor to screen isobutanol overproducer.* Microbial Cell Factories, 2019. **18**(1): p. 30.

List of publications

Publications

Food Research International (2013), 52 (1)

"Endophytes: Recent developments in biotechnology and the potential for flavor production"

ABRAHÃO, M.R.E; MOLINA, G.; PASTORE, G.M.

Critical Reviews in Biotechnology (2015), 35 (3)

"**Genetic and metabolic engineering of microorganisms for the development of new flavor compounds from terpenic substrates"**

BUTION, M. L.; MOLINA, G.**; ABRAHÃO,** M.R.E.; PASTORE, G.M.

Poster Presentations

ACS National meeting (2019) Spring- Orlando

"**Biotechnological aroma production using sesquiterpene *in situ* recovery".**

ABRAHÃO, M.R.E; van GULIK, W., CUELLAR, M.; PASTORE, G.M.; van der WIELEN, L.

18th European Congress on Biotechnology (ECB 2018)-Geneva

"Biotechnological production of sesquiterpene from glycerol"

ABRAHÃO, M.R.E; van GULIK, W., CUELLAR, M.; PASTORE, G.M.; van der WIELEN, L.

10th Slaca – Latin American Symposium of Food Science (2013) - Campinas

"Screening endophytes from *Myrciaria dubia* fruits and their biotransformation potential"

ABRAHÃO, M.R.E.; BUTION, M.L.; MOLINA, G.; de SOUSA, R.S.C.; da SILVA, M.J.; PAULINO, B.N.; PASTORE, G.M.

10th Slaca – Latin American Symposium of Food Science (2013) – Campinas

"Production of perillyl derivatives from fungal endophytes"

ABRAHÃO, M.R.E.; BUTION, M.L.; MOLINA, G.; da SILVA, M.J.; PASTORE, G.M.

Acknowledgements

I appreciate all the efforts from Prof. Dr. Patricia Osseweijer and Prof. Dr. Ir. Luuk van der Wielen towards the implementation of this Dual Degree program between Delft University of Technology and University of Campinas.

To my promotor, Prof. Dr. Ir. Luuk van der Wielen my gratitude for the opportunity to be part of the Bioprocess Engineering group at Delft University of Technology and for supporting me during challenging moments.

Prof. Dr. Glaucia Maria Pastore, thank you for being so supportive and enthusiastic during key moments, and even since the Master's project, encouraging me to be a proactive researcher.

Hereby I also express gratitude my copromotor, Dr. Walter van Gulik, who I will always have in memory as an excellent researcher, for all the comprehension, orientation, and expertise in Fermentation Technology. Dr. Maria Cuellar, as leader of the DIRC project, had also a remarkable impact on this project from her great experience with multiphasic systems.

I would like to thank all my colleagues from the DIRC project (Delft Integrated Recovery Program) from TUDelft and Delft Advanced Biorenewables for sharing these challenges. In special, Fabienne Feskens-Snoek, Susana Pedraza de la Cuesta and Carla Prat Llenas. I am grateful for the experiences in the laboratory and trainings.

To the technical team from Bioprocess Engineering section: Yi Song, Stef van Hateren and Max Zomerdijk, thank you very much. Song, thank you for your support with the bench reactors experiments. Max, I really admire your happiness and humor. Thank you for all the support

with GC assays. I also appreciate the technical support from Dirk Geerts, Rob Kerste, Jannie Kempff-Gruwel, Apilena Sapioper, Astrid van Uijen, Johan Knoll, Patricia van Dam and Martin Pabst and Dr. Karel Olavarria Gamez.

Ben Abbas and his impressive expertise about molecular biology and polymerase chain reaction was essential for the last two months of laboratory work. Thank you, Ben, for sharing your knowledge during such a busy time for both of us.

From TUDelft, Ans van Schaik, Rogier van Loghem, Prof. Dr. Ir. Bart van Arem, Prof. Dr. Adrie Straathof and Kawieta Ramautar, and from Unicamp: Debora Subira, Camila Julio, Isabela Girotto, Gustavo Paim, Liliana Rocha, Johni Prates and in special, Nadir Cassiano and: thank you for all the assistance with bureaucratic matters concerning the Dual Degree program. My former colleagues from Solvay, Paula Delgado and Jose Castilho were also supportive.

To my colleagues from The Dual Degree program my sincere admiration and respect for the experience and challenges together: Renato, Wesley, Tiago, Elisa, Rafael, Bianca, Ana, Carla and Lucas. My office colleagues Victor Koppejan and Monica Moreno Gonzalez, I appreciate how considerate you are.

I would like to acknowledge the cooperation of the Biochemical Processes team, in special my managers, Peter Burghout and Michel Beurret, and colleagues from Jonhson & Johnson Innovative Medicine and their empathy on critical times for the completion of this thesis.

To my parents Gilson and Stella, thank you for your unconditional love. Towards the completion of this thesis my dear brother Luis Felipe provided pivotal support with urgent family matters.

My friends, Aline Silva, Priscila Camelo, Larissa Tavares, Lorena Bragança, Lorena Bessas, Bruno Buso and cousin, Raisa: thank you for all the moments together.

The Jones have been my family in the Netherlands, sharing so many awesome moments. Words are just not enough to express my happiness to have you around me: Truus (*in memoriam*), Jolette, Richard, Robin, Milou, Oscar, and, in special, my husband, Alister. Aya & Yuki, our dogs, are just here for hugs and treats.

Curriculum vitae

Meissa Essenfelder was born in Governador Valadares, Minas Gerais, Brazil. She holds a Bachelor's degree in Food Engineering from the Federal University of Viçosa since 2010.

In 2011, Meissa moved to Adelaide Hills, Australia, to work on Quality Assurance of wines at the Shaw & Smith Winery. In 2012, she supported the 16th World Congress of Food Science and Technology (IUFoST) and became a member of the Laboratory of Bio Flavors and Bioactive Compounds, led by Dr. Glaucia Maria Pastore at the Faculty of Food Engineering, University of Campinas. Her research focused on the biotransformation of terpenes available in feedstocks into valuable organoleptic or bioactive molecules such as verbenone, verbenol and perillyl alcohol by wild endophytic fungi. Since 2014, Meissa holds a degree as Master of Food Science and in the same year, she joined the Research & Innovation team at the Industrial Biotechnology Laboratory at Rhodia (multinational Solvay group), working on the optimization of processes in bench scale bioreactors.

In 2016, Meissa moved to Delft to work on her Dual Degree program, as a PhD candidate at the Bioprocess Engineering section, Department of Biotechnology, Faculty of Applied Sciences, Delft University of Technology. Since 2020, Meissa joined the scientific team of Johnson & Johnson Innovative Medicine.

Bioprocess Engineering Section

Department of Biotechnology

Faculty of Applied Sciences

Delft University of Technology - NL

Laboratory of Bioflavours and Bioactive Compounds

Department of Food Science

Faculty of Food Engineering

University of Campinas - BR